The Pennsylvania State University
Applied Research Laboratory
P.O. Box 30
State College, PA 16804

A KALMAN FILTERING APPROACH TO WIDEBAND SCATTERING FUNCTION ESTIMATION AND UPDATING

By

Michael J. Roan

Technical Report No. TR 99-004
May 1999

Supported by:
Office of Naval Research

L. R. Hettche, Director
Applied Research Laboratory

REPORT DOCUMENTATION PAGE

Form Approved
OMB No. 0704-0188

1. AGENCY USE ONLY (Leave blank)	2. REPORT DATE	3. REPORT TYPE AND DATES COVERED

4. TITLE AND SUBTITLE
A Kalman Filtering Approach to Wideband Scattering Function Estimation and Updating

5. FUNDING NUMBERS
N00039-D-0042

6. AUTHOR(S)
Michael J. Roan

7. PERFORMING ORGANIZATION NAME(S) AND ADDRESS(ES)
Applied Research Laboratory
The Pennsylvania State University
P.O. Box 30
State College, PA 16804

8. PERFORMING ORGANIZATION REPORT NUMBER
TR 99-004

9. SPONSORING / MONITORING AGENCY NAME(S) AND ADDRESS(ES)
Office of Naval Research
Ballston Tower One
Arlington, VA 22217-5660

10. SPONSORING / MONITORING AGENCY REPORT NUMBER

11. SUPPLEMENTARY NOTES

12a. DISTRIBUTION / AVAILABILITY STATEMENT
Unlimited

12b. DISTRIBUTION CODE

13. ABSTRACT (Maximum 200 words)

Transmitted signals with high time bandwidth products tend to resolve multiple reflecting structural elements or highlights on the body that is being illuminated. This thesis develops a Kalman filtering approach to estimating the position and velocity of the multiple highlights on a single body undergoing complex motions. First, a general Kalman filter for direct recursive estimation of the spreading function is derived. Second, an algorithm which tracks peak locations within the spreading function is derived via an extended or linearized Kalman filter. The ability for the Kalman filter to track kinematic properties of a multihighlight scatterer is related to the transmitted signal's mean squared bandwidth, mean squared duration, and time-frequency content through the Cramer-Rao lower bound on estimation errors for time scale and time delay. It is shown that the ability of the Kalman filter to track peak locations within the object scattering function and recursively update these peak locations depends strongly on the use of signals with high time-bandwidth products. Finally, a performance monitor which provides a sound, monitorable performance measure of the tracker is introduced via the innovations spectrum. This performance monitor admits the ability of dynamic model updating for adaptive signal processing. This work sets a groundwork for further research into the application areas of image feature tracking, robotic vision, high resolution radar and sonar, and medical imaging.

14. SUBJECT TERMS	15. NUMBER OF PAGES
Transmitted signals, Kalman filter, Cramer-Rao, time-frequency, image feature tracking, robotic vision, high resolution radar and sonar, medical imaging.	126
	16. PRICE CODE

17. SECURITY CLASSIFICATION OF REPORT	18. SECURITY CLASSIFICATION OF THIS PAGE	19. SECURITY CLASSIFICATION OF ABSTRACT	20. LIMITATION OF ABSTRACT
UNCLASSIFIED	UNCLASSIFIED	UNCLASSIFIED	UNLIMITED

ABSTRACT

Transmitted signals with high time bandwidth products tend to resolve multiple reflecting structural elements or highlights on the body that is being illuminated. This thesis develops a Kalman filtering approach to estimating the position and velocity of the multiple highlights on a single body undergoing complex motions. First, a general Kalman filter for direct recursive estimation of the spreading function is derived. Second, an algorithm which tracks peak locations within the spreading function is derived via an extended or linearized Kalman filter. The ability of the Kalman filter to track kinematic properties of a multihighlight scatterer is related to the transmitted signal's mean squared bandwidth, mean squared duration, and time-frequency content through the Cramer-Rao lower bound on estimation errors for time scale and time delay. It is shown that the ability of the Kalman filter to track peak locations within the object scattering function and recursively update these peak locations depends strongly on the use of signals with high time-bandwidth products. Finally, a performance monitor which provides a sound, monitorable performance measure of the tracker is introduced via the innovations spectrum. This performance monitor admits the ability of dynamic model updating for adaptive signal processing. This work sets a groundwork for further research into the application areas of image feature tracking, robotic vision, high resolution radar and sonar, and medical imaging.

Table of Contents

LIST OF FIGURES

LIST OF TABLES

ACKNOWLEDGEMENTS

I would like to thank my thesis advisor, Dr. Leon Sibul, for his guidance and encouragement. I would also like to thank Dr. Randy Young for many fruitful technical discussions as well as fruitful trout fishing expeditions. Also, I would like to thank Dr. Lora Weiss, Dr. Dennis Ricker and Ken Hillsley for their expert advice and helpful conversations.

I would like to thank my family, for without their love, guidance, and true friendship this endeavor would have been doomed to failure. Most of all I would like to thank my wife, Kerstin, whose love and endless encouragement have helped me through many a dark hour. A most special thank you goes to Joe Brinko whose shining example of what mankind should be is with me every hour of every day.

This research was conducted at the Applied Research Laboratory of The Pennsylvania State University and supported by The Office of Naval Research Code 333, Dr. Kam Ng, Program Officer.

Chapter 1

INTRODUCTION

1.1 Motivation

In many applications, the propagation of a signal through a medium is used to derive information about the medium and about objects in the medium. This method has been used in RADAR, SONAR, and medical imaging as well a multitude of other applications. A primary, often undesirable effect which manifests itself in this process is the phenomenon of scattering. In the detection problem, (which is of primary concern in this thesis) a signal is transmitted into the medium, reflects (scatters) from the object to be detected and is received back at the receiver. The signal also scatters from the other objects in the medium, the medium itself, and travels along multiple paths in the medium, causing multiple transmitted signal replicas to arrive at the receiver at different times (delay spread)[1-3]. For high resolution signals [4], the target can be made up of multiple scatterers. In this case the signal may "over resolve" the target and lead to "splitting loss" [2]. In narrowband systems, the problem of fading [2] is prominent for distributed targets or spread channels. All of the above effects give the appearance(from a detection point of view) of multiple detections. The problem is then for a signal processor to determine which of the returns (if any) are from the target. The process of scattering manifests itself in a variety of forms including the multipath phenomenon and the scattering functions of any objects in the medium – including the object to be detected(in the case of RADAR and SONAR).

Recently proposed [4,6,7] wideband processors such as the wavelet transform domain (WTD) estimator-correlator (EC) attempt to overcome this by modeling the multi-highlight structure of an object as a spreading function. The multi-path phenomena is also treated as the channel spreading function. In the narrowband case, the spreading function specifies how the transmitted signal is "spread" in delay and Doppler. In the wideband case, the spreading function specifies how the transmitted signal is "spread" in delay and time-scale. Spreading functions are two-dimensional random functions and their second order statistics are given by scattering functions[8]. Because scattering functions can be related to the random scattering and propagation models, scattering functions are used as prior statistics for implementation of model based signal processors such as the WTD EC.

The WTD EC exploits the processing gain of high resolution (i.e. high time-bandwidth product) signals and uses an estimate of the target and channel scattering functions as prior statistics for implementation of the estimator branch of the processor [9]. The critical issue in the performance of the WTD EC is the accuracy of the scattering function that is used in the processor. A method of updating the scattering function estimates as new data becomes available is required. To accomplish this update, a Kalman filter approach will is used that exploits the innovations approach [10-14]. This method produces a mean-square sense optimal recursive scattering function estimation algorithm and provides a technique for monitoring convergence of the

estimates. Furthermore, the innovation method allows one to establish the validity of the underlying models.

1.2 General Statement of the Problem – Objective

The main objective of this thesis is to develop a complete algorithm for recursive scattering function updating and estimation. By complete, it is meant that starting with the transmitted signal, its shape, its parameters (i.e. duration and bandwidth), develop a Kalman filtering algorithm which illustrates the effects of these parameters on the filter's ability to perform recursive estimation. In the course of developing the Kalman filter the following will be accomplished:

1. Derive the Kalman filter for recursive scattering function updating and estimation.

2. Relate the Kalman filter quantities to physical properties of the signal and scatterer.

3. Place the Kalman filter in the context of a model based signal processor, thus illustrating the connection between tracking and detection.

4. Using simulations, show the effects of signal parameters on the ability of the Kalman filter to track kinematics.

The first goal of this thesis is to derive the Kalman filter for WTD scattering function estimates based on the innovations approach. This derivation will show how new information (innovation) will be used to form a new estimate of the scattering function based on the previous estimates and the innovations. It will be necessary to derive a WTD state equation for the system under investigation as well as a WTD measurement equation of the spreading function, as this is the quantity observed. This will be done within the framework of a wavelet transform based detection algorithm.

The next objective of the thesis is to investigate relationships between the Kalman filter parameters (e.g. measurement error) and the properties of the transmitted signal. The goal here is to establish the relationship between signal parameters and the Cramer-Rao lower bound on the error variance associated with observations of time-scale and time-delay.

The third objective of the thesis is to provide an implementation of the recursive updating algorithm. The results and performance of the algorithms will then be evaluated for selected examples. Another goal here is to illustrate, via the examples, the relationship between the physical problem (target position as a function of time) and the wavelet domain (time/time-scale) representation of the physical problem. Here the method of deriving the state equation and more importantly the state transition matrix from the physical problem is achieved. This critical step will illustrate the path from physical problem to scattering function prediction updating in the WTD.

Finally, the last objective is to show simulation results which highlight the transmitted signal parameter effects and how changes in the measurement error variance (related to the Cramer-Rao lower bound) [15-17] affect the Kalman Filter. Here, a possible performance monitor for the Kalman Filter algorithm, in the form of monitoring the "whiteness" of the innovations sequence[18] will be introduced.

1.3 Original Contributions

The main contribution of this thesis is the theoretical background, and algorithm development for using a Kalman filter to track the locations in the time delay scale plane of multiple reflections which arise from a single distributed abject which is illuminated with a high resolution pulse. This differs from conventional tracking/track association in that in these fields, each track represents a different object, here, all tracks lie on the same object. This algorithm can be used produce target spreading function estimates for use in model based signal processors such as the wavelet transform domain estimator-correlator. In the course of the development of the main theme of the thesis the following contributions were also made.

1. Derivation of the Cramer-Rao Lower Bounds on variances of estimation errors of time-delay and time-scale for a random amplitude scatterer using a wavelet transform detection scheme.
2. Derivation of an extended Kalman Filter for tracking kinematic properties of a physical system using wideband probing signals.

3. Relating the parameters of the transmitted signal to the ability of the Kalman filter to track the kinematics of the physical system.
4. Presentation of the results of simulations which illustrate all of the above contributions.

The main original contribution is the development of a unified approach to model-based signal processing that connects scattering function models, recursive model updating algorithms via Kalman filtering theory, wavelet transform implementation of the EC and signal design by CRLB analysis.

1.4 Assumptions

In this section, assumptions made in the thesis are discussed. The major assumptions are the noises present on the system are uncorrelated and Gaussian and that the scattering is uncorrelated. This is not always a necessary assumption and references are provided for those who wish to extend the work here to colored noises. Although multipath environments and their properties are discussed, in the examples, the medium has a single propagation path that is isovelocity. It is assumed that the initial estimates are within a region of convergence for the Kalman filter. Lastly, it is assumed assume in the kinematic portions of the development that the velocities are small (or analogously that the sample rate is high) so that the overall data rate is high enough for the Kalman filter to track. This assumption is made since the primary goal of the thesis is to illustrate the effects that the transmitted signal (or signal design issues) have on the ability of the

Kalman filter to track. Also, spreading and scattering function models and wideband representation (i.e. time-scale representation) of the return are assumed to be valid. It is also assumed that all signals are finite energy, square integrable functions so that they can be represented in the wavelet transform domain. It is also assumed that covariances of received echos and noise are positive definite functions that uniquely define a reproducing kernel Hilbert space (RKHS). Positive definiteness is also used to establish existence of inverse kernels [64]. In summary, it is assumed that all continuous signals and stochastic processes belong to separable L_2 Hilbert spaces with appropriate inner products. Because any infinite dimensional separable Hilbert space is linearly isometric to l_2 continuous and discrete representations are equivalent. Both representations are used within the thesis (Section 2.4.1).

1.5 Related Research

Many areas of application have reference to tracking, multiple target tracking, or contour tracking. In this section, the goal is to present related fundamental research in the areas of wideband spreading and scattering and to introduce related areas of current research where the features of an "object" is investigated. The definition of "object" depends on the application. First, the areas of research which encompass wideband spreading and scattering are introduced. This research is related to work in the thesis in that it provides a starting theoretical foundation on which to derive the Kalman filtering algorithms. Much of the work done in this area has been to characterize time-varying propagation channels with multiple propagation paths. This leads naturally a discussion

of spread spectrum systems and RAKE receivers as these systems attempt to recombine energy lost in multiple propagation environments. In this case the "object" to be tracked is the channel itself so that an optimum recombination can be performed. The relationship to the work in the thesis is that multiple paths are tracked for recombination. In multipath recombination, the paths appear as discrete points separated in delay. In applications such as feature tracking in image processing, entire continuous curves which appear in a video stream are tracked. This has applications in robotic lip reading, or tracking a person moving through a crowd: a security application. Finally, another large area of interest in tracking is track association and multiple target tracking where the problem is to maintain tracks of multiple independent objects. All of these areas are related to the thesis through tracking theory (Kalman filtering). This section points out the similarities and more importantly the differences between the existing body of work and the work in this thesis.

In this thesis, the problem of recursively estimating the parameters of a physical system through the use of probing signals is investigated. In proposing an algorithm using a Kalman filtering approach, many areas of current research in the realm of wideband signal processing [19-24] are applicable. Estimation as related to narrowband spreading functions has received extensive coverage in the literature [16,43]. These narrowband spreading function characterizations have been used for the characterization of time-varying propagation and scattering channels. Also, narrowband source localization and characterization has received considerable attention.

Characterization of these channels using wideband signals and concepts of wideband spreading functions has received recent attention [24-27]. However, in order to understand the underlying principles of wideband spreading, one must also investigate the properties of the wideband ambiguity functions of the transmitted signal [28-32].

The main problem in this thesis is to make recursive estimates of the properties of a physical system (i.e., position and velocity) called the state variables. One time estimation of physical parameters has been investigated using linear inverse techniques [33]. The problem of identifying and localizing an object in a changing environment using wideband inverse techniques, has also been thoroughly investigated [24]. The open problem of tracking changes in peak location within the measurement of the wideband spreading function, and relating these to the kinematics of an object using a model based approach is investigated in this thesis. In the area of model based signal processing the idea has been to include models within the signal processor to optimize system performance. The work of Candy [88,89] has been to use a model (environmental) based approach for detection and localization of acoustical sources. The work in the thesis differs in that the models used for tracking appear in the state transition matrix of the tracker. These models are of the kinematics of the object which is undergoing rotation, translation, or both.

This formulation of the wideband spreading function estimate is based on wavelet transform techniques which have received extensive recent attention [34-40]. In the case under investigation, a measurement is taken by using a wideband matched filter [4] which

produces a range-scale map which indicates the "position" of the object in time-delay and time-scale. These channel scattering function representations are exploited by spread spectrum communications for recombining the energy arriving at an antenna via multiple propagation paths.

In spread spectrum communications systems, a RAKE receiver structure has been used to recombine spread spectrum signals that propagate through slowly fluctuating channels [76]. In these systems, the arrivals of signals at an antenna are only (in most practical applications) separated in time delay (i.e., different propagation paths having different lengths produce multiple arrivals of a transmitted signal). The techniques proposed in this thesis can be used to extend this work by making the processes recursive/adaptive in nature for two dimensions. This has application in acoustical systems where time-scale can become appreciable [76].

The closest areas of research to which this work can be compared is in the two areas of contour and feature tracking in image processing and in multiple target tracking and track data association.

First in the area of image feature tracking, Blake [77] provides an analog in the sense that two dimensional (2D) image features are tracked as they move in an image using a model of the motion. This is a tracking algorithm which predicts how features within an image will appear in successive images based on a model which is used to predict the motion [78-81]. Conditional density tracking uses learned dynamical models, together

with visual observations, to propagate a random set over time. The results of this work have been applied to trackers for non rigid motion such as lip motion tracking for speech recognition. This work differs, however, from the work in the thesis in that intensity values are used to make up the feature rather than coherent maps. Also, the work in the thesis relates the transmitted signal parameters to measurement errors and ties these to tracker performance. The measurement errors are less clearly defined in the image tracking case and vary from case to case. Researchers at Carneige-Mellon [82, 83] have used a map correlation technique to track landmark features for mobile autonomous robot navigation/vision systems. Here a normalized correlation technique has been used to correlate masks of features with masks extracted from robot images, the features are "tracked" based on a maximized correlator output. Image feature tracking, however, does not depend on transmitted signals and detector outputs. Visibility of a feature in an image is analgous to detection, the difference lies in the fact that, in this thesis, one of the main points is to relate transmitted signal parameters to tracking performance. A related area of research where the transmitted signal parameters do matter is in radar tracking/track association.

In the area of radar tracking, track association, and data association for multiple target tracking, much work has been done [85-90]. Data/track association are concepts which have been used to group measurements with the appropriate track. In the case of multiple sensors, the data association is done to group the measurements from various sensors with the appropriate target. Work has been done to incorporate certain target characteristics into the tracking to improve the data association [91]. All of this work,

however, uses a separate tracker for each object to be tracked, therefore providing an innovations sequence (in the case of Kalman filtering) for each target. In this thesis, a single object, which has multiple highlights is tracked. The highlight motion is predicted according to a state transition which updates the position of each highlight according to a kinematic motion under the assumption of rigid body motion. This method provides a single innovations sequence which gives a measure of tracker performance. This is significantly different than using multiple trackers to track multiple objects and updating each separately.

Having reviewed the related research, the next subject is to determine the work to be done and its relationship to the existing body of related research. In this thesis, an algorithms for tracking the peak values and peak locations within a wideband spreading function are derived. This extends the work in the area of spreading function representations by giving a recursive spreading function estimation algorithm. It will be shown that a model based recursive algorithm for tracking the kinematic properties of multiple highlights on a body can be derived and implemented for several models. This extends work in image feature tracking (as points on a feature can be treated as multiple highlights). Also, work in track association can be extended by not only tracking the overall object trajectory, but by implementing (for high resolution radar) a "sub-tracker" which tracks the body's highlight structure. The outputs from this filter can be inputs (in the form of range profiles) tol multiple target tracking algorithms [85,87]. The following section provides an outline of the thesis.

1.6 Thesis Overview

This thesis is divided into six chapters including the introduction. The next chapter contains an overview of the theory necessary for completion of the work in the rest of the thesis. This overview begins with a background on Kalman filtering and its applications. The discussion then proceeds to cover the background necessary for understanding wideband systems, signals, and scattering phenomena. Since a major application of the work in the thesis is to improve the performance of the WTD EC, the background required to understand and extend the EC will be covered.

Chapter 3 is devoted to wideband signal analysis in the context of deriving the Cramer Rao lower bound on variances of estimation errors for time-delay and time-scale for wideband signals. Here, the derivation relates the lower bound on estimation error variances to the signal shape and signal parameters. This is important as these quantities will surface in the derivation of the Kalman filter in the next chapter.

Chapter 4 contains the area most important in the thesis. Here, the WTD Kalman filter scattering function predictor/corrector is derived and analyzed. The parameters of the wavelet transform domain Kalman filter (WTDKF) are investigated in detail and related to the overall performance. These parameters are related to those derived in Chapter 2 (the CRLB) and to transmitted signal parameter.

In chapter 5, two examples are presented which highlight the theoretical results derived in the previous chapters. The first example is of two spheres rotating about a central point. The Kalman filter attempts to track the angle one of the spheres makes with the perpendicular to the line of sight, and the normal velocity of the sphere as it moves through an arc. The second example is a highlight moving in a straight line, and the filter attempts to track the normal velocity and the time-delay to the scatterer. This chapter present results which tie together the signal duration and bandwidth, the Cramer-Rao lower bound, and the convergence of the Kalman filter.

Chapter 6 contains the conclusions which may be derived from the work contained in the thesis. Here, suggestions for further research are also presented.

Chapter 2

BACKGROUND

2.1 Introduction

The purpose of this chapter is to provide the necessary background and introduction to topics that are fundamental to the development later in the thesis. This chapter will provide an entry point at which to define notation used throughout the thesis. Finally, this chapter provides a discussion of previous research fundamental to the development of the work developed in later chapters.

Section 2.2 provides an introduction to the fundamental concepts of the wavelet transform. As the formulation of the Kalman filter is in the wavelet transform domain, this background will provide the necessary framework to understanding the concepts of spreading and scattering functions in the wavelet transform domain (WTD).

Section 2.3 is devoted to the concepts of the WTS wideband spreading function and the second moment of the spreading function, the real non-negative scattering function.

Section 2.4 contains a review of the WTD estimator-correlator (EC). This is included as the recursive scattering function updating algorithm was motivated by the

search for an optimal recursive algorithm for updating the spreading function estimate in the WTD EC.

Section 2.5 contains a review of the Kalman filter, extended Kalman filter (KF) and the KF recursive estimation algorithm.

2.1 Wavelet Transform Analysis

This section is to introduces the fundamental concepts in wavelet analysis in the context of signal analysis. It is intended as an overview of the concepts of time-frequency and time/time-scale analysis and signal resolution properties. In this section some of the assumptions common to wavelet analysis which will impact later discussions are reviewed.

2.1.1 Time-Frequency Analysis

The concept fundamental to the science of signal processing for much of the last century has been the Fourier transform. It has been the basis for many texts [42]. Basically stated, the Fourier transform (FT) is a correlation function. The FT correlates a time signal with a complex sinusoid at the desired frequency (2.1).

$$X(\omega) = F\{x(t)\} = \left\langle x(t), e^{-j\omega t} \right\rangle = \int_{-\infty}^{\infty} x(t) e^{-j\omega t}\, dt \qquad (2.1)$$

where <•,•> represents an inner product on the space of square-integrable functions, $L^2(R)$. The simultaneous measurements of time and frequency are incompatible since frequency cannot be measured instantaneously. Therefore, (2.1) represents the average frequency content over the length of the signal, and gives us no information about when precisely the frequency occurred [35].

To extend the usefulness of the Fourier transform, it can be extended by looking at a windowed portion of the signal and applying a possibly complex window g(t) time-limited to[-T<t<0] to the signal and then take the Fourier transform. Therefore, the windowed signal contains only the information in x(t) on the interval [t-T,t]. Taking the Fourier transform of the combined window-signal gives the windowed Fourier Transform (WFT).

$$X(f,\tau) = \left\langle x_w(t), e^{-j\omega t} \right\rangle = \int_{-\infty}^{\infty} x(t) g(t-\tau) e^{-j\omega t}\, dt \qquad (2.2)$$

X contains both time and frequency information. X contains information about the frequency content of x(t) near t-τ. The tradeoff here is that the shape, length, and dimensionality of the window determines the relative frequency and time resolution properties of the WFT. This is known as the uncertainty principle [35,42].

2.1.2 Time-Scale Analysis

Time-Scale analysis is often associated with the continuous wavelet transform (CWT). In the CWT a time compression or dilation operation is integral to the process. The amount of compression or dilation is referred to as time-scale. The CWT is a generalization of the WFT in the sense that the desired signal is correlated with a set of "wavelets". The CWT of a signal x(t) with respect to a mother wavelet $\psi(t)$ is [36]

$$X(s,\tau) = W_{\psi} x(s,\tau) \equiv \left\langle x, \psi_{s,\tau} \right\rangle = \frac{1}{\sqrt{s}} \int_{-\infty}^{\infty} x(t)\, \psi^{*}\left(\frac{t-\tau}{s}\right) dt \qquad (2.3)$$

One can see that the window in the WFT has been replaced by the mother wavelet ψ. The mother wavelet must satisfy the admissibility condition [36]. Figure 2.1 is provided to visualize the time scale operation.

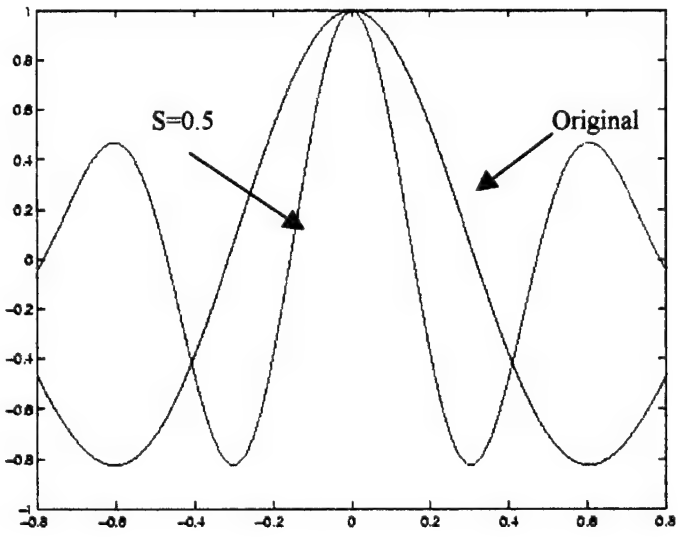

Figure 2.1: Morlet Mother Wavelet With Original and Compressed (s=0.5) Versions

Here the relative delay has been set to zero for simplicity. Since the compression of the mother wavelet contains more cycles per unit time, it measures higher frequency content in the correlation process. Dilation of the mother wavelet measures lower frequency content since fewer cycles are in the same time interval.

Secondly, an important concept in wavelet analysis is the reconstruction of the original signal also known as the inverse wavelet transform (IWT). First, however, a few conditions must be satisfied.

If the original signal is to be reconstructed, as said before the mother wavelet must satisfy the admissibility condition [36]

$$c_\psi = 2\pi \int_{-\infty}^{\infty} \frac{|\psi(\omega)|^2}{|\omega|} d\omega < \infty \tag{2.4}$$

which implies that the mother wavelet must have zero average value, that it is an oscillatory and bandpass function.

If the above condition is satisfied, the reconstruction formula (IWT) is given by [36]

$$x(t) = \frac{1}{c_\psi} \iint W_\psi x(s,\tau) \psi_{s,\tau}(t) \frac{ds\, dt}{s^2} \tag{2.5}$$

2.2.2 Wavelet Transform Domain Spreading/Scattering Functions

In this section, the concepts of WTD spreading functions and the second moment of the spreading function, the scattering function are introduced. The spreading function will be a function of both time-scale , s, and time-delay ,τ. The spreading function is a set of complex random variables which indicate how the transmitted signal "spreads" [43,44] in scale and delay. The total scattering function is a group theoretic convolution of the scattering caused by individual scattering mechanisms[8,45,46].

The purpose of this section is to introduce, qualitatively, the physical phenomena of spreading functions and their relationship to the quantitative estimates made on them using the wavelet transform.

In a typical detection problem, a probing signal is transmitted into a medium and reflected by motionless as well as moving objects in the medium. These reflections are received at some receiver(s) and processed. In a complicated environment such as the ocean and atmosphere, the medium itself can cause spread in delay and Doppler. This effect is referred to as multipath. To illustrate the phenomena, an example of a reflecting object in a multipath medium is given. If a high time-bandwith signal (see Chapter 3) is used, the individual reflectors on the target can be resolved. Therefore, each reflecting feature causes an individual return to be "seen" at the receiver. This reflector is referred to as a multi-highlight reflector.

The return from the target can be further complicated if the medium contains a multipath. Figure 2.2 shows the geometry for a multi-highlight object in a multipath environment.

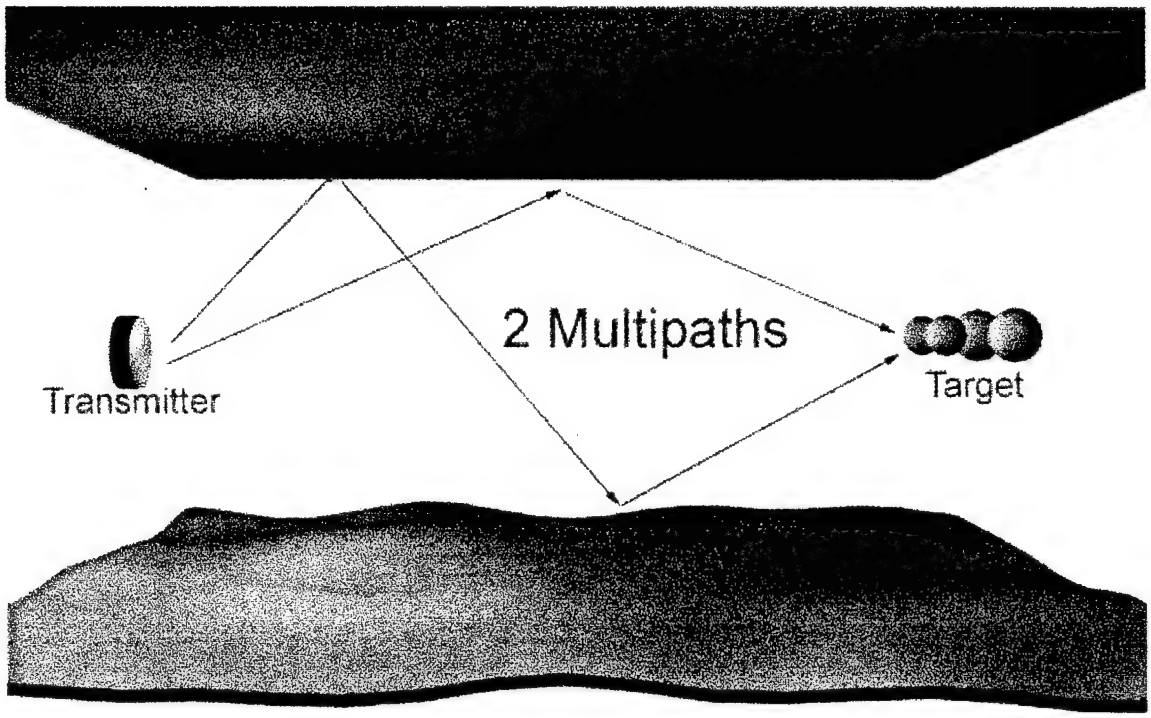

Figure 2.2: Transmitted Signal Scatters Over Two Paths

Figure 2.2 shows that in this example, the transmitted signal reaches the target over two separate paths. The difference in length of these two paths causes the signal to arrive at the target at different times. Upon reaching the target, the signal is further scattered by reflecting from each highlight on the target as seen in Figure 2.3.

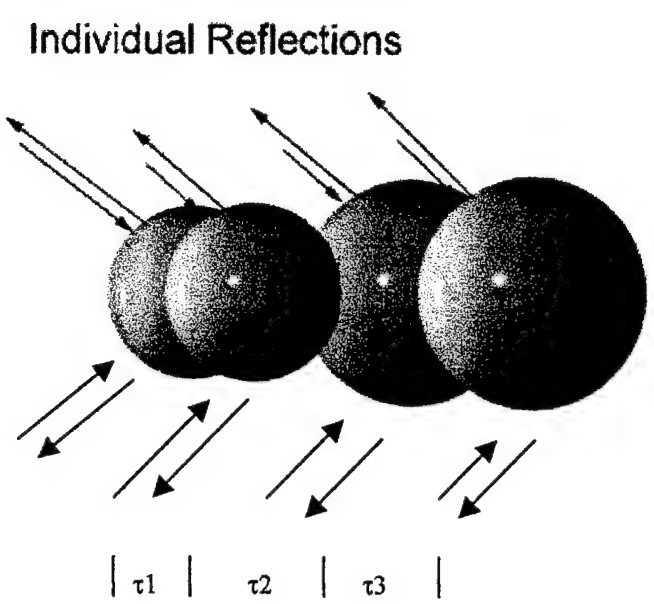

Figure 2.3: Target Scatter for a Multi-Highlight Target

Now, mathematical representations of the above physical phenomena are given. First, a model of the echo received at the receiver in Figure 2.2 must be introduced. This has been discussed widely in the literature [26, 33, 47]. The modeled echo is in the form of an inverse wavelet transform

$$r(t) = \int w(x)[U(x)f(t)]d\mu(x) + n(t) \tag{2.6}$$

where w(x) is either the narrowband or wideband spreading function, dμ(x) is the left invariant Haar measure on either the Heisenberg (narrowband) or Affine (wideband) group G, U(x) is a unitary representation of the corresponding group, f(t) is the transmitted signal, and the vector x represents either (τ,ϕ) or (τ,β) where τ is time delay, ϕ is Doppler shift, and β is time scale. [U(x)f(t)] is given by the following

$$\begin{aligned} [U(x)f(t)] &= z f(t-\tau)\, e^{j\phi(t-\tau)} \qquad \textit{narrowband} \\ [U(x)f(t)] &= \frac{1}{\sqrt{\beta}} f\left(\frac{t-\tau}{\beta}\right) \qquad \textit{wideband} \end{aligned} \tag{2.7}$$

Now, in order to obtain an estimate of the spreading function, the wavelet transform of (2.1) is taken using the transmitted signal as the mother wavelet, this gives

$$\begin{aligned} \int r(t)[U(x)f(t)]^* dt = \int\int w(x')[U(x)f(t)][U(x')f(t)]^* d\mu(x')dt \\ + \int\int n(t)[U(x')f(t)]^* d\mu(x')dt \end{aligned} \tag{2.8}$$

Rewriting (2.3)

$$\hat{w}(x) = \int\int w(x')K(x,x')d\mu(x')dt \tag{2.9}$$

where K is the auto-ambiguity function of the transmitted signal.

Equation (2.4) shows that the estimate of the spreading function is in the form of a convolution of the true spreading function with the auto-ambiguity function of the transmitted signal. If the spreading function is within the range space of the wavelet transform, then K is a reproducing kernel for the spreading function. This shows that the properties of the transmitted signal have an effect on estimates of the spreading function.

An estimate of the spreading function (as calculated using (2.9)) of the object shown is Figure 2.3 is given as the wavelet transform of the received data under the condition of no noise and that the reflections are mutually independent. If the wavelet transform of a return from the object in Figure 2.3 is taken four highlights spread in delay and each falling on a time-scale of 1 are expected. Figure 2.4 shows the theoretical wavelet transform of the return from the object with the transmitted signal as the mother wavelet.

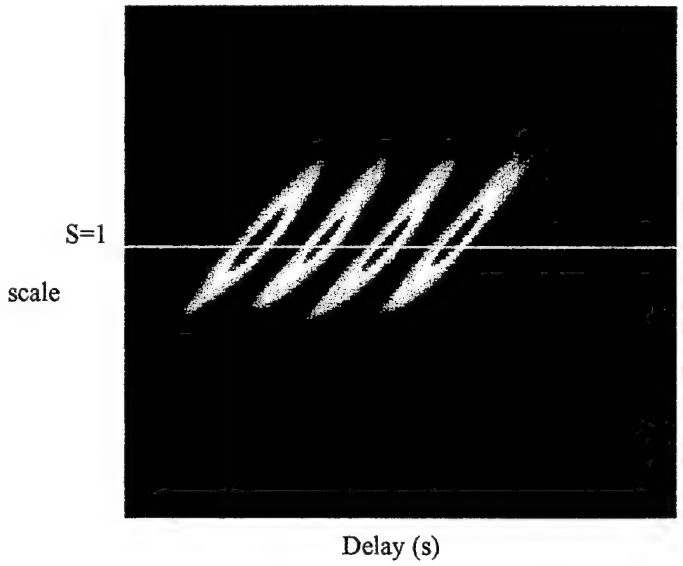

Figure 2.4: Object Spreading Function Estimate

For this illustrative example, four copies of the original signal's auto-ambiguity function, spread in delay, and lined up on a scale of 1 are obtained. Now, to get the total wideband spreading function, a group theoretic convolution of the target spreading function with the channel (multipath) spreading function must be performed. Completing the group theoretic convolution for this example, assuming a

channel scatter as seen in Figure 2.5, the overall spreading function estimate in Figure 2.6 is calculated.

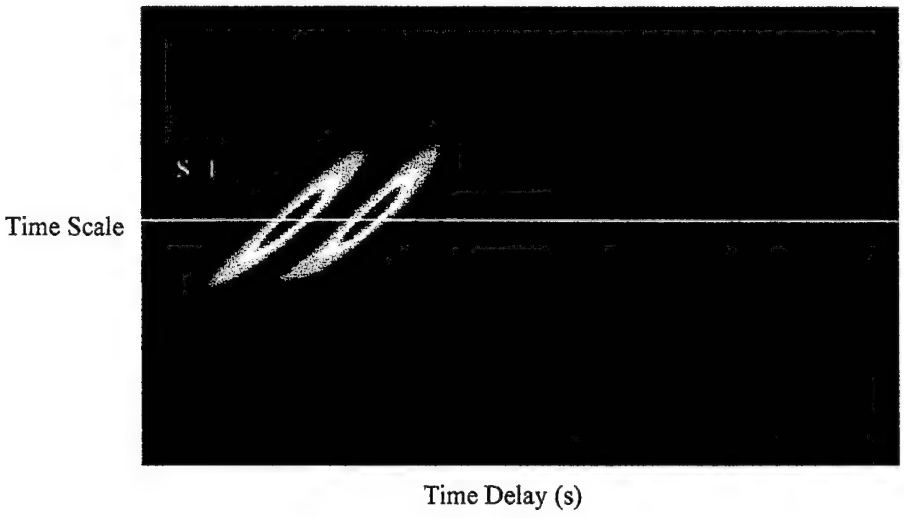

Figure 2.5: Channel Spreading Function Estimate

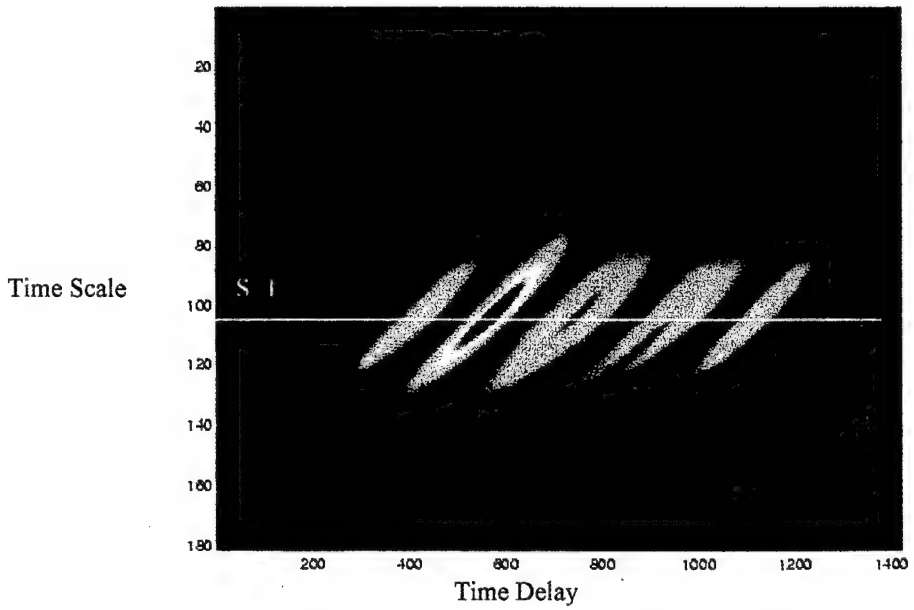

Figure 2.6: Overall Spreading Function Estimate for a 4 Highlight, 2 Multipath, Example.

As seen in figure 2.6, fading due to interactions between the highlights cause the result that all of the peaks are not at the same level. If there were no fading interactions, eight distinct peaks would be present. Through the use of high time-bandwidth (TW) product signals, this fading effect can be lessened, as the individual peaks are sharper hand have smaller main-lobe areas [30].

2.2 Estimator-Correlator Review

In this section, a brief review of the WTD estimator-correlator (EC) [6,7,48,49] is provided. Although the thesis is not about the EC, the motivation behind the Kalman filter scattering function updating algorithm lies within the domain of the EC. A major application of the work in the thesis is the WTD EC, and the WTD EC will be used in a few of the examples pertaining to performance analysis of the KF.

In an active system, a known signal, f(t) is transmitted into a channel. It is reflected and received back at the transducer as r(t) with

$$r(t) = y(t) + n(t) \tag{2.10}$$

Here, y(t) is the "total signal" containing all of the multipath and multihighlight components of the echo, and n(t) is colored non-stationary Gaussian reverberation. It is assumed that the "total signal" y(t) is again given by (2.7)[47]. Where w(x) is either the narrowband or wideband spreading function, $d\mu(x)$ is the left invariant Haar

measure on either the Heisenberg (narrowband) or Affine (wideband) group G, U(x) is a unitary representation of the corresponding group, f(t) is the transmitted signal, and the vector x represents either (τ,ϕ) or (τ,β) where τ is time delay, ϕ is Doppler shift, and β is time scale. [U(x)f(t)] is again given by the following

$$[U(x)f(t)] = f(t-\tau)\,e^{j\phi(t-\tau)} \qquad \textit{narrowband}$$
$$[U(x)f(t)] = \frac{1}{\sqrt{\beta}} f\left(\frac{t-\tau}{\beta}\right) \qquad \textit{wideband} \tag{2.11}$$

Equation (2) is a weighted integral of all delayed and time-scaled replicas of the transmitted signal with the spreading function being the weight. This weighted integral can be used to model both continuously time-frequency/time-scaled spread signals or discretely distributed multipaths and highlights. The total signal model given by (2.6) can be derived from the physics of propagation and scattering from distributed targets. The delay-Doppler spreading function model has been widely used in radar astronomy, sonar, and multipath communication [76, 77]. Of primary interest in this work is detection and characterization of scattering objects that have a rich and stochastic highlight structure. It is also significant that (2.7) is in the form of an inverse time-frequency/time-scale transform. This suggests that a natural implementation of wideband EC is the CWTD implementation. Next, the derivation of the CWTD EC is reviewed.

The EC computes the detection statistic *l* using

$$l = \langle \hat{y}, r \rangle_{R_o} \tag{2.12}$$

where $\hat{y}$ is the CME of y and $<\bullet,\bullet>_{R_0}$ denotes inner product on the reproducing kernel Hilbert space (RKHS) whose non-stationary noise covariance function $R_0(t,\tau)$ is the reproducing kernel for that Hilbert space.

In the Gaussian case, CME estimates of y(t) can be obtained from the orthogonality principle [47]

$$< y - \hat{y}, r >_H = 0 \tag{2.13}$$

where $<\bullet,\bullet>_H$ denotes an inner product defined by

$$< x, y >_H = E[\int x(t) y^*(t)\, dt] \tag{2.14}$$

For the multipath model of (2.1)

$$< y, r >_H = c_f \iint_{GG'} S(x,x') K(x,x') d\mu(x') d\mu(x) \tag{2.15}$$

where

$$K(x,x') = c_f \langle U(x)f, U(x')f \rangle_H \tag{2.16}$$

is the reproducing kernel for the space spanned by <g,U(x′)f> where c_f is the admissibility constant defined by (2.4).

Equation (2.12) contains S(x,x') the inhomogeneous scattering function defined by

$$S(x,x') = E\{w(x)w^*(x')\} \tag{2.17}$$

The orthogonality condition (2.10) itself is satisfied if

$$\hat{y}(t) = \int_G \int_{G'} S(x,x')\left(\iint r(z)Q_1(v,z)\,\left[U(x')f(v)\right]^*\right) dv\,dz\left[U(x)f(t)\right]d\mu(x')d\mu(x) \tag{2.18}$$

where $Q_1(v,z)$ is the inverse covariance kernel for the detection hypothesis H_1. That is

$$\int Q_1(v,z)R_1(z,t)dz = \delta(v-t) \tag{2.19}$$

and

$$R_1(z,t) = E[r(z)r^*(t)] \tag{2.20}$$

2.3.1 EC – Continuous & Discrete Representations

In this thesis, both the discrete and continuous representations of the EC are used equivalently. In this section, the relationship between the two forms of the EC detection statistic are reviewed.

It has been shown that from the log likelihood function the detection statistic in the form of (2.12) is obtained and that the signal estimate is an integral equation (2.6). By vectorizing the received data **r**, signal **s**, and noise **n** from equation (2.10) an equivalent discrete form of the EC can be formed as follows:

Consider discrete data,

$$\begin{aligned} r &= y + n \qquad (H_1) \\ r &= n \qquad (H_0) \end{aligned} \tag{2.21}$$

Where **y** is the signal vector containing all multipath and multihighlight components and **n** is the noise vector.

The data covariance is given by

$$E\{rr^H\} = \begin{Bmatrix} R_1 = R_{yy} + R_{nn} \\ R_0 = R_{nn} \end{Bmatrix} \tag{2.22}$$

Assuming Gaussian signals and noise, the detection statistic is proportional to $\exp(-r^H R_1^{-1} r)$ under H_1 and $\exp(-r^H R_0^{-1} r)$ under H_0. Therefore, the detection statistic is given by

$$l = r^H (R_0^{-1} - R_1^{-1}) r \tag{2.23}$$

This can be written as

$$\begin{aligned} l &= r^H R_1^{-1} (R_1 - R_0) R_0^{-1} r \\ &= ((R_1 - R_0) R_1^{-1} r)^H R_0^{-1} r \\ &= \hat{y}^H R_0^{-1} r \end{aligned} \tag{2.24}$$

Where $\hat{\mathbf{y}}$ is the conditional mean total signal estimate. This estimate is correlated with the optimally filtered data vector $R_0^{-1}r$.

The matrix difference (R_1-R_0) is equivalent to the signal covariance R_{yy}. Since the signal and interference are uncorrelated, $R_{yy}=E\{yr^H\}=R_{sy}$ and $R_1=E\{rr^H\}$ and the optimal signal estimate can be written as

$$\begin{aligned}\hat{y} &= R_{yr}R_{rr}^{-1}r \\ &= R_{yy}R_{rr}^{-1}r\end{aligned} \tag{2.25}$$

Now to get back to the continuous representation, define the expansion

$$x(t) = \bar{x}^t \bar{\varepsilon}(t) \tag{2.26}$$

For a scalar process x(t), $\bar{x}$ is a random vector and $\bar{\varepsilon}$ is a deterministic vector of orthonormal functions that make up a complete orthonormal set. The inverse relationship is given by

$$\bar{x} = \int x(t)\,\bar{\varepsilon}^*(t)\,dt \tag{2.27}$$

Orthonormality gives

$$\int_{-\infty}^{\infty} \varepsilon(u)\varepsilon^{H}(u)\,du = \int_{-\infty}^{\infty} \varepsilon\ (u)\varepsilon^{*}(u)\,du = I \tag{2.28}$$

Where I is the identity matrix. The scalar representation of the signal vector is therefore

$$\begin{aligned} \hat{y}(t) &= \hat{\bar{y}}(t)\varepsilon(t) \\ &= \varepsilon^{t}(t)R_{yy}R_{rr}^{-1}r \end{aligned} \tag{2.29}$$

By orthonormality,

$$R_{rr}^{-1} = \int_{-\infty}^{\infty} \varepsilon(v)\varepsilon^{H}(v)R_{rr}^{-1}dv \tag{2.30}$$

where

$$r = \int_{-\infty}^{\infty} r(z)\varepsilon^{*}(z)dz \tag{2.31}$$

Combining (2.29), (2.30) and (2.31) gives

$$\hat{y}(t) = \iint (\varepsilon^{t}(t)R_{yy}\varepsilon^{*}(v))(\varepsilon^{t}(v)R_{rr}^{-1}\varepsilon^{*}(z))r(z)dxdv \tag{2.32}$$

2.3.2 EC – WTD Implementation

The WTD implementation of the EC follows if the Frobenius-Shur-Godement theorem [36] is used to compute the inner product (2.12). Equation (2.12) can also be written in the form [7]

$$l = \int \hat{y}(t)\left(\int Q_0(t,z)\, r(z)\, dz\right)^* dt \tag{2.33}$$

where Q_0 is the inverse covariance kernel for the detection hypothesis H_0 (noise only) and

$$r_0(t) = \int Q_0(t,z)\, r(z)\, dz \tag{2.34}$$

similarly

$$r_1(t) = \int Q_1(t,z)\, r(z)\, dz \tag{2.35}$$

Thus, the detection statistic can be written as

$$l = \int \hat{y}(t)\, r_0^{\,*}(t)\, dt \tag{2.36}$$

Then, according the FSG theorem,

$$c_f \left\langle \hat{y}, r_0 \right\rangle = \int \left\langle \hat{y}, \left[U(x) f\right] \right\rangle \left\langle r_0, \left[U(x) f\right] \right\rangle^* d\mu(x) \quad (2.37)$$

by using equations (2.34), (2.35) and (2.37), (2.36) becomes

$$l = c_f \int_G \left(\int_{G'} S(x, x')\, W_f^1 r(x') d\mu(x') \right) \left(W_f^0 r(x) \right)^* d\mu(x) \quad (2.38)$$

where

$$\begin{aligned} W_f^1\, r(x) &= \iint r(z) Q_1(v, z) \left[U(x) f(v)\right]^* dv \\ &= \int r_1(v) \left[U(x) f(v)\right]^* dv \end{aligned} \quad (2.39)$$

and

$$\begin{aligned} W_f^0\, r(x) &= \iint r(z) Q_0(v, z) \left[U(x) f(v)\right]^* dv \\ &= \int r_0(v) \left[U(x) f(v)\right]^* dv \end{aligned} \quad (2.40)$$

For the wideband case, equations (2.39) and (2.40) are the weighted wavelet transforms of r(t) under the appropriate hypothesis (corresponding to Q_0 and Q_1). The final result is

$$\boxed{l = \int_G \hat{w}(x)\left(W_f^0 r(x)\right)^* d\mu(x)} \tag{2.41}$$

with admissibility constant [36]

$$c_f = \int_{-\infty}^{\infty} \frac{|f(\omega)|^2}{|\omega|} d\omega \tag{2.42}$$

the mean square estimate of the spreading function w(x) given by

$$\boxed{\hat{w}(x) = \int_G S(x, x')\, W_f^1 r(x')\, d\mu(x')} \tag{2.43}$$

This estimate of the spreading function is important for target characterization. Equations (41) and (43) describe the wavelet transform domain implementation of the EC. The processing, shown in Figure 1 is straight forward. The first step is to optimally filter [3] the data under the H_0 and H_1 hypothesis. Then, using the

transmitted signal replica as the mother wavelet, correlate the wavelet transform of the filter outputs. This generates generalized range/scale maps, of which the H_1 filtered map is convolved with the generalized scattering function (a priori – from models). The output of this operation is then correlated with the H_0 filtered map. For wide-sense stationary uncorrelated scattering (WSSUS) the correlation is coherent energy summation. However, if the WSSUS assumption is not made, and the generalized scattering function S(x,x') contains highlight correlation information, coherent highlight integration may be possible.

2.4 Kalman Filtering – A Brief Review

In this section, the concepts involved in the development of the Kalman filter are investigated. The topic is approached from the standpoint of model based signal processing. The purpose of this section is to provide the necessary background and references for the more complete derivation of the recursive scattering function estimator developed later in Chapter 4.

The problem that the Kalman filter has been developed to solve is to reconstruct estimates of a state, say x(t), from a set of noisy measurements y(t) [51]. There are many forms of the Kalman filter [52-54], the predictor-corrector form [51] of the filter will be the focus. This allows a model-based approach to the signal processing. The major features of the Kalman filter are presented in the next section.

2.4.1 The Kalman Filter Predictor-Corrector Algorithm

The Kalman filter algorithm requires the use of several quantities that will be reviewed throughout this section. Referring to the algorithm in Figure 2.7, individual steps of the algorithm can be followed. First, at time t, the previously filtered estimate x(t-1|t-1) and error covariance P(t-1|t-1) exist. The goal is to make the best estimate of the current state based on the previous estimates (t-1 samples). This is the prediction phase of the algorithm. Using the state-space model, the state estimate x(t|t-1) and the error covariance P(t-1|t-1) are predicted. Once the prediction phase is completed, the innovations covariance R_e and the Kalman gain K(t) are calculated. When a measurement y(t) is available, the innovations, or new information [11,51,55] is determined. The old state estimate x(t-1|t-1) is used to form the new, or corrected, state x(t|t), and covariance P(t,t). The error, or innovation, is the difference between the measurement y(t|t-1) and the prediction. The innovation is weighted by the Kalman gain to correct the old state estimate x(t|t-1). The error covariance is similarity corrected. Then, the algorithm is cycled at time t+1. Figure 2.7 depicts the entire algorithm [51].

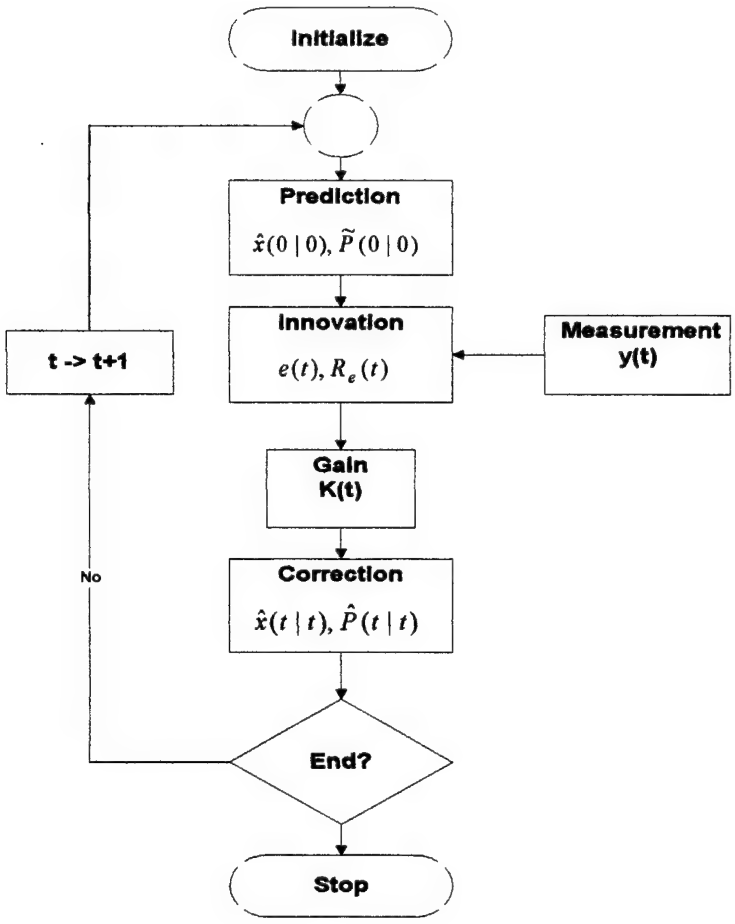

Figure 2.7 Kalman Filtering Algorithm

Candy [51] provides an example of the algorithm through two time steps which provides insight into the operation of the filter and the calculation of the individual quantities. The example is reproduced here..

Example 4.1 This example illustrates the calculations performed in the algorithm in the above section given initial estimates. The calculations are carried out for times t=1 and t=2. State noise in this example is zero.

$t = 1$ Start Time

$\hat{x}(1\mid 0) = A(0)\hat{x}(0,0)$	Estimate x(1|0) using state transition A
$\widetilde{P}(1\mid 0) = A(0)\widetilde{P}(0\mid 0)A'(0)$	Estimate error covariance P using state transition A
$R_e(1) = C(1)\widetilde{P}(1\mid 0)C'(1) + R_v(1)$	Calculate Innovations Covariance at t=1 Using Measurement Matrix C
$K(1) = \widetilde{P}(1\mid 0)C'(1)R_e^{-1}(1)$	Calculate Kalman Gain K at t=1
$e(1) = y(1) - C(1)\hat{x}(1\mid 0)$	Use Measurement y at t=1 to calculate innovations e
$\hat{x}(1\mid 1) = \hat{x}(1\mid 0) + K(1\_e(1)$	Calculate Updated State Estimate at t=2
$\widetilde{P}(1\mid 1) = [I - K(1)C(1)]\widetilde{P}(1\mid 0)$	Calculate Error Covariance Estimate at t=2

$t = 2$ Increment Time

$\hat{x}(2\mid 1) = A(1)\hat{x}(1,1)$	Estimate x(2|1) using state transition A
$\widetilde{P}(2\mid 1) = A(1)\widetilde{P}(1\mid 1)A'(1)$	Estimate error covariance P using state transition A
$R_e(2) = C(2)\widetilde{P}(2\mid 1)C'(2) + R_v(2)$	Calculate Innovations Covariance at t=2 Using Measurement Matrix C
$K(2) = \widetilde{P}(2\mid 1)C'(2)R_e^{-1}(2)$	Calculate Kalman Gain K at t=2
$e(2) = y(2) - C(2)\hat{x}(2\mid 1)$	Use Measurement y at t=2 to calculate innovations e
$\hat{x}(2\mid 2) = \hat{x}(2\mid 1) + K(2)e(2)$	Calculate Updated State Estimate at t=2
$\widetilde{P}(2\mid 2) = [I - K(2)C(2)]\widetilde{P}(2\mid 1)$	Calculate Error Covariance Estimate at t=2

This is simply a brief review of the operation of the Kalman filter. Chapter 4 provides a detailed derivation of the Kalman filtering algorithm used as well as a detailed analysis of all of the quantities involved. In this problem tracking of the

Kinematic properties of a system using probing signals as the measurements of the state will be done. The state of the system will be derived as well the measurement equation. The main focus will be on the problem of designing a signal that provides the resolution necessary for the Kalman filter to track. Also discussed is how quantities which arise within the Kalman filter derivation can be used to provide performance monitoring of the entire system.

2.5 Application of the Target Scattering Function Algorithm in the WTD EC

In this section the applicability of the Kalman filtering algorithm in an adaptive model based signal processor, namely, the WTD EC is discussed. The WTD EC uses an estimate of the wideband spreading function of the target (and channel) in the calculation of the EC detection statistic. The output of our Kalman filter will be an estimate of the target portion of the spreading function for use in the estimator branch of the EC. This is illustrated in Figure 2.8.

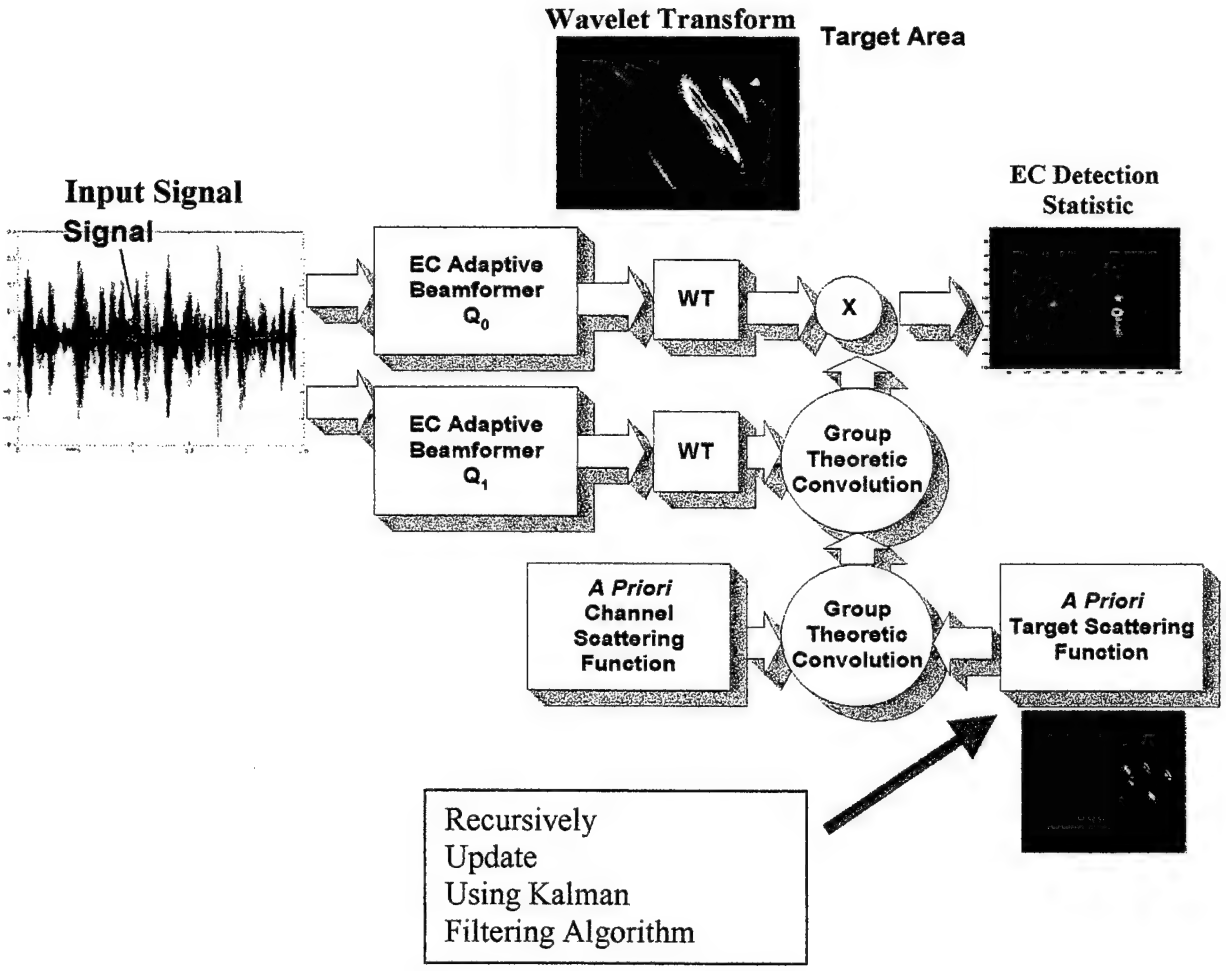

Figure 2.8: Application of Kalman Filter to WTD EC

In this case, an attempt to update the target spreading function estimate based on the kinematics of the problem would be done. The EC detector output would be maximized on a ping to ping basis, and provide performance monitoring of the overall system.

Chapter 3

ESTIMATION ERRORS – THE CRAMÉR-RAO LOWER BOUND

3.1 Introduction

In this chapter, the Cramér-Rao (C-R) bound [16,17] for the minimum variance of joint estimates on time-scale and time-delay is derived for wideband echoes that are processed with a wideband (wavelet transform) matched filter. The C-R bound on Doppler shift for narrowband signals is well known [16], but the extension to the more general case of high time-bandwidth signals and time-scale is not. The typical measure of resolution of a signal is the width at the –3dB points on a transmitted signal's auto-ambiguity function. This measure is meaningful, however, only in the absence of noise. When noise of any kind is present, the resolution of the signal is limited not only by the main lobe width (a function of time bandwidth product (TW)), but also by the signal to noise ratio. Therefore, in order to accurately speak of resolution, the C-R bound must be used, as it is a measure of the coupled effect of noise and main lobe width.

3.2 The Auto-Ambiguity Function – Resolution

Resolution is the property by which one can distinguish (in both time-scale and time-delay) between separate returns in a range-scale map. Since in this thesis, the detection

and estimation problem is under consideration, this is a good place to lay out the problem in context.

3.3 The Detection and Estimation Problem – No Noise

In this problem, a high resolution signal (large TW) is transmitted into a medium in which it is desired to resolve two independent point scatterers which are separated by a distance d (Figure 3.1) moving with normal velocities v1 and v2.

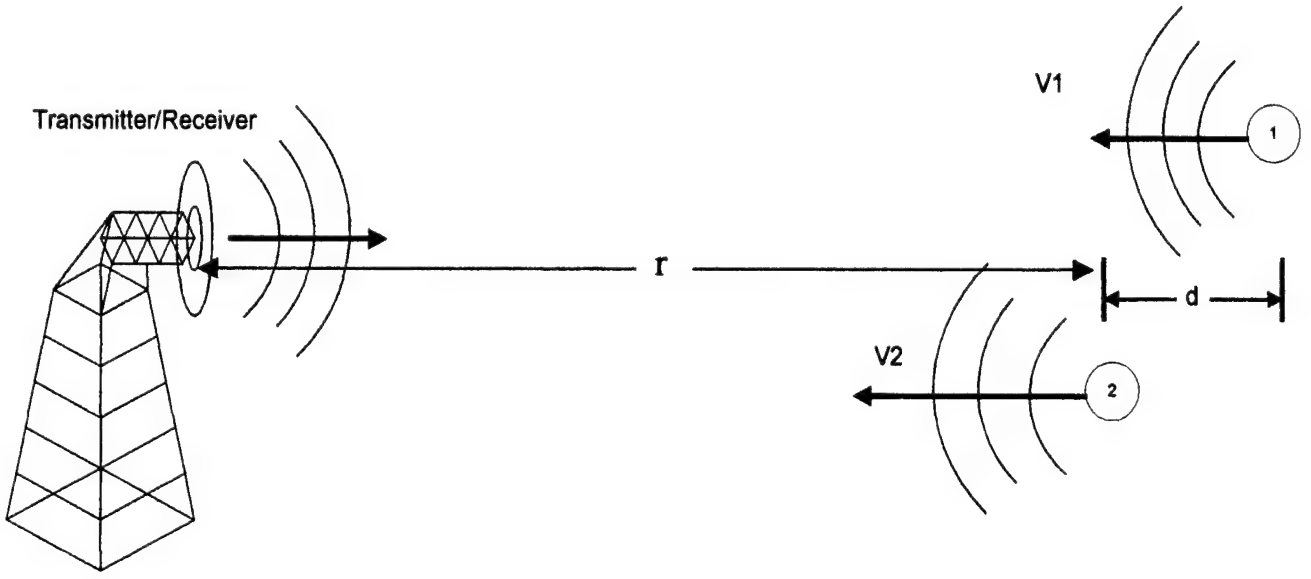

Figure 3.1: Problem Geometry

As seen in Figure 3.1, the first object is a distance r from the transmitter/receiver (Tx/Rx). Both objects are moving with normal (toward or away from the Tx/Rx) velocities v1 and v2. A high TW signal is transmitted into the medium (homogenous/infinite) and reflects

from the objects. This causes the total echo to contain two echoes each of which is time-scaled (compressed or expanded depending on the direction of the motion). Now, the data is match-filtered using the transmitted signal as the mother wavelet, a range – scale map of the echo (Figure 3.2) is produced.

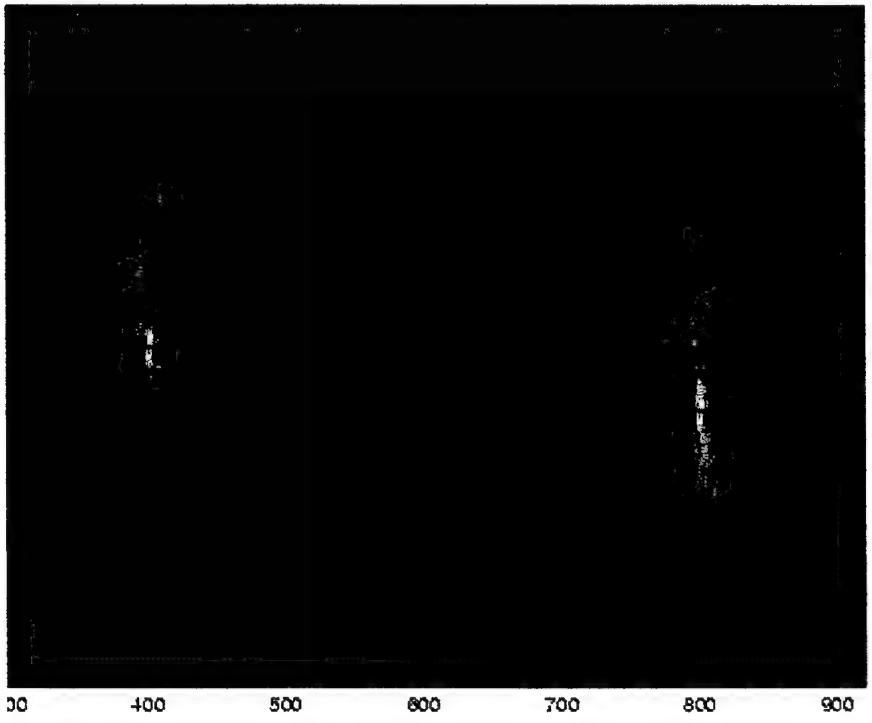

Figure 3.2: Range-Scale Map

where each of the peaks in the figure represents the delay and time-scale location of the individual scatterers. Now if the signal has less resolution and the scatterers are close together, as is seen in Figure 3.3, the location of the actual peak becomes increasingly ambiguous as the signal ambiguity function becomes less sharp.

Figure 3.3: Ambiguity Main Lobes Begin To Overlap

As seen in Figure 3.3, when the resolution is low, the ability to distinguish individual scatterers in the range-scale plane is reduced. In Figure 3.4, it is seen that two scatterers that are closer in range are indistinguishable as the ambiguity functions overlap.

Figure 3.4: Scatterers Become Indistinguishable

In summary, the higher the TW product, the smaller the main lobe area [6], thus increasing the ability to distinguish individual scatterers. The addition of noise in any form further complicates the ability to estimate the position of the scatterers in the time-scale plane.

3.4 Detection and Estimation – Additive Noise

Now the effects of adding noise of any kind to the problem are investigated. Plotting the ambiguity function for multiple delay hypothesis and for a single scale hypothesis s_0, a plot seen in Figure 3.5 is obtained.

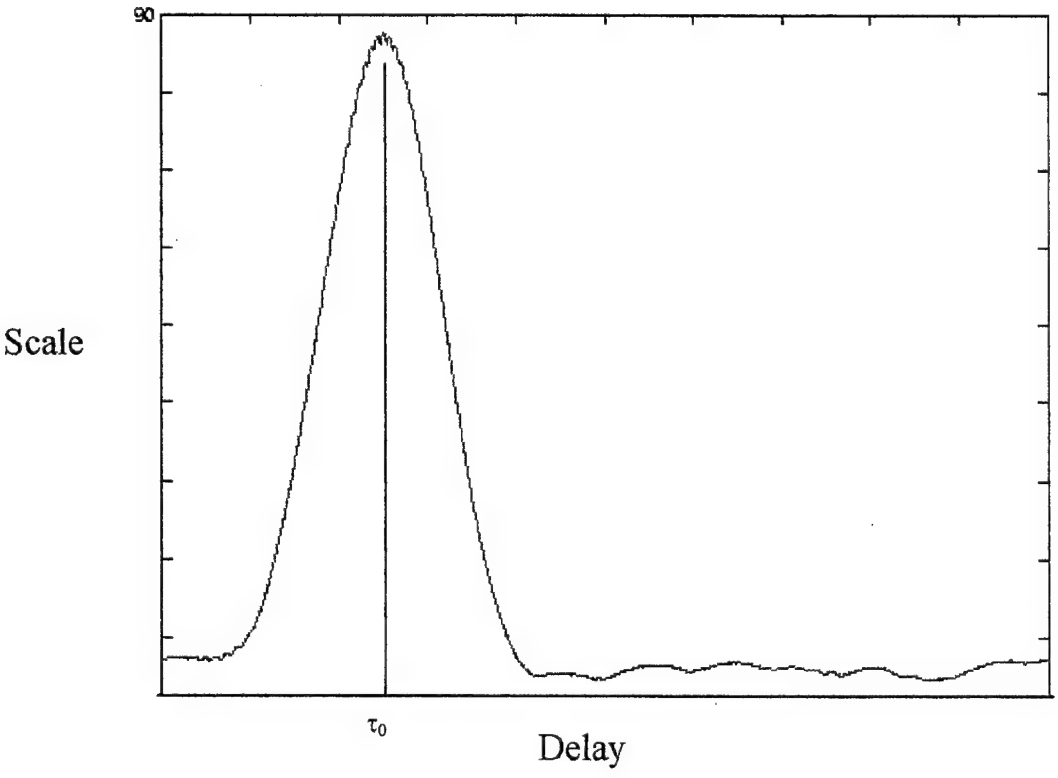

Figure 3.5: Ambiguity Function Without Noise for Scale Hypothesis s_0

Adding noise to the time-series that produced the ambiguity function has the effect that the actual delay (i.e., the delay τ_0) is much more difficult to estimate (Figure 3.6). The estimated delay in not equal to the actual peak. This effect is exaggerated at lower signal-to-noise ratios and broader ambiguity function main lobes. It is the *bound on the variance* of this estimate that is the desired quantity. This bound is called the Cramer-Rao lower bound [56].

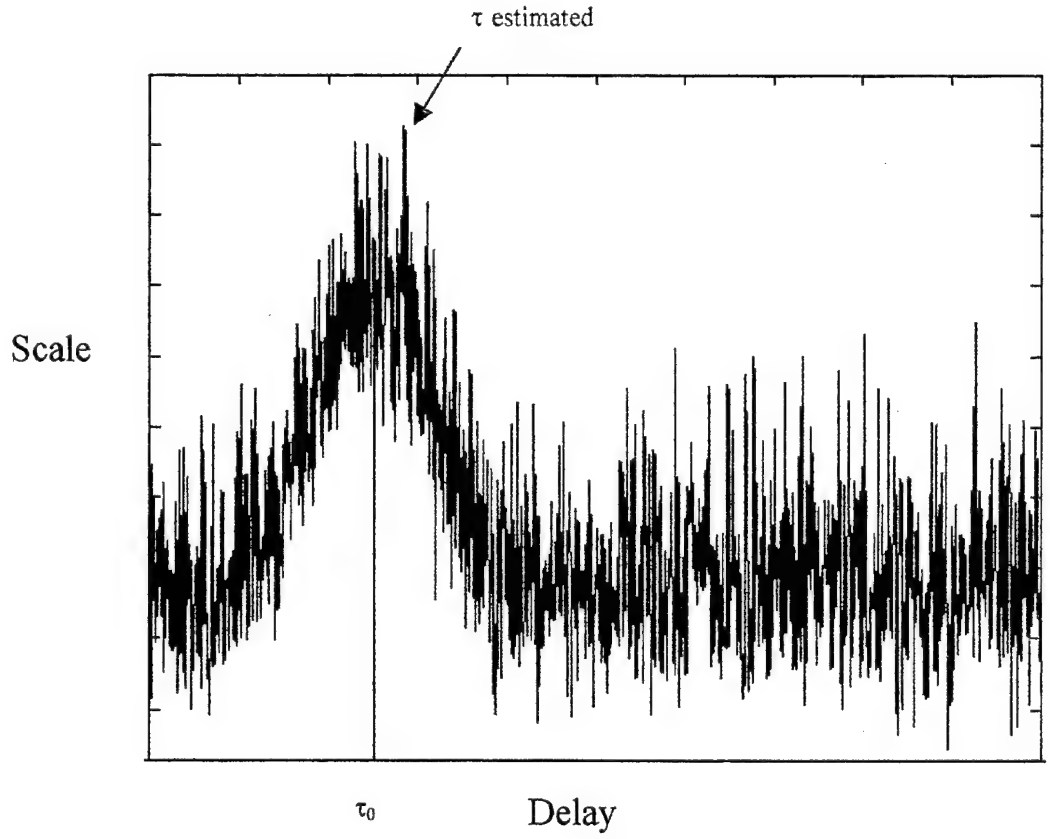

Figure 3.6: Ambiguity Function With Noise Added

In summary, it is desired to calculate a bound on the variance of estimates that can be made on the location of a scatterer in the scale-delay plane. This bound, the C-R bound,

will include the coupled effects of ambiguity main lobe area and signal-to-noise ratio. This is a useful quantity for both signal design and detector performance analysis.

3.5 C-R Lower Bound Derivation

In this section the C-R bound starting with the general wideband representation of a received echo with noise added is derived. In order to simplify the derivation it is assumed that the noise is uncorrelated with the signal, that it is white, and is Gaussian distributed.

3.5.1 Wideband Representation of the Echo

Assuming that the scatterer is a slowly fluctuating point target moving with constant velocity through a homogenous, infinite medium. The echo from the scatterer received at the receiver (Figure 3.1) is modeled as [4,6,7,16]

$$r(t) = \sqrt{E_t}\,\tilde{b}\sqrt{s}\,f(s(t-\tau)) + n(t) \tag{3.1}$$

here E_t is the transmitted signal energy, $\tilde{b}$ is a zero mean, complex, Gaussian random variable, and $E\{|b^2|\}=2\sigma_b^2$. n(t) is an independent, zero-mean, white, Gaussian process with covariance given by

$$E[n(t)n^*(t)] = N_0\delta(t-u) \tag{3.2}$$

From Equation (3.1), s and τ are the non-random scale and delay parameters to be estimated and for which the C-R bound will be calculated.

3.5.2 The Detector

In order to continue the derivation, it is necessary to define the detector structure being used (i.e., define the detection statistic as a function of s and τ). In this case, a wideband matched filter operation (wavelet transform) given by

$$L(s,\tau) = \int_{-\infty}^{\infty} r(t)\sqrt{s}\, f^*(s(t-\tau))dt \tag{3.3}$$

is performed. Where L is the detection statistic, s is the hypothesized time scale, τ is the hypothesized time delay and r(t) is given by (3.1). The next step is the derivation is to derive the likelihood function. This has been done in [16] and the result stated here

$$\ln \Lambda(s,\tau) = \frac{1}{N_0}\frac{E_r}{N_0 + E_r}\left\{\left|L(s,\tau\right|^2\right\} \tag{3.4}$$

Here N_0 is the noise energy and E_r is the total echo energy.

Having obtained equations (3.3) and (3.4), the next step is to investigate the Fisher information matrix [57,58].

3.5.3 The Fisher Information Matrix

In order to estimate the non-random parameters s and τ, the Fisher information matrix must first be derived. The lower bounds on the estimates (C-R bounds) are given by the diagonal components of the inverse of the Fisher information matrix. The Fisher information matrix is derived in detail in [16] the results are stated here. For a given likelihood function the elements of the information matrix are given by the following

$$J_{ij} = -E\left[\frac{\partial^2 \ln \Lambda}{\partial a_i \partial a_j}\right] \tag{3.5}$$

Where $\ln\Lambda$ is given by (3.4) and a_i and a_j are s and τ respectively. As these are non-random parameters, the expectation in (3.5) is over r(t) and n(t). Using (3.5) the individual elements of the information matrix are given by [56,57]

$$J_{11} = -E\left[\frac{\partial^2 \ln \Lambda}{\partial \tau^2}\right] \tag{3.6}$$

$$J_{22} = -E\left[\frac{\partial^2 \ln \Lambda}{\partial s^2}\right] \tag{3.7}$$

$$J_{12} = J_{21} = -E\left[\frac{\partial^2 \ln \Lambda}{\partial s \partial \tau}\right] \tag{3.8}$$

Inserting (3.4) into (3.6),(3.7), and (3.8) produces

$$J_{11} = -E\left[2c\,\mathrm{Re}\left[\frac{\partial L}{\partial \tau}\frac{\partial L^*}{\partial \tau} + L\frac{\partial^2 L^*}{\partial \tau^2}\right]\right] \tag{3.9}$$

$$J_{22} = -E\left[2c\,\mathrm{Re}\left[\frac{\partial L}{\partial s}\frac{\partial L^*}{\partial s} + L\frac{\partial^2 L^*}{\partial s^2}\right]\right] \tag{3.10}$$

$$J_{21} = J_{12} = -E\left[2c\,\mathrm{Re}\left[\frac{\partial L}{\partial s}\frac{\partial L^*}{\partial \tau} + L\frac{\partial^2 L^*}{\partial s \partial \tau}\right]\right] \tag{3.11}$$

where

$$c = \frac{1}{N_0} \frac{\overline{E}_r}{N_0 + \overline{E}_0} \tag{3.12}$$

It is now necessary to evaluate each of the equations (3.9), (3.10), and (3.11) separately. As the algebra is intense, only the term J_{11} will be derived (Appendix A) in detail. The other terms have very similar derivations.

The individual terms as given by (3.9), (3.10), and (3.11) with (3.3) substituted for L are given in final form as:

$$J_{11} = s^2 \left[\overline{\left(\frac{\omega}{s}\right)^2} - \overline{\left(\frac{\omega}{s}\right)}^2 \right] \tag{3.13}$$

$$J_{22} = -2cE_r \left[4\pi^2 \overline{(\omega t)} - \frac{1}{4} + \alpha_t \right] \tag{3.14}$$

As can be observed in equation (3.13), the J_{11} term is a function of mean squared bandwidth indicated by the bar and the J_{22} term is proportional to a quantity α_t, called the alpha moment [30]. By inverting these quantities, the C-R bounds on time-delay and time-scale are calculated. In the next section, illustrative examples of these quantities as a function of signal duration, bandwidth, and signal to noise ratio are given.

3.6 Examples of the C-R Lower Bound

In this section, example calculations of the CRLB for time delay and time scale are presented. In order to see the effects of changing various transmitted signal parameters, a few simplifying assumptions are made here. The first major assumption is that the estimation errors of time-scale and time-delay are uncoupled [16]. In order for this to be true, the signal envelope must be real and the signal must be symmetric about the frequency axis [59]. Making these assumptions, only the J_{11} and J_{22} terms are needed to calculate the C-R bounds. This simplifies the calculations as the cross terms J_{12} are not needed any longer. It is a research issue to investigate further the signal design problem in terms of estimation error decoupling. The C-R bounds, making the above assumptions, can be written as [60]:

$$\mathrm{var}[\tau-\hat{\tau}] = (2cE_r)^{-1}\left[\overline{\left(\frac{\omega}{s}\right)^2} - \overline{\left(\frac{\omega}{s}\right)}^2\right]^{-1} \tag{3.15}$$

And

$$\mathrm{var}[s-\hat{s}] = (2cE_r)^{-1}\left[4\pi^2\,\overline{(\omega t)} - \frac{1}{4} + \alpha_t\right]^{-1} \tag{3.16}$$

As expected, the bounds are functions of signal parameters as well as signal to noise ratio. The following sections contain examples of the CRLB for time-scale and time-

delay to illustrate the dependance on signal parameters. Also, it is well known that the alpha moment appearing in equation (3.16) above is not only a function of signal parameters, but also a function of the signal shape. The alpha moment is larger for signals which have their higher instantaneous frequency content located at the end points of the signal [61,62]. This has an effect on the CRLB, and therefore, two signal types will be used to illustrate the point. A VFM signal which has a time-frequency plot as given in Figure 3.7 and a roof-top FM (RTFM) which has a time-frequency plot as plotted in Figure 3.8 will be used for the examples to follow.

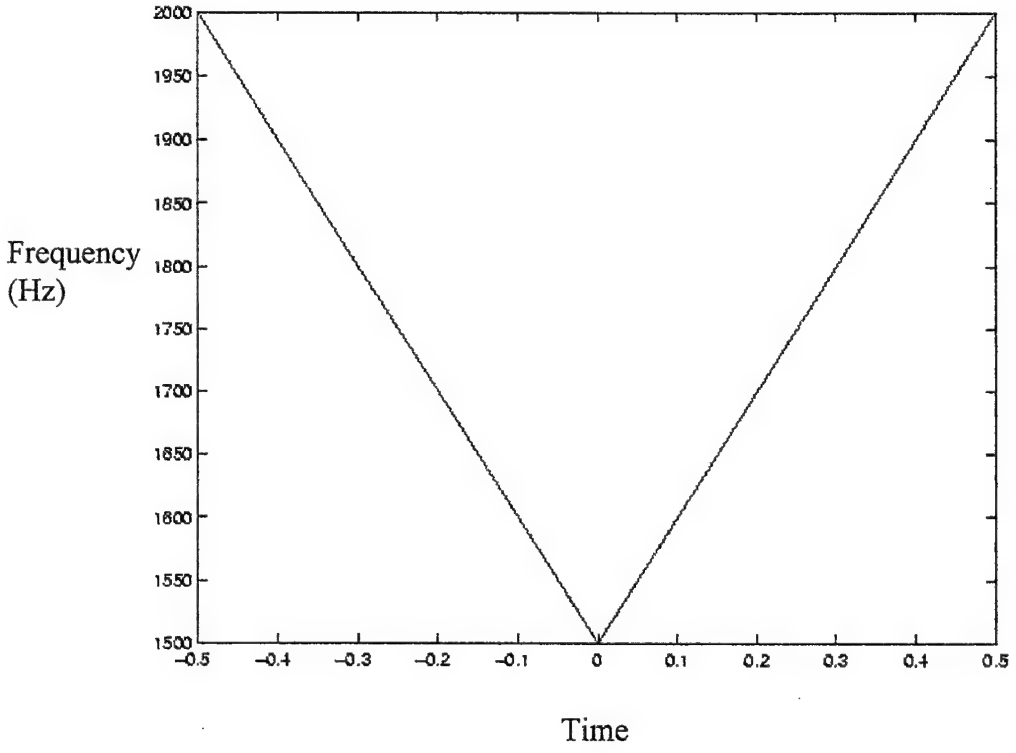

Figure 3.7: Time Frequency Plot for VFM Signal

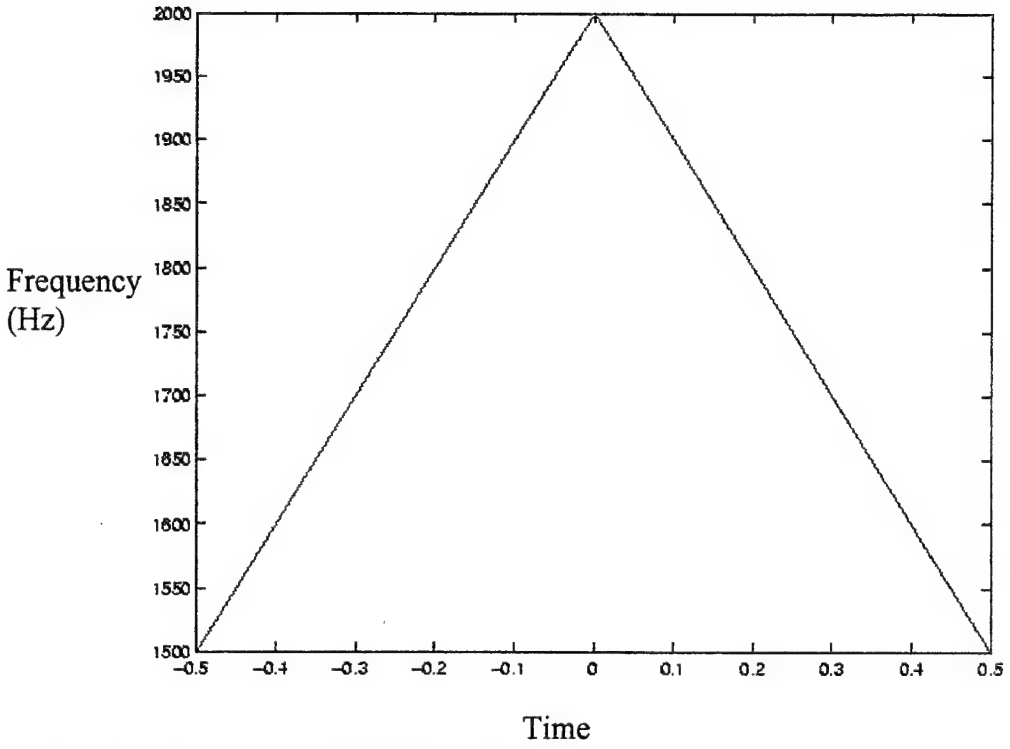

Figure 3.8: Time Frequency Plot for Roof-Top Signal

3.6.1 CRLB for Time Delay

In this section plots of the CRLB for time delay are given. These plots are only given for the VFM signal as the CRLB for time delay is independent of signal shape. It is also seen that the CRLB for time-delay is a function only of mean squared bandwidth and signal to noise ratio. Figure 3.8 is a plot of the CRLB for time delay as a function of mean squared bandwidth.

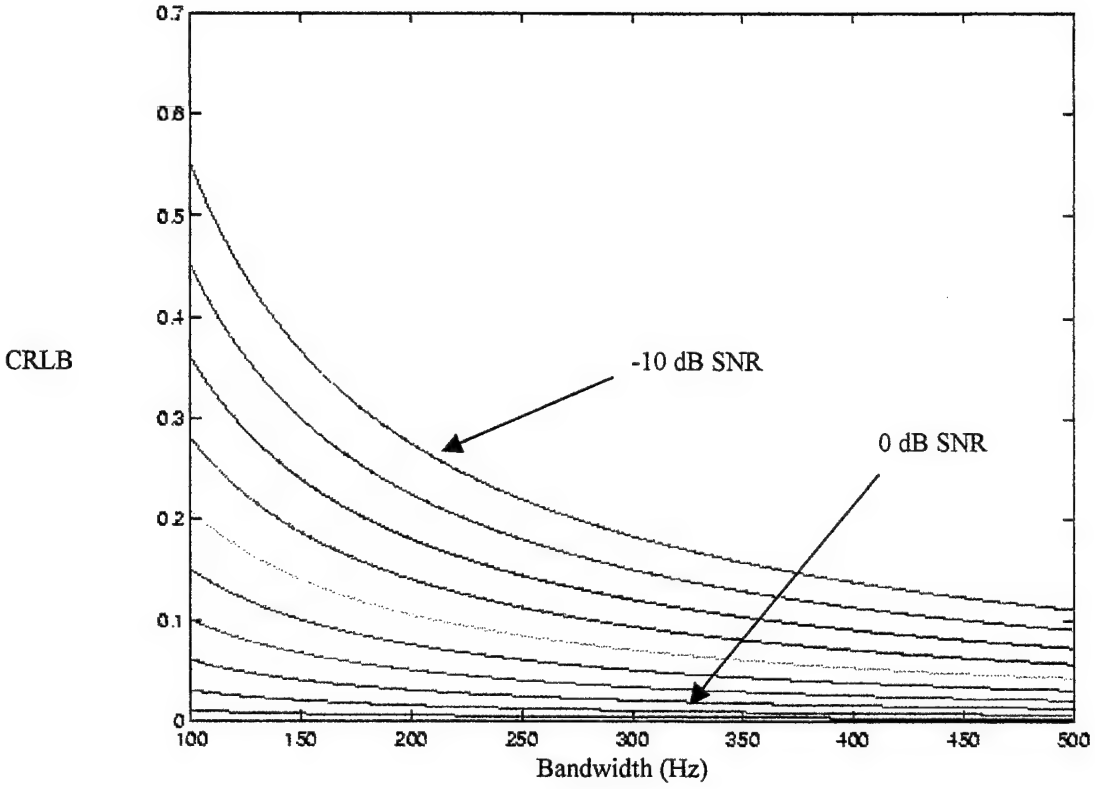

Figure 3.9: CRLB for Time Delay for Varying SNR as a Function of Bandwidth

Figure 3.9 confirms the expectation raised in section 3.2, that is, as the SNR is decreased, progressively worse estimates on the time delay are made. Also, increased bandwidth can recover some of the loss due to signal to noise ratio, this is a positive argument for using wideband signals for estimation of range. Figure 3.9 shows that as the bandwidth is increased, the CRLB is lowered. This trend shows that for a fixed signal to noise ratio, statistically speaking, by using signals with the higher frequency components at the ends of the signal in time, better estimates of range can be made in the detection problem. How these progressively worse estimates affect the ability of the Kalman filtering routine to converge is the subject of Chapter 5.

3.6.2 CRLB for Time-Scale

In this section the more complex issue of the CRLB for time-scale estimation errors is investigated. In this case, the CRLB is not only determined by the transmitted signal parameters such as duration, bandwidth, and center frequency, but also on the alpha moment, which is itself a function of the signal shape [61-63]. This section will present examples that illustrate this fact. In this section, the CRLB for time-scale will be calculated for a variety of transmitted signal parameters and for the two signals envelopes: VFM and RTFM. It is a simple matter to derive the alpha moment analytically for the VFM and RTFM using the equation [60, 61, 62]

$$\alpha_t = \frac{1}{T} \int_{\frac{-T}{2}}^{\frac{T}{2}} t^2 \omega^2(t)\, dt \tag{3.17}$$

If the inverse of the alpha moment (which is proportional to CRLB) it is seen that, as expected, the CRLB for time scale is lower when the instantaneous frequency content is higher at the endpoints of the signal. Figure 3.10 is a plot of the CRLB for time-scale as a function of duration for the VFM and RTFM for equal mean square bandwidths of 1000 Hz.

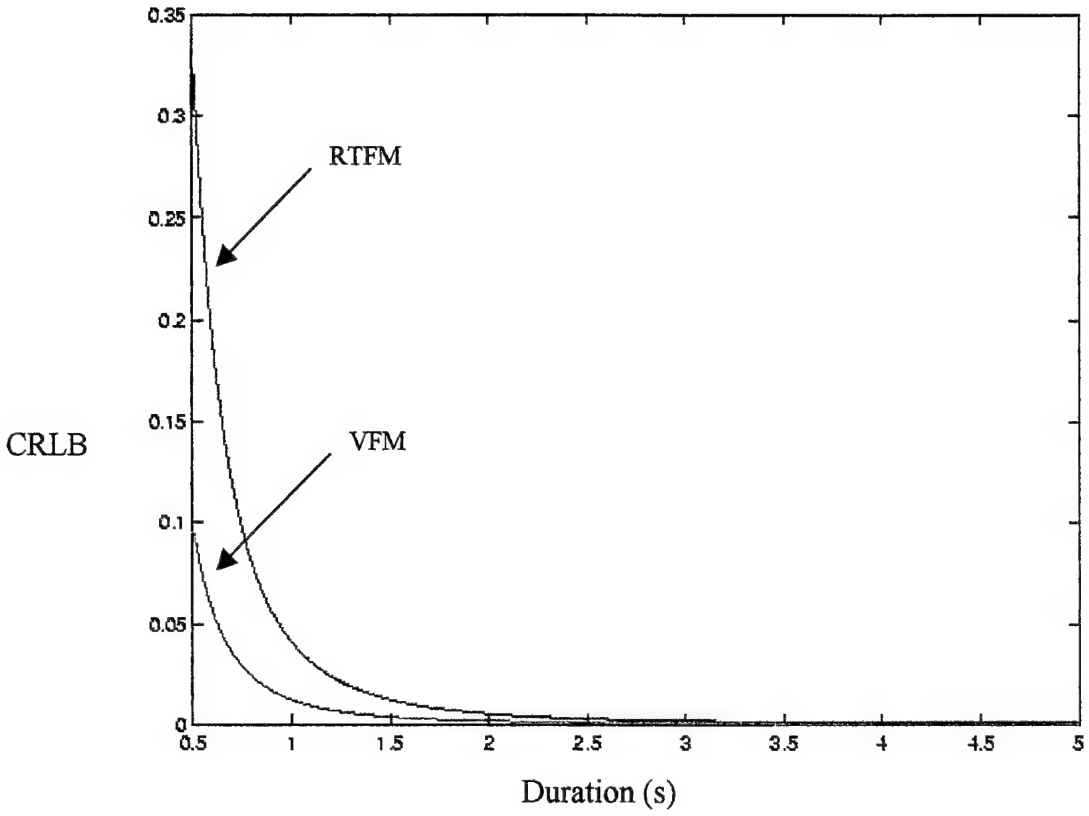

Figure 3.10: CRLB for VFM and RTFM vs. Duration

As can be seen in Figure 3.10, the CRLB is lower for the VFM for the same mean squared bandwidth and durations. This indicates that better estimates can be made if the higher frequency components are pushed out to the ends of the signal (in time). However, as is seen in Figure 3.11, this effect is lessened as the total bandwidth gets much higher.

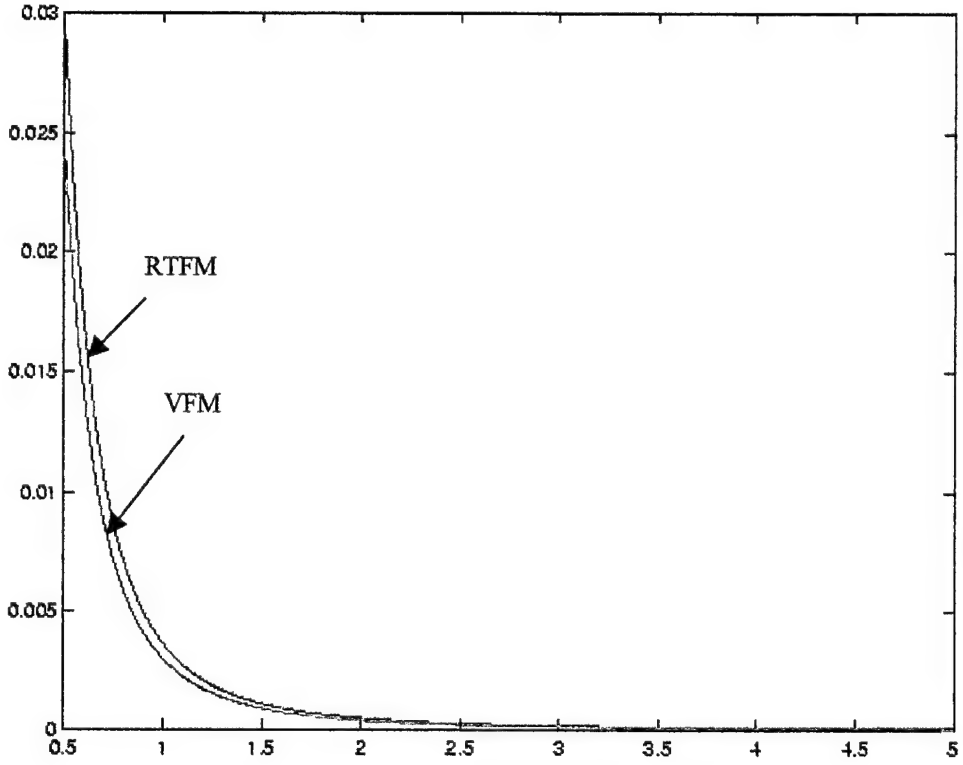

Figure 3.11: Time Scale CRLB for 5kHz Bandwidth VFM and RTFM

3.7 Conclusions

The CRLB for time-delay and time-scale for the case of wideband signals has been derived and their dependence on the transmitted signal's parameters have been investigated. As expected, it has been shown that as the effective duration is increased, the ability to estimate time-scale is increased. Also, as the mean squared bandwidth is increased, the ability to estimate time-delay is improved. It was shown that the CRLB for delay and scale can be related to the parameters of the transmitted signal and to the alpha moment. The alpha moment is a function of signal bandwidth as well as signal shape.

The important conclusion is that the CRLB for the variance on estimation errors made on time-scale and time-delay can be related to the time-bandwidth product of the transmitted signal. This is an important signal processing issue as it has been shown that processing gain (in the detection problem) is proportional to time-bandwidth product for point scatterers. The purpose of this derivation and analysis in terms of the overall thesis is that the CRLB for delay and scale dictates a minimum variance on the errors associated with estimating time-delay and time-scale. These quantities will be used in the next chapter in the form of a measurement equation in the Kalman Filter. In the forthcoming development, the performance of the Kalman filter will be shown to be tightly tied to the measurement error covariance matrix. As it will be shown, the elements within the measurement error covariance matrix are the variances predicted by the CRLB . This relationship is critical, as the best possible performance achievable in the Kalman filter depends on (among other things) the CRLB for time-scale and time-delay. Having shown that the CRLB is tied to the transmitted signal parameters, a complete concept can be formed, tying realistic measurement quantities to expected Kalman filter estimator performance.

Chapter 4

Wavelet Domain Scattering Function Predictor/Corrector Kalman Filtering

4.1 Introduction

As discussed in Chapter 1, two approaches to updating the *a priori* scattering function information are investigated in the thesis. The first, to be discussed in this chapter is the direct recursive estimation of the spreading function based on spreading function estimates using a Kalman filter. Upon completion of the derivation it was found that the complexity of the results (i.e., four dimensional state transition and measurement equations) pointed to approaching the problem using a simplified approach. The simplified approach is the tracking of peak locations within the spreading function using an extended Kalman filter. This approach is more easily implemented, and can be used to update spreading function estimates by updating the scattering function found in Equation (2.40). The simplified approach is introduced at the end of Chapter 4, and in implemented in Chapter 5.

This chapter contains the derivation and analysis of the Kalman filtering approach to scattering function recursive estimation and updating. Presented here are the results of the derivation of the Kalman filter for WTD scattering function estimation and updating based on the innovations approach [11,51]. The parameters of the Kalman filter (e.g., the criterion and quality) are analyzed in terms of the WTD observables (e.g., spreading and scattering functions) and the performance parameters of the Kalman filter are compared to and analyzed with the performance measures of

the WTD EC. It is shown that relationships exist between the scalar figure of merit derived in Chapter 2 and the criterion of the Kalman filter (i.e. the trace of the error covariance). It is also shown that the EC detection statistic error function is related to the Kalman filter error covariance.

4.2 Innovations Approach to the Kalman Filter

In this section, the Kalman filter for recursive scattering function updating using the innovations approach outlined by Kailath [11] is derived. The general introductory theory of the Kalman filter operation was given in Section 2.2.

4.2.1 State Equation

The first relationship required in the derivation of the Kalman filter is referred to as the state equation [51]. Here, a state equation in terms of the spreading function will be given as

$$w(x) = A(x-1)w(x-1) + u(x-1) \tag{4.1}$$

Here, x is given as $x \in R^2$ or $x=[\tau\ s]$ where τ is the variable of time delay and s is the variable of time-scale. The state equation gives the relationship between the x-1 (previous scale and delay) and the current scale and delay x. The relationship (1) ,therefore, gives the relationship of the new spreading function w(x) to the previous spreading function w(x-1) where the (x-1)

portion of the expression indicates the previous s and τ (i.e. if x=[s τ] then x-1=[s_{t-1} τ_{t-1}]. This is accomplished by a known variable A called the state transition matrix. The state transition matrix is an appropriately dimensioned matrix which is derived from the physics of the problem (see Section 5.2 and 5.3 for specific examples). For the purposes of the derivation it is sufficient to state that the state equation (1) models the system under investigation in general. A is an appropriately dimensioned matrix called the state transition matrix. Here, q is the state noise which is assumed to be zero mean and white with covariance R_q and q is uncorrelated with w, the spreading function.

The next step in the derivation is to arrive at a measurement equation.

4.2.2 The Measurement Equation

In order to begin the Kalman filter derivation, it is first necessary to find (for our EC processing structure) the proper representation of the measurement equation of the general form

$$w_m(x) = C(x)w_o(x) + n(x) \tag{4.2}$$

here w_d is the observed spreading function, C is a matrix operating on the desired variable, and n is a noise process. The subscript m denotes the fact that this is an

observed (measured) variable and the subscript o denotes that this is the desired variable or the variable to be estimated from the observations.

As seen in Section 2.3 in the outline of the WTD EC, the measurement equation under reverberation limited conditions is given by:

$$r(t) = y(t) + n(t) \tag{4.3}$$

where r(t) is the received data, y(t)is the signal with reverberation , and n is a colored noise process. Recall Section 2.1 that y(t) for the EC is given by:

$$y(t) = \int_G w(x)[U(x)f(t)]d\mu(x) \tag{4.4}$$

where w(x) is the spreading function of Section 2.3, U(x) is a unitary operator operating on either the Heisenberg (narrowband) or affine (wideband) group, f(t) is the transmitted signal and $\mu(x)$ is the left invariant Haar measure for the appropriate group.

Substituting (4.4) into (4.3) and taking the wavelet transform of both sides:

$$\int r(t)[U(x)f(t)]^* dt = \int\int w(x')\,[U(x')f(t)]\,[U(x)f(t)]^*\, d\mu(x')\, dt + \int n(t)[U(x)f(t)]^* dt \tag{4.5}$$

In the first integral on the right hand side the time dependent terms can be grouped together in the time integral pulled into the G integral resulting in

$$\int r(t)[U(x)f(t)]^* dt = \int w(x') \left[\int [U(x)f(t)]\,[U(x)f(t)]^*\, dt\right] d\mu(x) + \int n(t)[U(x)f(t)]^* dt \quad (4.6)$$

Recognizing that the time integration in the first term on the right hand side of (4.6) represents the reproducing Kernel which spans the space of signals admissible f(t), (4.6) can be written as

$$w_m(x) = \int w_o(x')\, K(x,x') \quad d\mu(x') + \int n(t)[U(x)f(t)]^* dt \quad (4.7)$$

Noting that the second term is the wavelet transform of the received noise, for brevity

$$w_m(x) = \int w_o(x')\, K(x,x') \quad d\mu(x) + n_{wf}(x) \quad (4.8)$$

where the subscript wf denotes the wavelet transform with f(t) as the mother wavelet. The measurement equation is beginning to take shape. It is now necessary to show that the integral operator (really a convolution integral) can be written as a matrix operator. In general, an operator can be represented as a matrix operator with respect to a set of basis functions [64]. For this convolution integral, the matrix operator representation is valid.

Using a simple one dimensional example to illustrate the method, an example of converting a convolution integral to a convolution sum is given. Starting with a simple form (for illustrative purposes) with a convolution integral [65]

$$y(t) = \int_{-\infty}^{\infty} h(\tau)x(t-\tau)\, d\tau \quad (4.9)$$

Now, for this example x(t) is a general time series and h(t) is the impulse response of a linear filter. Equation (4.9) can be written as a convolution sum for discrete data as

$$y(n) = \sum_{k=-p}^{p} x[k]h[n-k] \tag{4.10}$$

where n is the time index and k is the delay index. To show that this can be written as a matrix operator, simply write Y=y[n] n=1,2,3... and X=x[n] n=1,2,3,..... and show that for windowed (i.e. finite duration) signals:

$$\begin{bmatrix} y[1] \\ y[2] \\ \vdots \\ y[n] \end{bmatrix} = \begin{bmatrix} h[1-(-p)] & h(1-(-p+1) & \cdots & h[1-(p)] \\ h[2-(-p) & \ddots & & \\ \vdots & & \ddots & \\ h[n-(-p) & \cdots & & h[n-p] \end{bmatrix} \begin{bmatrix} x[1] \\ x[2] \\ \vdots \\ x[n] \end{bmatrix} \tag{4.11}$$

By carrying out the, multiplication it is seen that each term in the vector y[n] is obtained from the matrix multiplication in (4.11) (which results in the sum 4.10) for each term. So in matrix notation (4.11) can be written as

$$\underline{Y} = \underline{\underline{h}}\,\underline{X} \tag{4.12}$$

By an analogous derivation for the 2 dimensional convolution integral

$$\begin{bmatrix} w_y(x_1) \\ w_y(x_2) \\ \vdots \\ w_y(x_i) \end{bmatrix} = \begin{bmatrix} K(x_1,x_1') & \cdots & & K(x_i,x_1') \\ K(x_1,x_1') & \ddots & & \\ \vdots & & \ddots & \vdots \\ K(x_j,x_1') & \cdots & & K(x_i,x_j') \end{bmatrix} \begin{bmatrix} w_x(x_1') \\ w_x(x_2') \\ \vdots \\ w_x(x_i') \end{bmatrix} \tag{4.13}$$

Therefore, the integral operator can be written as the matrix operator K(x,x') and it follows that the measurement equation is in the correct form (4.2) as

$$\underline{w_y} = \underline{\underline{K}}(x,x')\ \underline{w_x}(x') + \underline{n_{wf}}(x) \tag{4.14}$$

This completes the derivation of the measurement equation for our wideband spreading function. Equation (4.14) coupled with (4.1) enables the continuation of the innovations approach of the derivation as given by Kailath [11].

4.2.3 Kalman Filter Derivation – Innovations Approach

The problem is posed here as

Given a noisy set of measurements $w_m(i)$ i=1,2,3...X (X being the current state X=[s τ] characterized by (4.13), find the linear minimum (error) variance estimate of the state characterized by (4.1). That is, find the best estimate of $w_o(X)$ given the measurement data up to time (time delay/time-scale pair) x where $\underline{W_m}(x)$=[$w_m(1)$ $w_m(2)$..... $w_m(x')$]. Here $\underline{W_m}(x)$ is the set of observations of the spreading function.

The minimum (error) variance criterion is given by

$$J(X \mid x) = E\{\tilde{w}_o'(X)\tilde{w}_o(X) \mid W_m(x)\} \tag{4.15}$$

or using the standard conditional mean notation and noting that ~ denotes estimate

$$\tilde{w}_o(X \mid x) = E\{\tilde{w}_o(X) \mid W_m(x)\} \tag{4.16}$$

which states that the estimate of the true spreading function at the "time" given data up to X is equal to the expected value of the true spreading function conditioned on the measurement of the spreading function. Thus, the criterion is written as

$$J(X \mid x) = E\{\tilde{w}_o'(X \mid x)\,\tilde{w}_o(X \mid x) = trace(\tilde{P}(X \mid x)) \tag{4.17}$$

Where $\tilde{P}$ is the estimated error covariance.

There are three special cases of the state estimation problem:

1. The l-step predicted estimate.
2. The filtered estimate.
3. The fixed lag smoothed estimate.

The "filtered" estimate $\tilde{w}_o(x \mid x)$ is of interest here as this is the form which gives recursive estimates in a prediction/correction form. It is given by

$$\tilde{w}_o(x \mid x) = E\{\tilde{w}_o(x) \mid W_m(x)\} \tag{4.18}$$

First, the dynamic form on the estimator is chosen and the estimator is constrained to be linear.

In the dynamic case, the linear estimator [51] is

$$\underline{\hat{W}}_{MV}(N) = R_{w_o w_m}(\underline{N}) R_{w_m}{}^{-1}(\underline{N}) \underline{W}_m = \mathrm{K}_{MV}(\underline{N}) \underline{W}_m \tag{4.19}$$

where:

$$\hat{W}_{MV}(\underline{N}) = [\hat{w}'(1) \cdots \hat{w}'(N)]' \tag{4.19a}$$

Is the batch minimum variance (MV) spreading function estimate and

$$W_m = [w_m{}'(1) \ldots w_m{}'(N)]' \tag{4.19b}$$

is the batch measurement and K_{MV} is the Kalman gain.

This is a "batch" minimum variance solution to the state estimation problem, since all p-vector data $\{w_m(1) \ldots w_m(N)\}$ are processed in one batch. However, for the purposes of the thesis, a recursive solution to the estimation problem of the form:

$$\hat{W}_{new} = \hat{W}_{old} + KE_{new} \tag{4.20}$$

is needed.

In order to achieve the recursive solution, it is necessary to transform the covariance matrix R_{w_m} to be block diagonal, since

$$R_{w_y} = \begin{bmatrix} E\{w_m(1)w_m'(1)\} & \cdots & E\{w_m(1)w_m'(N)\} \\ \vdots & \ddots & \vdots \\ E\{w_m(N)w_m'(1)\} & \cdots & E\{w_m(N)w_m'(N)\} \end{bmatrix} = \begin{bmatrix} R_{w_m}(1,1) & \cdots & R_{w_m}(1,N) \\ \vdots & \ddots & \vdots \\ R_{w_m}(N,1) & \cdots & R_{w_m}(N,N) \end{bmatrix} \quad (4.21)$$

Having R_{w_m} be block diagonal implies that all of the off-diagonal matrices $R_{w_y}(i,j) = 0$ for i≠j. This in turn implies that all of the $w_m(x)$ must be uncorrelated with or orthogonal to $w'_m(x)$.

Therefore, a sequence of independent p-vectors {e(x)} can be constructed such that

$$E\{e(x)e'(k)\} = 0 \quad for x \neq k \quad (4.22)$$

The sequence e(x) can be constructed using the orthogonality property

$$[w_m(x) - E\{w_m(x) \mid W_m(x-1)\}] \perp W_m(x-1) \quad (4.23)$$

Defining the innovation or new information as:

$$e(x) = w_m(x) - \hat{w}_o(x \mid x-1) \quad (4.24)$$

with the orthogonality property that

$$\text{cov}(w_m(X), e(x)] = 0 \quad for X \leq x-1 \quad (4.25)$$

Since e(x) is a time-uncorrelated p-vector sequence

$$R_e(N) = \begin{bmatrix} R_e(1) & \cdots & R_e(1) \\ \vdots & \ddots & \vdots \\ R_e(1) & \cdots & R_e(N) \end{bmatrix} \tag{4.26}$$

for each $R_e(i) \in R^{pxp}$.

The correlated measurement vector can be transformed into an uncorrelated innovation vector though a linear transformation , say L, given by,

$$W_y = L\,e \qquad L \in R^{pnxpn} \tag{4.27}$$

where L is a non-singular transformation matrix and $\underline{e}$:=[e′(1)…e′(N)]′.

Multiplying (4.26) by its transpose and take the expected value to obtain

$$R_{W_m}(\underline{N}) = LR_e(\underline{N})L' \tag{4.28}$$

now, inverting:

$$R^{-1}{}_{W_m}(\underline{N}) = (L')^{-1}R_e^{-1}(\underline{N})L^{-1} \tag{4.29}$$

Similarly,

$$R_{w_o w_m}(\underline{N}) = R_{w_x e}(\underline{N})L' \tag{4.30}$$

Now, substitute these results into (4.19) to obtain

$$\underline{\hat{W}}_{MV}(N) = R_{w_x w_y}(\underline{N})R_{w_y}{}^{-1}(\underline{N})\underline{W}_y = [R_{w_x e}(\underline{N})L'][(L')^{-1}R_e^{-1}(\underline{N})L^{-1}](L\underline{e}) \tag{4.31}$$

Simplifying yields

$$\underline{\hat{W}}_{MV}(N) = R_{w_x e}(\underline{N})R_e^{-1}(\underline{N})\underline{e} \tag{4.31a}$$

Since the e(x) are time uncorrelated, $R_e(\underline{N})$ is block diagonal. From the orthogonality properties of the innovations, e, it can be shown that $R_{w_o e}(\underline{N})$ is lower-block triangular, that is:

$$R_{w_o e}(\underline{N}) = \begin{Bmatrix} R_{w_x e}(x,i) \\ R_{w_x e}(x,x) \\ 0 \end{Bmatrix} for \begin{Bmatrix} x > i \\ x = i \\ x < i \end{Bmatrix} \tag{4.32}$$

substituting into (4.31)

$$\hat{W}_{MV}(N) = \begin{bmatrix} \hat{w}_x(1,1) \\ \vdots \\ \hat{w}_x(N,N) \end{bmatrix} = \begin{bmatrix} R_{w_x e}(1,1) & & 0 \\ \vdots & \ddots & \\ R_{w_x e}(N,1) & \cdots & R_{w_x e}(N,N) \end{bmatrix} \begin{bmatrix} R_e^{-1}(1) & & 0 \\ & \ddots & \\ 0 & & R_e^{-1}(N) \end{bmatrix} \begin{bmatrix} e(1) \\ \vdots \\ e(N) \end{bmatrix} \tag{4.33}$$

Any row of (4.32) can be written as

$$\hat{w}_x(x,x) = \sum_{i=1}^{x} R_{w_o e}(x,i) R_e^{-1}(i) e(i) \tag{4.34}$$

If the last term of the sum in (4.33) is extracted, from (4.18)

$$\hat{w}_x(x,x) = \underbrace{\sum_{i=1}^{z} R_{w_x e}(x,i) R_e(i) e(i)}_{\hat{W}_{old}} + \underbrace{R_{w_x e}(x,x) R_e^{-1}(x) e(x)}_{\mathrm{K}} \tag{4.35a}$$

Or

$$\hat{W}_{new} = \hat{w}_x(x,x) = \hat{w}(x \mid x-1) + \mathrm{K}(x) e(x) \tag{4.35b}$$

Where $\mathrm{K}(x) = R_{w_x e(x)}(x,x) R_e^{-1} = \tilde{P}(x \mid x-1) C'(x) R_e^{-1}(x)$ is the Kalman weight, C is the measurement matrix, and $\tilde{P}(x \mid x-1)$ is the updated error covariance estimate.

Recall that

$$\hat{w}_m(x \mid x-1) = \underline{\underline{K}}(x,x') w_o(x \mid x-1) \tag{4.36}$$

Using the measurement equation (4.14) and (4.24) the innovations sequence can be decomposed as

$$e(x) = w_m(x) - \underline{\underline{K}}(x,x') \hat{w}_o(x \mid x-1) = \underline{\underline{K}}(x,x')[w_o(x) - \hat{w}_o(x \mid x-1)] + W_f n(x) \tag{4.37}$$

$$e(x) = \underline{\underline{K}}(x,x') \tilde{w}_o(x \mid x-1) + W_f n(x) \tag{4.38}$$

Consider the innovations covariance $R_e(x)$ using the expression,

$$R_e = \underline{\underline{K}}(x,x')\tilde{P}(x \mid x-1)\underline{\underline{K}}'(x,x') + R_{W_G n(x)} \tag{4.39}$$

and

$$R_{w_{ox}e} = E\{w_o(x)e'(x)\} = E\{w_o(x)[\underline{\underline{K}}(x,x')\tilde{w}_o(x \mid x-1) + W\,n(x)]'\}$$

or

$$R_{w_x e} = E\{w_o(x)\tilde{w}_o(x \mid x-1)\}\underline{\underline{K}}'(x,x') \tag{4.40}$$

Using the definition of $\tilde{w}_o$ and substituting for w_o

$$R_{w_o e} = E\{[\hat{w}_o(x \mid x-1) + \tilde{w}_o(x \mid x-1)]\,\tilde{w}_o(x \mid x-1)\}\underline{\underline{K}}'(x,x') \tag{4.41}$$

So that

$$R_{w_o e} = E\{[\hat{w}_o(x \mid x-1)\tilde{w}_o(x \mid x-1)]\}\underline{\underline{K}}'(x,x') + E\{[\tilde{w}_o(x \mid x-1)\tilde{w}_o(x \mid x-1)]\}\underline{\underline{K}}'(x,x')] \tag{4.41a}$$

From the orthogonality property of the estimation error for dynamic variables, that is

$$E\{(W_m(X))\tilde{w}_o'(x \mid x-1)\} = 0 \qquad for X \le x-1 \tag{4.42}$$

The first term in (4.41) is zero because of (4.42) therefore (4.41) becomes

$$R_{w_o e} = \tilde{P}(x \mid x-1)\underline{\underline{K}}'(x, x') \tag{4.43}$$

Therefore, the Kalman gain is

$$\mathrm{K}(x) = R_{w_o e}(X)R_e^{-1}(x) = \tilde{P}(x \mid x-1)\underline{\underline{K}}'(x, x')R_e^{-1}(x) \tag{4.44}$$

Before the corrected state estimate can be calculated, the predicted estimate is needed, that is:

$$\hat{W}_{old} = \hat{w}_o(x \mid x-1) = E\{w_o(x) \mid W_m(x-1)\} \tag{4.45}$$

Employing the state space model (4.1) and from the linearity properties of the conditional expectation,

$$\hat{w}_x(x \mid x-1) = E\{A(x-1)w_x(x-1)\} \tag{4.46}$$

write (4.46) as

$$\hat{w}(x \mid x-1) = A(x-1)\hat{w}(x-1 \mid x-1) \tag{4.47}$$

or

$$\hat{W}_{old} = \hat{w}_o(x \mid x-1) = A(x-1)\hat{w}_o(x-1 \mid x-1) \tag{4.48}$$

The error covariance is given by

$$\tilde{P}(x \mid x-1) = A(x-1)\tilde{P}(x-1 \mid x-1)A'(x-1) \tag{4.50}$$

The corrected covariance $\tilde{P}(x-1 \mid x-1)$ is calculated using the corrected estimation error and (4.35a) to obtain

$$\tilde{w}(x \mid x) = w_o(x) - \hat{w}_o(x \mid x) = w_o(x) - \hat{w}_o(x \mid x-1) - K(x)e(x) \tag{4.51a}$$

or

$$\tilde{w}(x \mid x) = \tilde{w}_o(x \mid x-1) - K(x)e(x) \tag{4.51b}$$

Using (4.51b) the required covariance is calculated:

$$\begin{aligned}\tilde{P}(x \mid x) = \tilde{P}(x \mid x-1) - K(x)E\{e(x)\tilde{w}_o'(x \mid x-1)\} - E\{w_o(x \mid x-1)e'(x)\}K'(x) \\ + K(x)R_e(x)K'(x)\end{aligned} \tag{4.52}$$

From the orthogonality property $E\{\tilde{w}_o(x \mid x-1)e'(x)\} = 0$ the error covariance is now given by:

$$\begin{aligned}\tilde{P}(x \mid x) = \tilde{P}(x \mid x-1) - \mathrm{K}(x)\underline{\underline{K}}(x,x')\tilde{P}(x \mid x-1) - \tilde{P}(x \mid x-1)\underline{\underline{K}}'(x,x')\mathrm{K}'(x) \\ + \mathrm{K}(x)R_e(x)\mathrm{K}'(x)\end{aligned} \tag{4.53}$$

Factoring $\tilde{P}(x \mid x-1)$ from the first two terms and using the expression (4.44) for K(x) in the last term

$$\begin{aligned}\tilde{P}(x \mid x) = [I - \mathrm{K}(x)\underline{\underline{K}}(x,x')]\tilde{P}(x \mid x-1) - \tilde{P}(x \mid x-1)\underline{\underline{K}}'(x,x')\mathrm{K}'(x) \\ + \tilde{P}(x \mid x-1)\underline{\underline{K}}'(x,x')R_e^{-1}R_e(x)\mathrm{K}'(x)\end{aligned} \tag{4.54}$$

Observing that the last two terms cancel the error covariance is given by

$$\tilde{P}(x \mid x) = [I - \mathrm{K}(x)\underline{\underline{K}}(x,x')]\tilde{P}(x \mid x-1) \tag{4.55}$$

This completes the derivation of the Kalman filter algorithm for the wideband spreading function recursive updating.

4.3 Analysis of Kalman Filter Derivation Results

In this section the major results of the previous section are discussed. First the criterion, the mean square scattering function error will be analyzed. Second, the dimensions and possible uses of these quantities in a signal processing structure will be presented and an explanation of how the quantities are interrelated is given. Table 4.1 contains the results of the Kalman filter derivation for recursive scattering updating.

Table 4.1 Summary of the Kalman Filter for Recursive Scattering Function Estimation and Updating.

Prediction
$\hat{w}_o(x \mid x-1) = A(x-1)\hat{w}_o(x-1) + q(x-1)$ (State Prediction)
$\widetilde{P}(x \mid x-1) = A(x-1)\widetilde{P}(x-1 \mid x-1)A'(x-1)$ (Covariance Prediction)
Innovation
$e(x) = w_m(x) - \hat{w}_m(x \mid x-1) = w_m(x) - \underline{\underline{K}}(x,x')\hat{w}_m(x \mid x-1)$ (Innovation)
$R_e = \underline{\underline{K}}(x,x')\widetilde{P}(x \mid x-1)\underline{\underline{K}}'(x,x') + R_{W_G n(x)}$ (Innovation Covariance)
Gain
$K(x) = \widetilde{P}(x \mid x-1)\underline{\underline{K}}'(x,x')R_e^{-1}$ (Kalman Gain/Weight)
Correction
$\hat{w}_o(x \mid x) = \hat{w}_o(x \mid x-1) + K(x)e(x)$ (State Correction)
$\widetilde{P}(x \mid x) = [I - K(x)\underline{\underline{K}}(x,x')]\widetilde{P}(x \mid x-1)$ (Covariance Correction)
Initial Conditions
$\hat{w}_x(0 \mid 0)$ $\widetilde{P}(0 \mid 0)$

The rest of this chapter will be dedicated to the analysis of the quantities outlined in Table 4.1.1. All of the quantities outlined, however, most of our focus will be on the *correction* terms, the *innovations*, and the *Kalman gain*.

4.3.1 Prediction Terms

In this section the prediction relationships presented in Table 4.1 are discussed. The state prediction is simply the state equation (4.1). This equation gives the relationship between the values of the predicted spreading function at the current (τ,s) conditioned on (τ,s) at the last time t-1 (what, in the derivation, are referred to as x and x-1 respectively). The predicted spreading function at these two "times" are related by the state transition matrix A. In words, the new estimate of the spreading function is the old estimate transformed by the state transition matrix A. A itself is derived directly from the physics of the problem (See Chapter 5). The state transition matrix in the WTD related the new scale and delay to the old is based on the motion of objects in the medium.

The second item, the error covariance $\widetilde{P}$, given in Table 4.1 has the same kind of relationship between new and old values as the state prediction via the state transition matrix. In this case the new value of the error covariance is the old value transformed using A as given in Table 4.1

The assumptions made in the derivation pertaining to the prediction parts of the algorithm are as follows:

1. A is a known matrix.
2. The additive process noise is zero-mean and spectrally white with correlation matrix defined by:

$$E\{q(x)q^H(x')\} = \begin{cases} Q_1(x) & x = x' \\ 0 & x \neq x' \end{cases} \tag{4.56}$$

4.3.2 Innovations

The innovations approach [55] is the heart of the derivation. In this section, the properties of the innovations or "new data" [51] and the innovations relationship to the scattering function updating algorithm are discussed. Also, the innovations sequence itself ,e(x), as well as the innovations covariance, $R_e(x)$ will be discussed.

The first property used in the derivation of the Kalman Scattering Function Algorithm is that the Mx1 vector e(x) represents the new information in the observed data $w_y(x)$. The innovations process has the following properties [66]:

1. The innovations process e(x), associated with the observed data $w_y(x)$ at "time" x is orthogonal to all past observations e(1) e(2)...e(x-1) given by

$$E\{e(k)w'_m(k)\} = 0 \qquad 1 \leq k \leq (x-1) \tag{4.57}$$

2. The innovations process e(x) consists of a sequence of vector random variables that are orthogonal to each other:

$$E\{e(k)e'(k)\} = 0 \qquad 1 \leq k \leq (x-1) \tag{4.58}$$

3. The sequence of vector random variables $\underline{W}_m(x)$, and the sequence of vector random variables $\underline{e}(x)$ have a one-to-one correspondence. This means that one can be obtained from the other by means of linear stable operators without the loss of information. The sequence of vector random variables defining the innovations process is obtained using a Gram-Schmidt orthogonalization procedure [67].

As seen in Table 4.1, the transition "matrix", A, and the measurement "matrix", $\underline{\underline{K}}$ are actually a tensors. These matrices can be transformed to a more recognizable form size by realizing what these tensor notations mean and by using a lexiographic ordering scheme [68-70]. This can be done to transform the tensor-matrix form to a matrix vector form without the loss of information. However, the size of the resulting transformation matrix can be problematic for implementation.

In the next section, an extended Kalman filter which tracks the peak locations within the spreading function is introduced for the case in which direct measurements of the kinematic quantities are not available. In this derivation only the peak locations within the spreading function are tracked. Time-scale and time-delay are estimated from a delay-scale map. However, it is desired to track state variables that differ from the measurement variables.

4.4 Extended Kalman Filter Derivation

In this section, the extended Kalman filter [71] to track a single highlight moving in a circular motion is derived. The state variable is a vector quantity containing the velocity v_n and angle θ as shown in Figure 4.1.

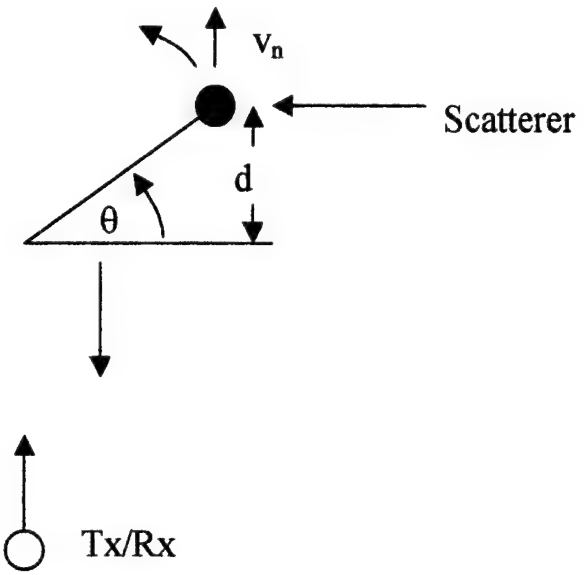

Figure 4.1: Circular Motion Geometry

It is assumed that the highlight has an initial position given by the vector

$$\bar{x}_0 = \begin{bmatrix} v_0 \\ \theta_0 \end{bmatrix}$$

Which are uncertain by the amounts σ_v and σ_θ. The true highlight "position" moves randomly about its unknown nominal location with standard deviations σ_v and σ_θ. The highlight is illuminated with a pulse and the time-scale and time-delay of the

return are measured using a wideband matched filter. This measurement has associated with it error due noise and an inherent error in the ability of the transmitted pulse to estimate the true time-delay and time-scale. This was discussed extensively in Chapter 3 in the form of the Cramér-Rao lower bound. The estimation errors on time-delay and time-scale are given by standard deviations σ_τ and σ_s. The derivation of the extended Kalman Filter (EKF) is begun by first introducing the state equation

$$\bar{x}_k = A\bar{x}_{k-1} + \overline{W}_{k-1} \tag{4.59}$$

where $\overline{W}_{k-1}$ is the state noise which is white, Gaussian, zero mean, and has a known variance. The matrix A is a state transmission matrix which relates past to future values of the state vector which is given as

$$\bar{x}_k = \begin{bmatrix} v_k \\ \theta_k \end{bmatrix} \tag{4.60}$$

Next a measurement equation is needed as in the previous sections, however, here, the state variables cannot be observed directly as the measured quantities are functions of the observed quantities. The measurement equation is given by

$$\bar{z}_k = \overline{H}_k(\bar{x}_k) + \overline{V}_k \tag{4.61}$$

where $\bar{z}_k$ is the measurement vector, $\overline{H}_k(\bar{x}_k)$ is the measurement as a function of the state variables and $\overline{V}_k$=[V_s V_θ]' the measurement noise, which is white,

Gaussian, zero mean, and has a diagonal covariance R_k with diagonal elements defined by the CRLB derived in Chapter 3. Our measurement equation is therefore given in terms of the kinematic variables, and observables as

$$\begin{bmatrix} s(k) \\ \tau(k) \end{bmatrix} = \begin{bmatrix} \dfrac{c - v_n(k)}{c + v_n} \\ \dfrac{2d}{c}\sin\theta(k) \end{bmatrix} + \begin{bmatrix} V_s \\ V_\theta \end{bmatrix} \tag{4.62}$$

Now, to start the iteration, initial estimates of the state and the error covariance are needed. These are given by

$$\bar{x}_0 = \begin{bmatrix} v_0 \\ \theta_0 \end{bmatrix} \qquad P_0 = \begin{bmatrix} \sigma^2{}_{v_0} & 0 \\ 0 & \sigma^2{}_{\theta_0} \end{bmatrix} \tag{4.63}$$

First, this initial estimate is projected ahead to the first measurement

$$\hat{x}_1(-) = A_0 \hat{x}_0 \tag{4.64}$$

Now, using the state transition matrix derived in Section 5.3, the estimate of the variance on the estimate can be calculated. This is given as

$$\hat{P}_1(-) = A_0 P_0 A_0^T \tag{4.65}$$

now, the update of the state variable estimate is given by

$$\hat{x}_1(+) = \hat{x}_1(-) + K_1[\overline{Z}_1 - H_1(\hat{x}_1)] \tag{4.66}$$

which when 4.62 and 4.64 are substituted becomes

$$\begin{bmatrix} \hat{v}_k \\ \hat{\theta}_k \end{bmatrix} = \begin{bmatrix} \hat{v}_k(-) \\ \hat{\theta}_k(-) \end{bmatrix} + K_k \begin{bmatrix} s_{1k} - \dfrac{c + \hat{v}_k(-)}{c - v_n} \\ \tau_k - \dfrac{2d}{c}\sin\hat{\theta}(-) \end{bmatrix} \tag{4.67}$$

Now the Kalman gain K_k is calculated. In the linear case it is a function of H_k, the measurement matrix.

Using the vector Taylor series expansion

$$\overline{H}(\overline{x} + \Delta\overline{x}) = \overline{H}(\overline{x}) + \frac{\partial \overline{H}}{\partial \overline{x}}\Delta\overline{x} + \textit{Higher Order Terms} \tag{4.68}$$

Having made the assumption of negligible acceleration, the higher order terms are dropped. This is only possible if the observation interval is short enough to ensure second order effects are negligible. Dropping the higher order terms

$$\Delta\overline{H} = \frac{\partial \overline{H}}{\partial \overline{x}}\Delta\overline{x} \tag{4.69}$$

where

$$\frac{\partial \overline{H}}{\partial \overline{x}} = \overline{\overline{H}} \tag{4.70}$$

and

$$H_{ij} = \frac{\partial \overline{H}_i}{\partial \overline{x}_j}$$

Are the elements of the new measurement matrix which is given by

$$\overline{\overline{H}} = \begin{bmatrix} \frac{\partial \overline{H}_1}{\partial \overline{x}_1} & \frac{\partial \overline{H}_1}{\partial \overline{x}_2} & \cdots & \frac{\partial \overline{H}_1}{\partial \overline{x}_j} \\ \frac{\partial \overline{H}_2}{\partial \overline{x}_1} & \frac{\partial \overline{H}_2}{\partial \overline{x}_2} & & \vdots \\ & & \ddots & \vdots \\ \frac{\partial \overline{H}_i}{\partial \overline{x}_1} & \cdots & \cdots & \frac{\partial \overline{H}_i}{\partial \overline{x}_j} \end{bmatrix} \tag{4.71}$$

Which in our case is a 2x2 matrix for the time-scale as a function of velocity and time delay as a function of the angle θ.

The iteration can now be completed by calculating the Kalman gain K_k

$$K_k = P_k(-)H_k^T(\hat{x}_k(-))[H_k(\hat{x}_k(-))P_k(-)H_k^T(\hat{x}_k(-)) + R_k]^{-1} \tag{4.72}$$

and the error covariance is given by

$$P_k(+) = [I - K_k H_k(\hat{x}(-))]P_k(-) \tag{4.73}$$

This completes the iteration of the extended or linearized Kalman filter. This is the form of the algorithm used in the remainder of the thesis to implement the examples.

4.5 Conclusions

In this chapter, a Kalman filter for updating and estimating wideband spreading functions using the innovations approach has been calculated. Through the use of the extended or linearized Kalman filter, the algorithm that tracks the kinematics of the problem using measurements of time-delay and time scale in a wideband range-scale map is derived. In the next chapter, the extended Kalman filter will be implemented for objects undergoing various types of motion. The ability of the Kalman filter to maintain a track on the peak locations within the spreading function of the object will be investigated for signals with varying bandwidths and durations.

Chapter 5

Recursive Kalman Scattering Function Estimation – Implementation

5.1 Introduction

This chapter introduces, via two examples, the implementation of the recursive scattering function updating algorithm. The first example will be of two rough spheres attached by a non-scattering rod. The spheres and rod rotate as a single object in the plane which contains the transmitter/receiver. The second example consists of a set of point scatterers linearly arranged and moving with a constant velocity and with only transverse motion with respect to the observer. For both of these examples, these state and measurement Equations (4.1) and (4.2) will be calculated explicitly, and the effects of transmitted signal parameters on KF performance will be presented and explored in detail.

5.2 Example 1: Two Rotating Rough Spheres

For this example, the geometry of the scatterers is as shown in Figure 5.1.

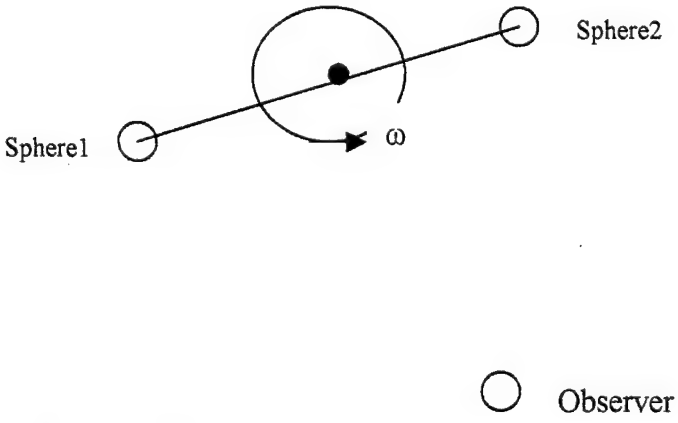

Figure 5.1: Example 1 Geometry

The system consists of two rough spheres connected by a non-reflecting rod which is rotating with angular frequency ω. The system will be illuminated with a high resolution VFM pulse with various durations and bandwidths which correspond to the measurement error variance bounds (CRLB) given in Table 5.1.

Table 5.1: Transmitted Signal Parameters

Signal	Duration (s)	Bandwidth (Hz)	var$[s - \hat{s}]$	var$[\tau - \hat{\tau}]$
VFM1	.25	1000	1e-1	1e-1
VFM2	.5	1000	1e-2	1e-1
VFM3	1	1000	1e-3	1e-1
VFM5	1	1	1e-1	1e-1
VFM6	1	100	1e-1	1e-2
VFM7	1	1000	1e-1	1e-3

It is also known that the signal to noise ratio affects the CRLB for both time-scale and time delay as discussed in Chapter 3. However, the final effect on the Kalman filter is the same as changing the transmitted signal parameters. The final effect being that the convergence as a function of measurement error is guided by the error covariance regardless of the effects. However, it should be noted that the signal to noise ratio's effect on the CRLB is multiplicative as discussed in Chapter 3, and therefore is an important factor. As most realizable systems are reverberation or peak transmitted power limited, it is the signal parameters over which the system designer has the best

control, and therefore present the more interesting (and useful) results of the Kalman filter response as a function of transmitted signal parameters.

The pulse has sufficient time-bandwidth product to resolve the rough spheres in time and frequency. By taking the auto-wavelet transform of the signal, the auto-ambiguity function of the SFE pulse is produced. This is shown in Figure 5.3.

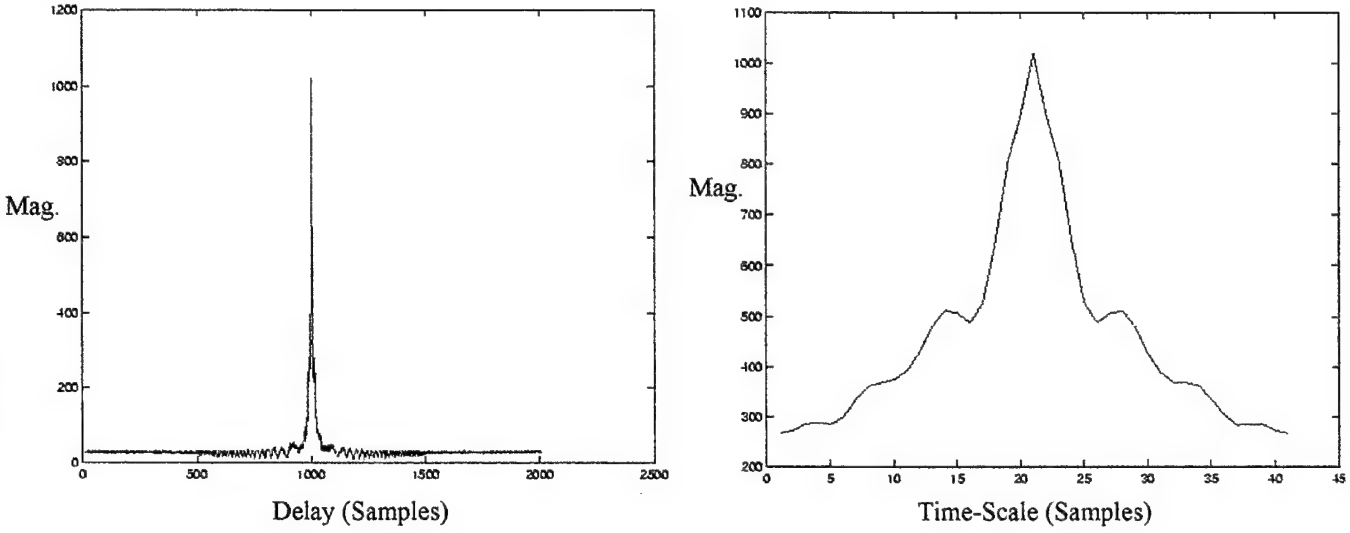

Figure 5.3: Auto-Ambiguity Function of a 1s 1000Hz VFM

5.3 Derivation of the State Transition Matrix

In this section, the equation of state for the system presented in section 5.2 is derived. By considering a few assumptions about the system. First, neglecting the effects of acceleration. In this, it is assumed that the system is rotating slowly enough to neglect angular acceleration, but fast enough to produce a measurable scaling of the return. Second, a reference point is chosen such that when the rod connecting the spheres is

perpendicular to the line of sight to the sensor, the relative delay is zero. The scale at this point is a maximum due to the fact that the component of velocity of the spheres is parallel to the line of sight, making it a maximum, thus producing the maximum scale. When the rod connecting the spheres is parallel to the line of sight, the component of tangential velocity parallel to the line of sight is zero – producing zero scale. Here the delay (+ and -) is a maximum. Figure 5.4 shows the details.

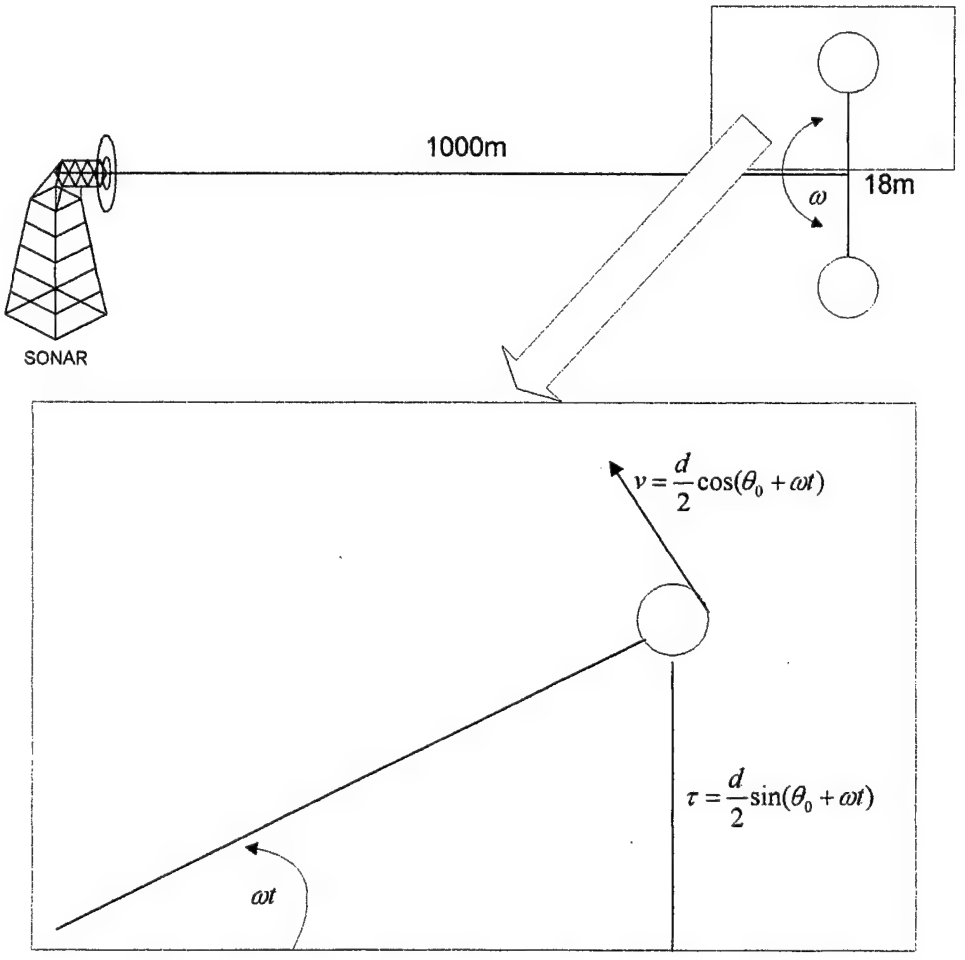

Figure 5.4 Scale and Delay as a Function of Position or Time

Now knowing each scale and delay as a function of time, the state transition matrix is derived.

In the x-y plane, it is known [72] that the coordinate transformation, in this case a rotation, is given by the following:

$$\begin{bmatrix} x \\ y \end{bmatrix}_{new} = \begin{bmatrix} \cos\theta & -\sin\theta \\ \sin\theta & \cos\theta \end{bmatrix} \begin{bmatrix} x \\ y \end{bmatrix}_{old} \tag{5.1}$$

where $\theta=\theta_0+\omega t$.

The trick is to derive a similar expression for the new scale and delay. This is done by writing down the following equation:

$$\begin{bmatrix} s \\ \tau \end{bmatrix}_{new} = [G] \begin{bmatrix} s \\ \tau \end{bmatrix}_{old} \tag{5.2}$$

Where G is a 2x2 matrix. The following are also used:

$$s_{new} = \frac{1+\frac{v}{c}}{1-\frac{v}{c}}; \quad v = \frac{d}{2}\cos(\theta_0 + \omega t) \tag{5.3a}$$

$$\tau_{new} = \frac{2}{c}(r + \frac{d}{2}\sin(\theta_0 + \omega t)) \tag{5.3b}$$

$$s_{old} = \frac{1+\frac{v}{c}}{1-\frac{v}{c}}; \quad v = \frac{d}{2}\cos(\theta_0) \tag{5.3c}$$

$$\tau_{old} = \frac{2}{c}(r + \frac{d}{2}\sin(\theta_0)) \tag{5.3d}$$

Using (5.3a-d) in 5.2 and solving for G

$$\begin{bmatrix} s \\ \tau \end{bmatrix}_{new} = \begin{bmatrix} 1+\dfrac{\omega d\cos(\omega t)}{2(c-\omega\dfrac{d}{2}\cos(\omega t_0))} & 0 \\ 0 & 1+\dfrac{d\sin(\omega t)}{2(r+\dfrac{d}{2}\sin(\omega t_0))} \end{bmatrix} \begin{bmatrix} s \\ \tau \end{bmatrix}_{old} \tag{5.4}$$

Equation (5.4) is the form needed for the state transition matrix. In order to show that this is the correct state transition matrix, the actual and noiseless state predicted scales and delays are plotted in Figure 5.4

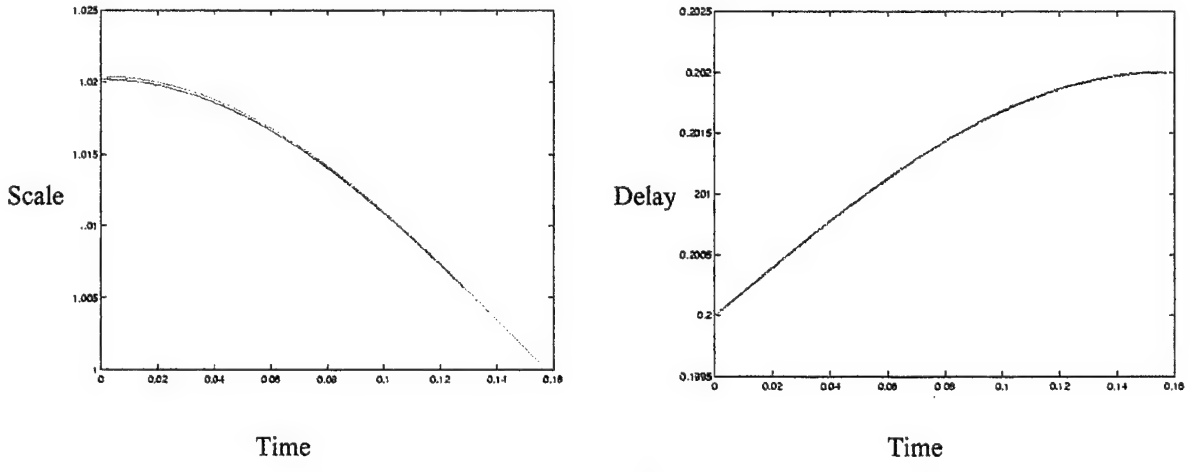

Figure 5.5: Expected and Predicted Values of Scale and Delay vs. Time

Figure 5.5 shows that the state transition matrix produces the desired results, producing the new scale and delay at time t, given the measurement at time t-1 – meaning the

previous measurement. Now, for the purposes of the simulation the state equation is used:

$$\hat{w}_{T|T-1}(x) = A(t,t-1)\hat{w}_{T-1}(x) \tag{5.5}$$

This gives the value of the spreading function at time T conditioned on the previous value at T-1. The state noise is considered to be zero mean, white, Gaussian noise with a known covariance R_{vv}.

5.4 Rough Rotating Spheres – Data Creation Algorithm

In this section, the algorithm used to produce the data necessary for the examples in this chapter is discussed. It is desired to track time-scale and time-delay, and therefore two data sets are produced. First, the time-scale and time-delay for the model portion of the algorithm is created. Second, the measurements of the actual system (i.e. the data) are calculated. Here, the noisy measurements are produced that are statistically correct having variances of white Gaussian noise added which correspond to the predicted CRLB for the transmitted signal used. Not only are the measurements noise, but inaccuracies in the model are introduced via the measurements. The idea here is that the model does not accurately represent the actual system. For example, in the examples to follow, the distance, d, between the spheres is larger for the simulated measurement data that for the model. In this way, the ability of the Kalman filter to track measured data is tested. Also, the point is found at which inaccuracies in the measurements (as a function of transmitted signal duration and bandwidth) inhibit the ability of the Kalman filter to estimate the actual time-delay and time-scale as a function of time. Figures 5.6 and 5.7

give the plots of time-scale and time-delay for the measured and model portions of the data creation algorithm.

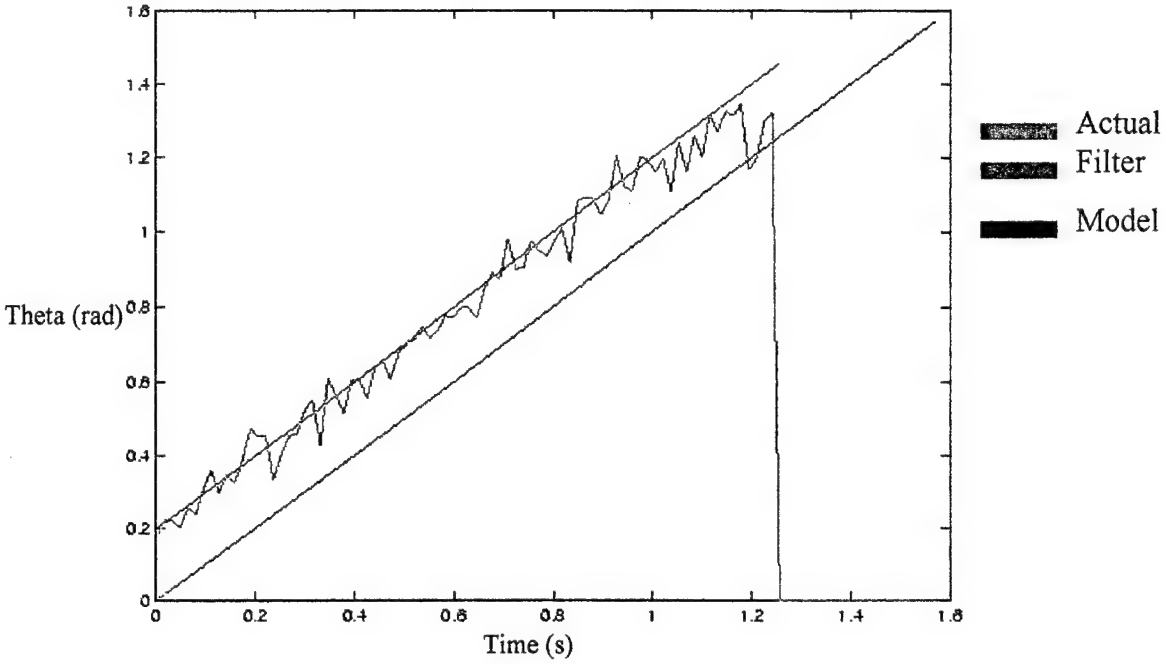

Figure 5.6: Theta as a function of time for Measurement and Model

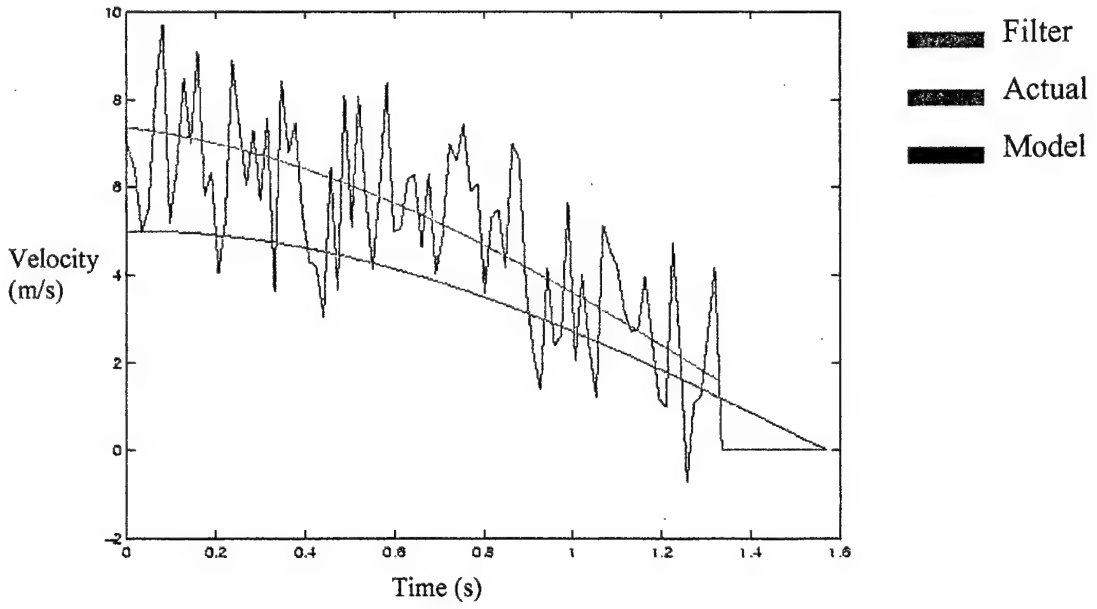

Figure 5.7: Velocity as a function of time for Measurement and Model

Changing only the distance between centers, significant differences in the model and measurement quantities can be produced for both time-delay and time-scale (theta and velocity).

By using the above algorithm, various aspects of tracking, detection, and signal design can be related. This is accomplished by observing that the TW improves processing gain [4] (lowering measurement inaccuracies). Work in Chapter 3 showed that longer durations and higher bandwidths lower the CRLB for estimates that can be made on time-delay and time-scale. This, in turn, as illustrated in the following section, affects the ability of the Kalman filter to track.

5.5 Rotating Spheres – Results

The results of the processing for the rotating spheres example which was discussed above are now given. First, the results for time-delay measurements which correspond to the angle theta (as seen in Figure 5.8-5.10) are given.

It is desired to show the effect of changing the mean-squared bandwidth of the transmitted signal on the Kalman filter's ability to track. Beginning with Figure 5.8 which contains plots of three quantities vs. time. These are the model theta, the actual (measured) theta, and the updated or filtered theta, the quantity of interest.

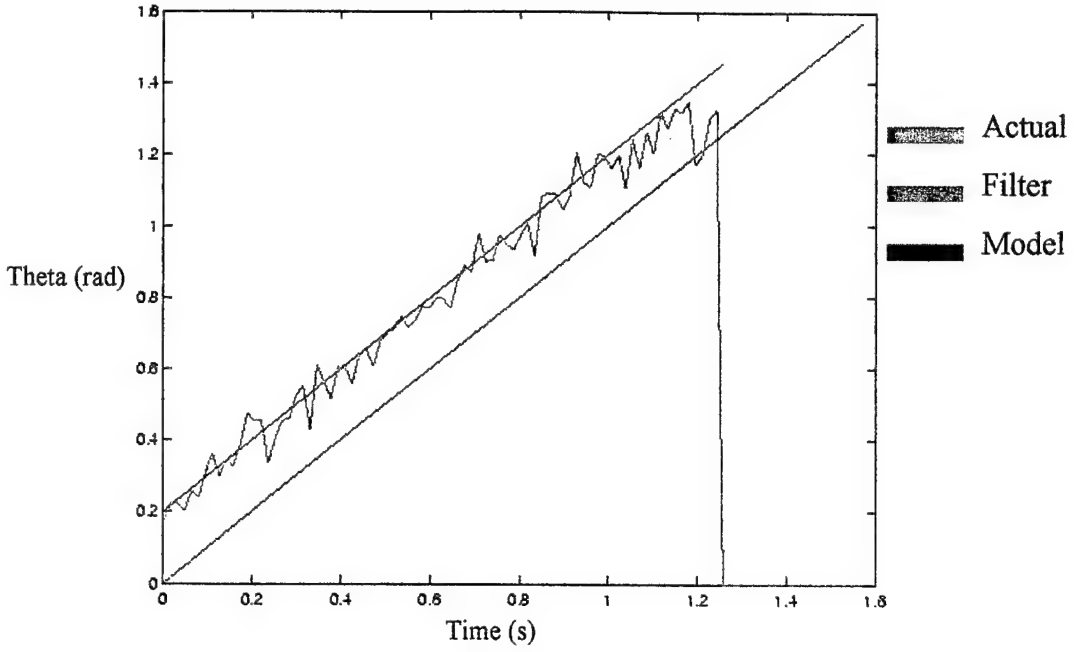

Figure 5.8: Theta Vs. Time: Transmitted Signal VFM 1 (Duration 1s, BW 1000 Hz)

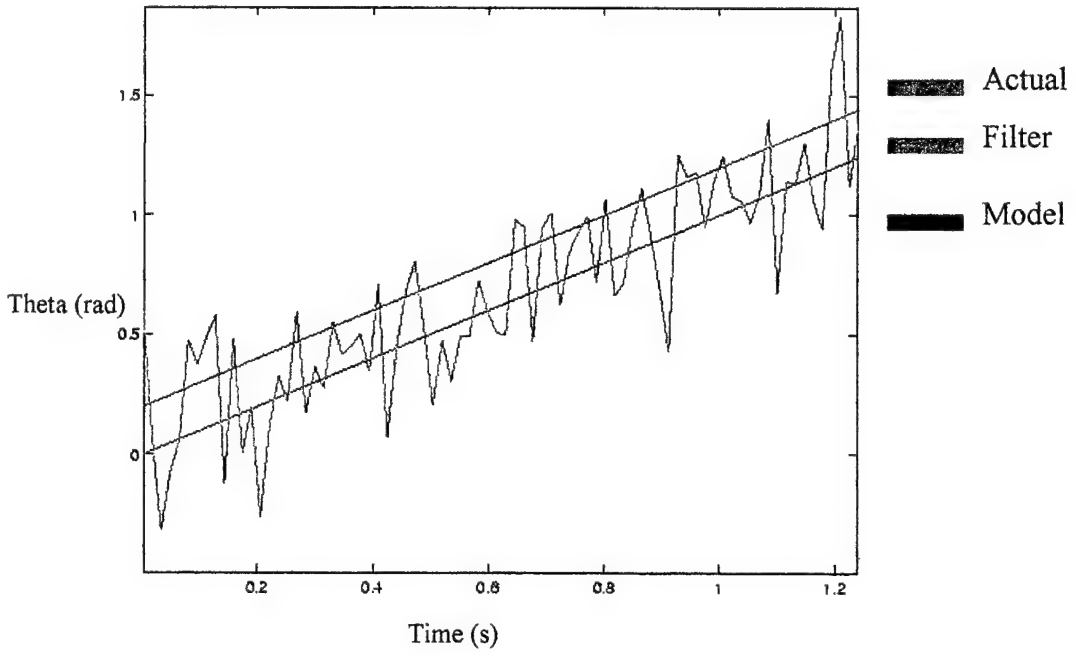

Figure 5.9: Theta Vs. Time: Transmitted Signal VFM 1 (Duration 1s, BW 100 Hz)

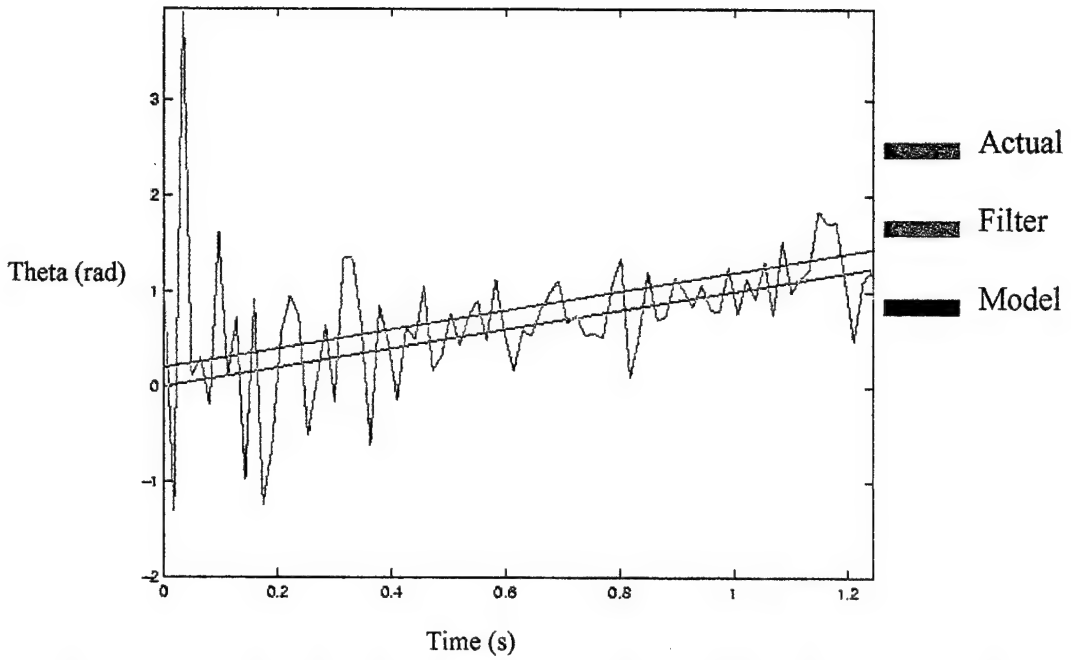

Figure 5.10: Theta Vs. Time: Transmitted Signal VFM 1 (Duration 1s, BW 1 Hz)

As seen from the above series of plots, the bandwidth of the signal determines the convergence. Figure 5.8 shows that the filtered estimates reflect what is going on in the actual kinematics. However, as the bandwidth is decreased, the filter follows the model completely and no longer tracks the actual kinematics. This is entirely due to the effective bandwidth of the VFM signal, as all other parameters have been kept constant. The series 5.5-5.7 is interpreted as follows. First the higher bandwidth VFM has enough resolution to accurately track the spheres as they rotate as seen in Figure 5.8. Second, Figure 5.8 shows that a 10x reduction in bandwidth causes the filter to diverge (i.e. ignore the measurements). Lastly when the bandwidth is reduced essentially to a tone, the noise of the measurements is very large and at first fluctuates wildly, until the gain is so small that the measurements are ignored completely.

5.6 Linear Highlight Motion – Results

In this section, the results of Kalman filtering algorithm operating on a different kinematic system are presented. In this system, a highlight in linear motion. For the simplicity of illustration, the results for the single highlight are given.

5.6.1 Linear Motion – State Transition Matrix Derivation

In this section, the state transition matrix for a single highlight, moving with constant velocity v_0 in a straight line is derived. The geometry for this scenario is given in Figure 5.8.

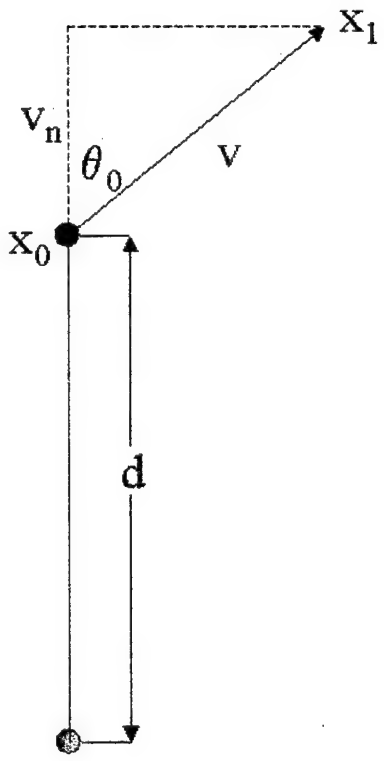

Figure 5.11. Linear Highlight Motion Geometry

The state transition matrix is derived as before in Section 5.3. However, in this instance, the normal velocity is constant and therefore A_{11}=1. The quantity to track which changes with time is the relative delay. This is given by the standard geometric/trigonometric relationships. The result for the state transition matrix is

$$\begin{bmatrix} s \\ \tau \end{bmatrix}_{new} = \begin{bmatrix} 1 & 0 \\ 0 & \dfrac{v_0(t+1)\sin\theta_0}{\tau_0} \end{bmatrix} \begin{bmatrix} s \\ \tau \end{bmatrix}_{old} \tag{5.6}$$

where τ_0 is the one way delay time from the transmitter/receiver to the highlight at x_0 and θ_0 is the angle the trajectory the highlight makes with a perpendicular to the line of sight.

This example differs from the previous example in that the extended Kalman filter for the delay is not necessary. Here delay appears as both a measured and modelled parameter. This changes only one quantity in the Kalman filter derivation, which is the element of H_{22}. Here, H_{22} =1 since the measured quantity is simply the quantity to track. For this example, all of the parameters used in the first example are also used in this example. The signals used are the same, with changes in duration and in bandwidth. The algorithm for production of data is the same, however the parameter changed to produce model vs. measured data is the angle θ_0. This again causes the modeled velocity (normal) and delay as a function of time to differ from the measured.

5.6.2 Linear Highlight Motion, Velocity Tracking

This section presents the results for the velocity tracking portion of the simulation. Three results are presented. First, given in Figure 5.12 a plot containing three curves. These are: in green, the filtered output, red is the actual trajectory, blue is the modeled normal velocity. In this case the measurement accuracy is such that the Kalman filter tracks immediately to the data.

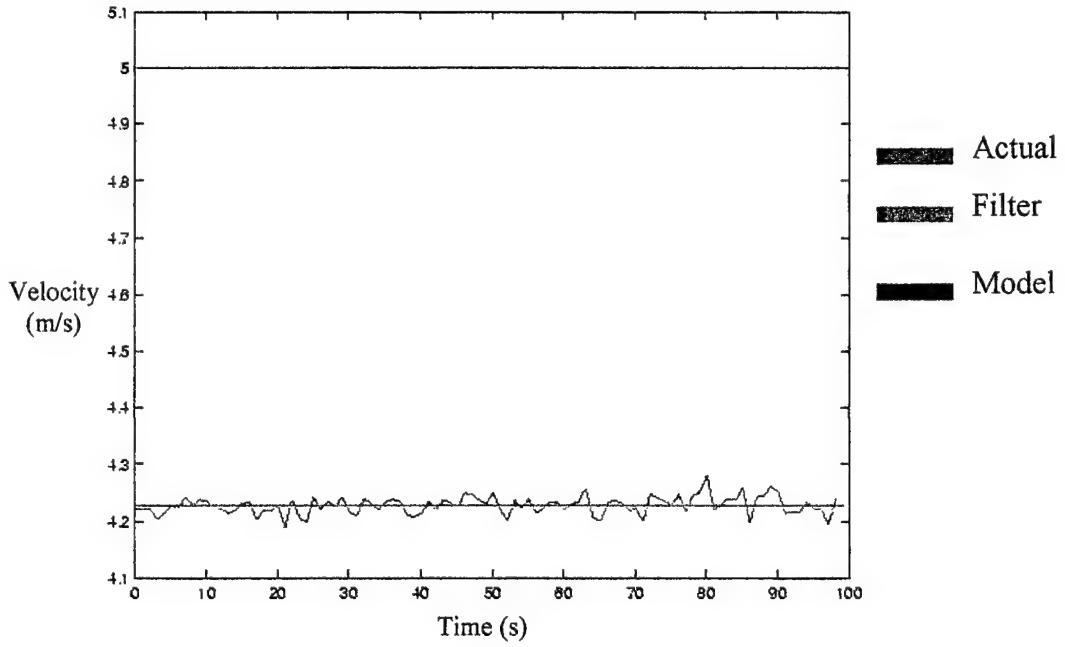

Figure 5.12: Velocity vs. Time Transmitted Signal: VFM 1

The next plot, Figure 5.13, shows how the filter begins to lose the track as the measurement error is increased.

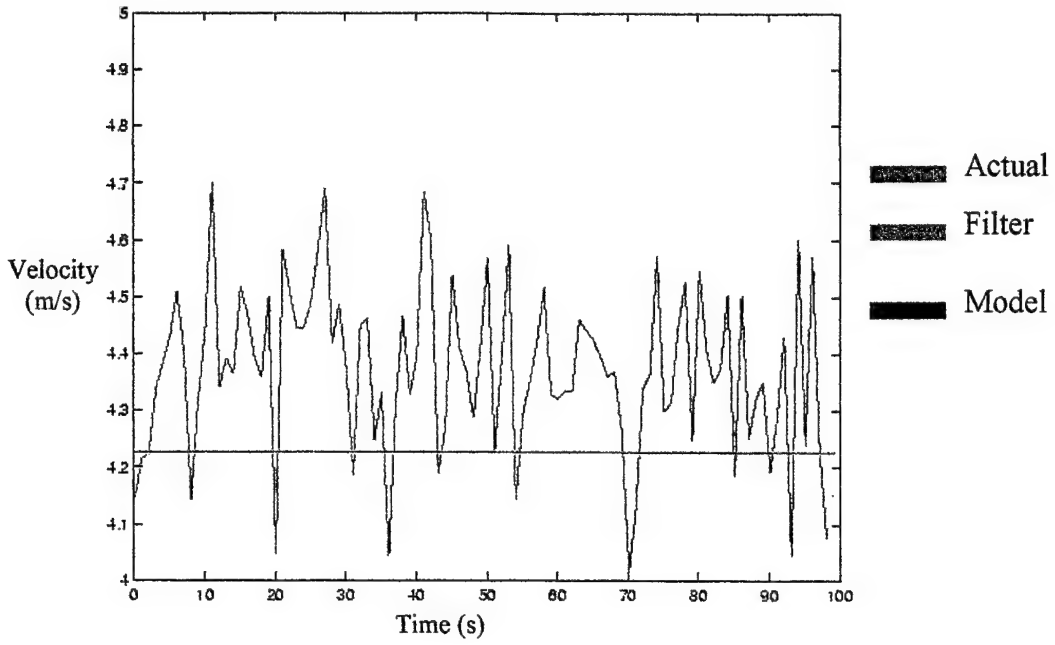

Figure 5.13: Velocity vs. Time: Transmitted Signal: VFM2

The last plot shows how the filter rejects the new data and tracks to the model.

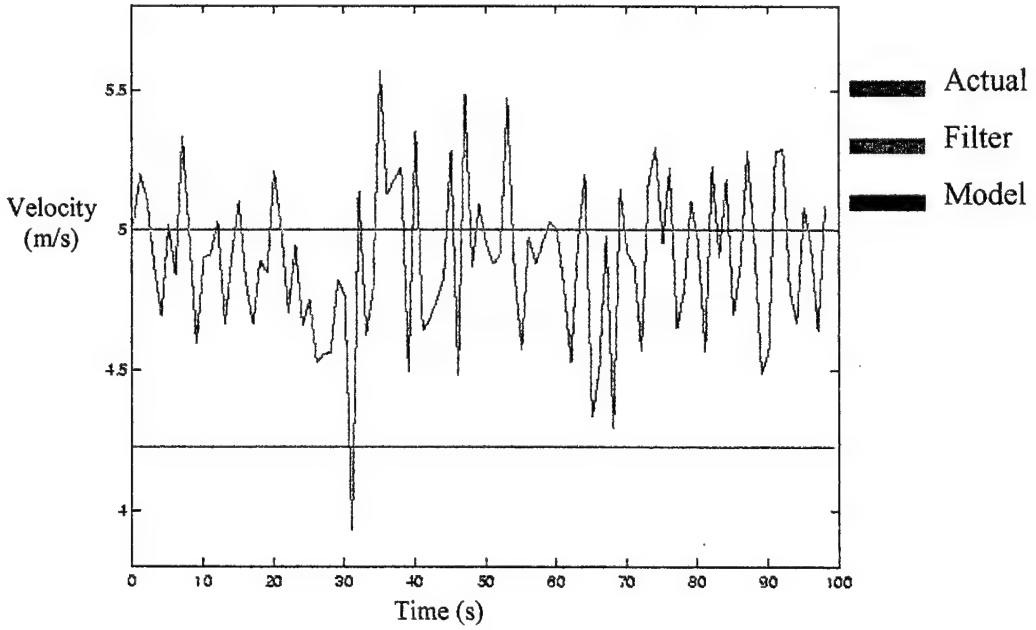

Figure 5.14: Velocity vs. Time: Transmitted Signal: VFM3

5.6.3 Linear Highlight Motion: Delay (Range) Tracking

In this section the results of the delay portion of the simulation are given. Again, the three plots given correspond to the signals given in Table 5.2. It is seen that as the bandwidth is increased, for a fixed SNR, the ability of the Kalman filter to track the delay can be directly related to the transmitted signal's bandwidth. In Figure 5.14 it is seen that the Kalman filter tracks to the received data. This is due to the fact that the measurement error is very small, and therefore, the filter "believes" the data.

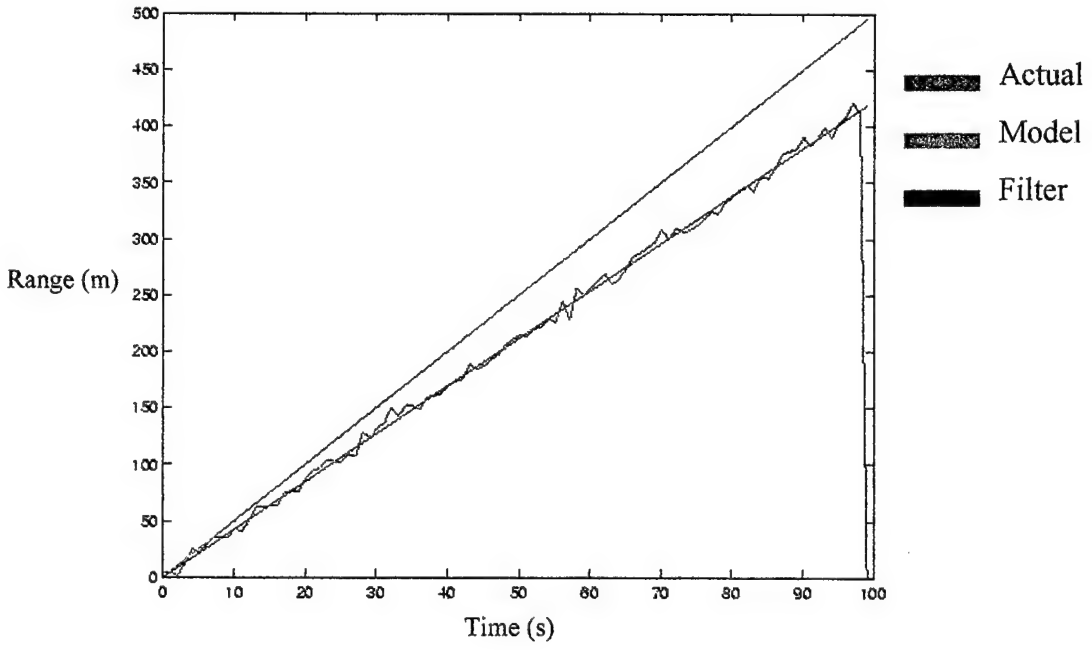

Figure 5.15: Range vs. Time, Transmitted Signal: VFM4

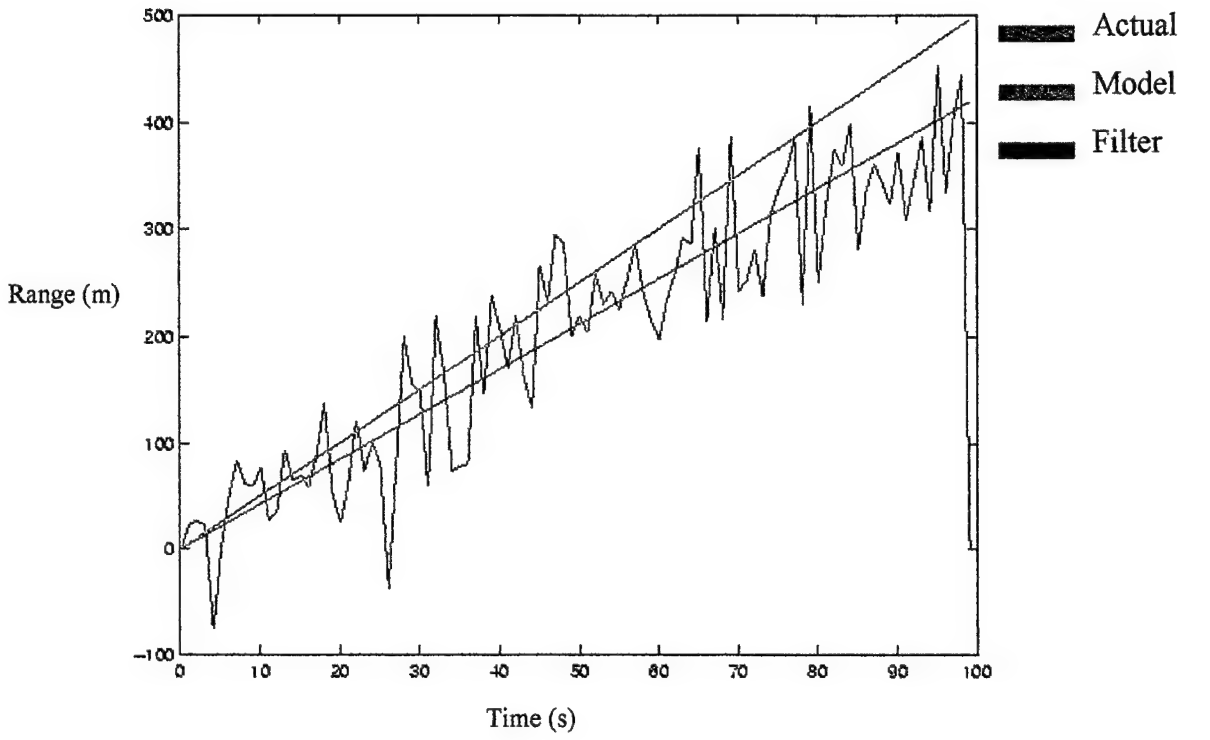

Figure 5.16: Range vs. Time, Transmitted Signal VFM5

Figure 5.16 shows that the Kalman filter tracks to the data even though the measurement errors are beginning to get high. The filter finally breaks down and begins to track to the model in Figure 5.17.

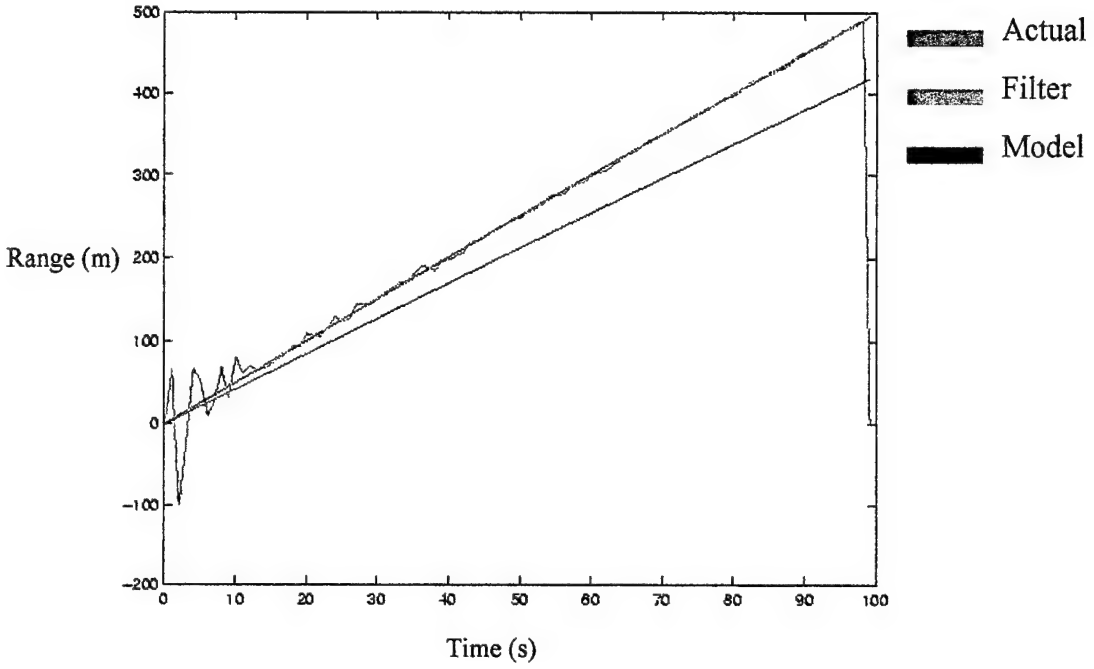

Figure 5.17: Range vs. Time, Transmitted Signal VFM5

5.7 Performance Monitoring

In this section, a method of determining the performance of the Kalman filter is introduced. This method includes the monitoring of the spectrum of the innovations sequence. The innovations sequence was discussed in detail in Chapter 4. It is known from this discussion, that for the optimal estimator [51] the innovations sequence is white. In this section, the results of calculating the innovations sequence for the sphere moving in circular motion are presented. For this example, plots of the Kalman filter output for the velocity and for the angle theta are given. In the example chosen, the

Kalman filter is able to track the true velocity, however, the delay portion of the filter does not converge to the true angle. This is shown in Figure 5.18.

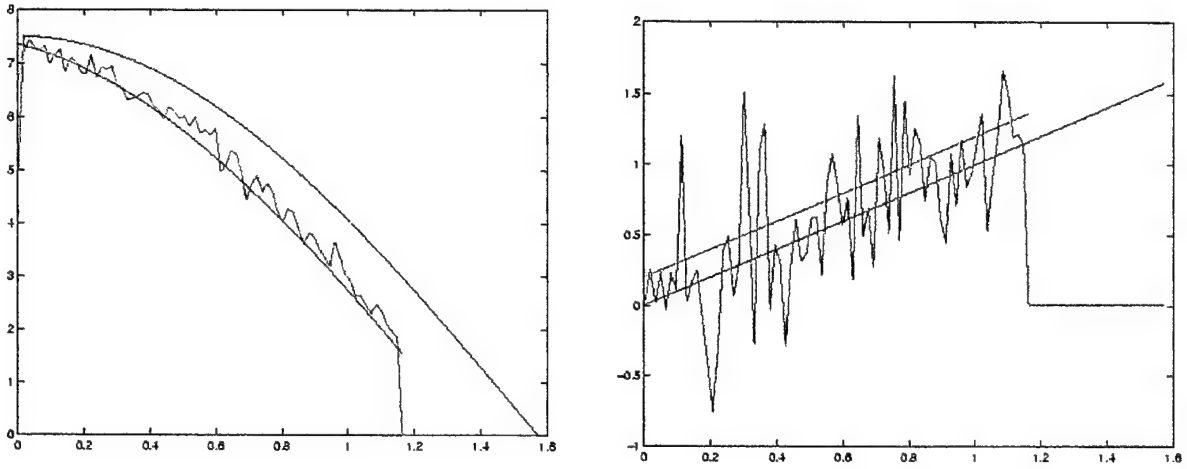

Figure 5.18. Velocity and Angle Kalman Filter Output, Model, and True

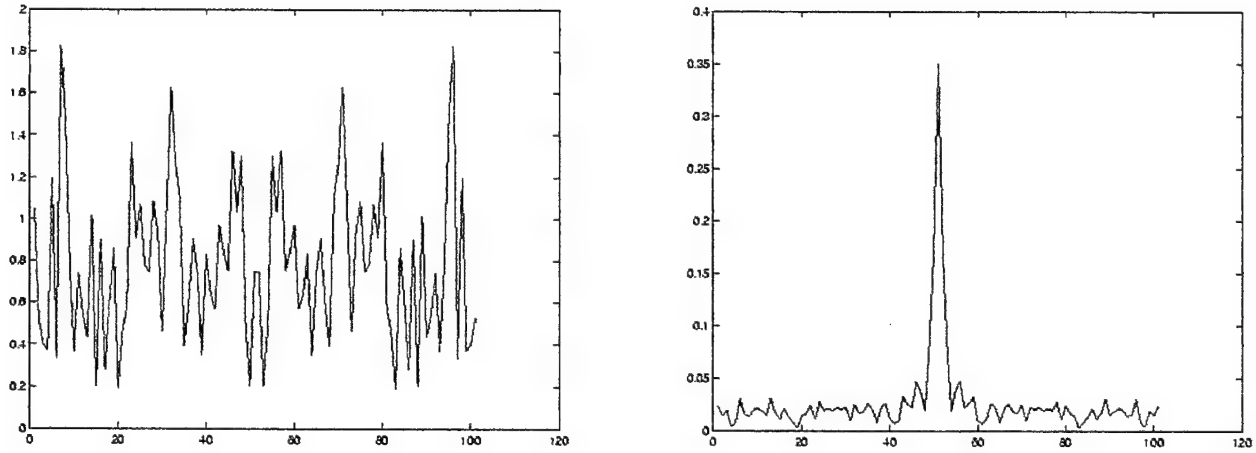

Figure 5.19: Innovations Spectrum for Optimum and Sub-Optimum Kalman Filters

From the above Figure 5.19, it is seen that the "whiteness" of the spectrum of the innovations sequence is a good indicator as to the operation of the Kalman filter. One can imagine a recursive model updating algorithm being incorporated into the state equation portion of the tracker in order to optimize the Kalman filter in terms of broadening the spectrum of the innovations sequence and thus optimizing the Kalman filter.

5.8 Conclusions

The above observations lead to the conclusion that the transmitted signal's parameters, i.e. duration, bandwidth, and even shape (as this too affects the CRLB as shown in Chapter 3) can affect the ability to track the highlights in time-scale and time-delay. It has been shown that the Kalman tracking algorithm is easily reconfigured for different Kinematic scenarios. The main point of this work is to show that the issues of signal design, detection, and tracking can be intimately related. The above analysis shows that the theoretical calculations of the Cramer –Rao lower bound on the variance of the estimates that can be made have a direct impact on the Kalman filters ability to converge to the actual scenario and to balance the model and measurement portions of the tracking algorithm. The above examples have shown that a model based detection/tracking algorithm can be designed for which there exist observables (i.e., innovations and Kalman Gain) which provide a direct measure of the performance of the tracker.

CHAPTER 6

Summary, Conclusions and Further Research

6.1 Summary of Results

The primary focus of this thesis has been to derive, implement and investigate a recursive algorithm, based on a model based Kalman filtering approach, to estimate and update the location of peaks in the wideband spreading function which correspond to the kinematic properties of an object. In this, primarily interest has been in the physical variables of position and velocity with the actual observables being time-scale and time-delay in a range-scale map produced by a wideband matched filter. Several original contributions were made in the completion of this task.

The primary contributions made in this thesis are:

- Derivation of the multidimensional Kalman filter for total spreading function updating and estimation.
- Reduction of the dimensionality of the above derivation to handle updating and estimation of the peak locations in a range-scale map.
- Relating the state variables to the measured quantities in the extended Kalman filter derivation.
- Derivation of the Cramér – Rao lower bound for time-scale and time-delay for the wideband signal model and wideband detector.
- Implementation of the Kalman filter for spreading function updating and executing illustrative examples.

- Provide a theoretical and experimental (through simulation) common thread which begins with the transmitted signal design, ambiguity properties of the transmitted signal and the estimation properties of the signal including the effects of noise (CRLB) and connects these properties to the eventual convergence issues of the extended or linearized Kalman filter.

The thesis began by introducing the necessary background for development of the Kalman filtering algorithm. This included a cursory review of wavelet transforms, Kalman filtering, and applications of the output of our filter to model based signal processors in the form of the wavelet transform estimator-correlator.

Then, using the slowly fluctuating point target signal model, the Cramér-Rao lower bound on the estimation errors for time-scale and time-delay for wideband transmitted signals was derived. This contribution is important as this relates transmitted signal properties such as alpha moment, envelope shape in the time-frequency plane, bandwidth, and duration, to variances on errors associated with making estimates on time-delay and time-scale using a wideband matched filter detector.

Having the relationships discussed in the previous paragraph, the Kalman filter which tracks the kinematic properties of the system based on the measurements (estimates) made on time-delay and time-scale using the wideband probing signal can be discussed. Within the derivation of the Kalman filter a measurement equation becomes an important quantity. In this case a matrix form of the wideband matched filter is the measurement.

Associated with the measurement equation, is a quantity referred to as the measurement error, this measurement error is assumed to be zero mean, Gaussian, and white with a known variance, namely, the Cramér-Rao lower bound is used. In this way, the transmitted signal parameters are related to the errors associated with the measurements, these errors can then be related to the ability to track the kinematic parameters of the physical system using the Kalman filter. It should also be mentioned that the parameters of the detection process, such as signal to noise ratio also appear in the Cramér-Rao lower bound.

Following the derivation of the total wideband spreading function predictor-corrector version of the Kalman filter, the problem is reduced form a tensor-matrix problem to a matrix-vector problem by using a lexiographic ordering technique. In this way, an extended Kalman filter that tracks only the highlights of interest (peaks in the range-scale map which are local phenomena for which the CRLB is valid). In this way state equations which predict the kinematics of multiple highlights can be derived, thus, reducing the dimensionality of the problem. In this way, a model updated state equation is used with a wideband matched filter measurement equation to predict kinematic properties based on the past measurements.

Once the extended Kalman filtering algorithm was derived, a computer implementation/simulation was made. Using the simulation, two data sets were produced. The first data set corresponded to the model. The second set corresponded to the physical system. These were intentionally made to be different to test the ability of

the Kalman filter to track the physical system even though the model did not accurately reflect the physical processes. In other words, the ability of the Kalman filter to balance the accuracy of the measured data to the expected values predicted by the model (state equation) was tested. In this way, it could be shown that the signals with wider bandwidth produces lower CRLB's on time-delay, and thus allowed us to have better estimates on time-delay. This in turn allowed the Kalman filter to better track the physical position of the scatterer. Also, it was shown that longer duration signals produced lower CRLB's on time-scale. This in turn showed that the accuracy of estimates on time-scale could be better "believed" by the Kalman filter. This in turn was used to show that the Kalman filter could better track the true velocity of the scatterer. Interestingly, plotting curves of the CRLB for delay and scale showed that signal to noise ratio and duration or bandwidth could be "traded off" in the sense that if a lower SNR exists, a higher bandwidth or longer duration signal can be used to overcome the shortcoming. Figure 6.1 illustrated the topics covered and their interrelation. Using the above framework, each of the blocks in Figure 6.1 illustrates a starting point for further research. This is the topic of the next section.

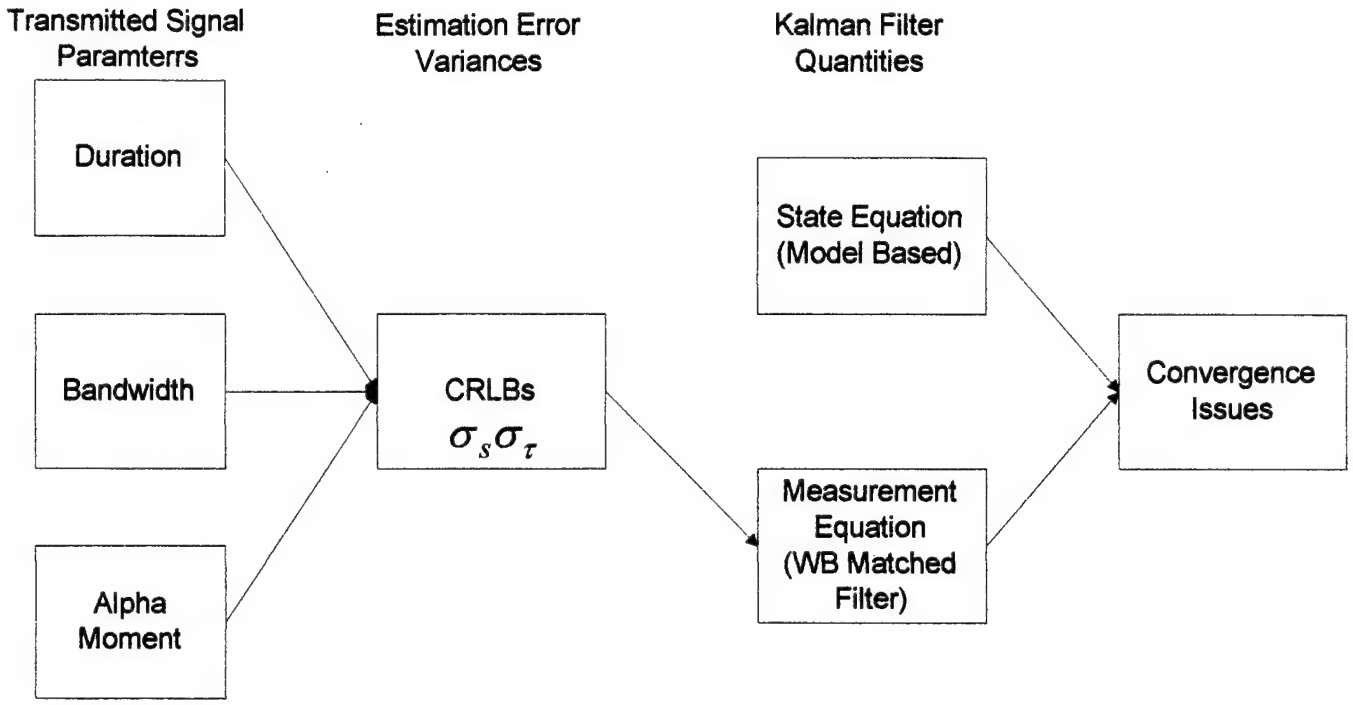

Figure 6.1: Outline of Topics Covered and Their Interrelationship

6.2 Recommendations For Further Research

In this thesis several questions which are stand alone topics for further research have arisen. In this section, avenues for pursuing these topics are discussed.

In Chapter 3, CRLB's for time-delay and time-scale were derived. Examples for the uncoupled estimated by making assumptions on the shape of the signal, and by using a real signal were produced. One important topic for further research is to do an exhaustive study of the full CRLB for any signal. This will involve the more difficult to interpret

cross term J_{12}. As this is an important signal design issue, an extensive parametric study should be completed to show how the transmitted signal parameters affect coupled estimates.

Next, the Kalman filter should be implemented for a larger number of highlights for a more realistic object should be investigated. This should include an exhaustive study of the tuning parameters for tracking the highlight structure of a complex object. Included in this study should be a study of the robustness of the approach, as well as a study of the effects of errors in the initial estimates should be investigated.

Stability issues should also be investigated along with the issue of efficient implementation for a larger number of highlights. Bierman [73] has extensively investigated the problem of efficient implementations for Kalman filtering routines.

Lastly, the cases for non-white and/or non-Gaussian measurement and state noises should be investigated. In this case, the noise in the measurements should include reverberation terms. This in itself is an important and self contained research topic, namely, deriving the CRLB for time-delay and time-scale under reverberation limited conditions.

In the larger picture it would be desirable to further, in a fundamental sense, the multidimensional issues raised in Chapter 4. Remembering that in Chapter 4, it was shown that the state equation and measurement equations contain four dimensional matrix multiplications. Mathematics, specifically tensor analysis coupled with operator

theory should be investigated deeply to gain better understanding of the relationships between these tensor/matrix operations and operator theory. In the case of the state equation, it was shown that each sub-matrix operating on a state variable was a state transition of that variable. The tensor relationship in the measurement equation is far less clear. Usually, to dispense with the higher dimensionality, assumptions such as wide-sense-stationary –uncorrelated scattering are invoked. Better mathematical understanding of these mechanisms may allow the relaxation of some of these assumptions and provide a more general solution to the wideband problems at hand.

Further, work completed here should be used to highlight the importance algorithms for multi-feature/highlight object tracking. Future research should investigate the use of learning algorithms for application to model based signal processing. This would enable systems to learn from the environment and change their own operating parameters to better interact with the environment. These would be truly intelligent systems. In the future, autonomous systems should be developed to apply learning algorithms to update statistical models. Applications would include image tracking, dynamic, real-time, medical imaging displays, high resolution radar and sonar, and intelligent vision systems for industrial robots. The ideas begun in this thesis, if taken to their ultimate development would enable robotic systems to create a "mental image" of an object and track its motion based on the robot's "knowledge" of kinematics (i.e., range of possible motion). Using the kinematics in combination with the ability to follow object features through rotations and translations (i.e., various aspects over time) provides a robust tracking ability for future detection/estimation systems.

BIBLIOGRAPHY

[1] Urick, R.J., Principles of Underwater Sound, 3rd Edition, McGraw Hill, New-York, 1983.

[2] Burdic, W.S., Underwater Acoustic System Analysis, 2nd Edition, Prentice Hall, Englewood Cliffs, New-Jersey, 1991.

[3] Etter, P.C., Underwater Acoustic Modeling, Elsevier Applied Science, London, 1991.

[4] Young, R.K., Wavelet Theory and its Applications, Kluwer Academic Publishers, Boston, 1993.

[5] Bello, P. "Characterization of Time-Variant Linear Channels," *IEEE Trans. On Communication Systems*, pp. 360-393, Dec. 1963.

[6] Sibul L.H., Weiss L.G., and Dixon T.L., *"Wavelet Transform Domain Implementation of the Estimator Correlator for Detection of Distributed Objects in Stochastic Propagation Media"*, Proc. Of the Conf. On Info. Sciences and Systems, Johns Hopkins, March 19-21, 1997.

[7] Sibul L.H., Sidahmed S.T. , Dixon, T.L. , Weiss L.G.,"Wavelet Domain Implementation of the Estimator-Correlator and Weighted Wavelet Transforms," invited paper at the *13th Annual Asilomar Conference on Signals, Systems, and Computers*, Pacific Grove, CA, Nov 3-6, 1996.

[8] Weiss, L.G., Wideband Inverse Scattering and Wideband Deconvolution of Acoustic Signals Using Wavelet Transforms, Ph.D. Thesis, Penn State University, 1993.

[9] Roan, M.J. and Sibul, L.H., "Performance Quantification for The Wavelet Transform Domain Estimator-Correlator", *CISS*, Princeton University, New Jersey, March 22-24, 1998.

[10] Kailath, T. "The Innovations Approach to Detection and Estimation Theory", *Proc. IEEE*, Vol. 58, 1970.

[11] Kailath, T., Lectures on Kalman and Weiner Filtering, Academic Press, New York, 1970.

[12] Anderson, B.D. and Moore, J.B., Optimal Filtering, Prentice Hall, Englewood Cliffs, New Jersey, 1979.

[13] Candy, J.V. and Rozsa, P., "Safeguards Design for a Plutonium Concentrator An Applied Estimation Problem", *Automatica*, Vol. 16, 1980.

[14] Marlin, W.C. and Stubberud, "The Innovation Process With Applications to Identification", in C.T. Lewis (Ed.), Control and Dynamic Systems, Academic Press, New York, 1976.

[15] Tretter, S.A., Introduction to Discrete Time Signal Processing, Wiley, New York, 1976.

[16] Van Trees, H.L., Detection, Estimation and Modulation Theory, Part III, Wiley, New York, 1971.

[17] Cramér, Mathematical Methods of Statistics, Princeton University Press, Princeton, New Jersey, 1946.

[18] Silo, V., Kung, X., Adaptive Signal Processing Algorithms, Stability and Performance, Prentice Hall, Englewood Cliffs, New Jersey, 1995.

[19] Fowler, M.L., Signal Detection Using Time-Frequency and Time-Scale Methods, Ph.D Thesis in Electrical Eng., Penn State University, December, 1991.

[20] Ricker, D.W. "The Doppler Sensitivity of Large TW Phase Modulated Waveforms", *IEEE Trans. Sig. Proc.* Vol. 40, No. 10, pp. 2406-2413, Oct. 1992.

[21] Altes, R.A., "Some Invariance Properties of the Wideband Ambiguity Function", *JASA*, Vol. 53, No. 4, pp. 1154-1160, 1973.

[32] Altes, R.A., "Target Position Estimation in Radar and Sonar, Generalized Ambiguity Analysis for Maximum Likelihood Parameter Estimation", *Proc. IEEE* Vol. 67, pp. 920-930, 1979.

[23] Weiss, L.G., "Wavelets and Wideband Correlation Processing", *IEEE Signal Processing Magazine*, pp. 13-32, January, 1994.

[24] Weiss, L.G., "Time-Varying System Characterization for Wideband Input Signals", Signal Processing, Vol. 55, pp. 295-304, 1996.

[25] Green, P.E., Radar Astronomy – Chapter 1, Evans, J.V, (Ed.), MIT Lincoln Laboratory, McGray Hill, New York, 1968.

[26] Sibul, L.H., Roan, M.J., and Hillsley, K.L., "Wavelet Transform Techniques for Time Varying Propagation and Scattering Characterization", *32nd Asilomar Conf. On Signals, Systems, and Computers*, Pacific Grove, CA., Nov. 1-4, 1998.

[27] Naparst, H.C., "Dense Target Signal Processing", *IEEE Trans. On Information Theory*, Vol. 37, No. 2, pp. 317-327, March 1991.

[28] Tewfik, "Wavelets in Optimal Radar Range-Doppler Imaging", *26th Asilomar Conf. on Signals, Systems, and Computers*, Pacific Grove, CA., Oct. 26-28, 1992.

[29] Altes, R.A., "Some Invariance Properties of the Wideband Ambiguity Function", *JASA*, Vol. 53, No. 4, pp. 1154-1160, 1973.

[30] Altes, R.A., "Target Position Estimation in Radar and Sonar, Generalized Ambiguity Analysis for Maximum Likelihood Parameter Estimation", *Proc. IEEE* Vol. 67, pp. 920-930, 1979.

[31] Young, R.K., Wideband Space Time Processing and Wavelet Theory, Ph.D. Thesis, Penn State University, August, 1991.

[32] Kelly, E.J. and Wishner, R.P., "Matched-Filter Theory for High Velocity Targets", IEEE Trans. On Military Electronics, Vol. 9, pp. 56-69, 1965.

[33] Dixon, T.L., Wideband Imaging of Distributed Objects Using Wavelet Transforms and Generalized Inverse Theory, Ph.D. Thesis, Penn State University, August, 1994.

[34] Maas, P., "Wideband Approximation and Wavelet Transforms" in Grunbaum, F.A., and Bernfield, (eds.), Radar and Sonar Part II, Springer-Verlag, New York, 1992.

[35] Kaiser, G., A Friendly Guide to Wavelets, Birkhauser, Boston, 1994.

[36] Daubechies, I., Ten Lectures on Wavelets, SIAM, Philidelphia, 1992.

[37] Daubechies, I., "The Wavelet Transform, Time-Frequency Localization, and Signal Analysis", *IEEE Trans. on Information Theory*, Vol. 36, pp. 961-1005, 1990.

[38] Hernandez, E., and Weiss, G., A First Course on Wavelets, CRC Press, Boca Raton, Fl., 1996.

[39] Meyer, Y, and Ryan, R.D., Wavelets and Applications, SIAM, 1993.

[40] Strang, G. and Nguyen, T., Wavelets and Filter Banks, Wellesley-Cambridge Press, Welleslely, MA., 1996.

[41] Proakis, J.G., Digital Communications, Mcgraw-Hill, New York, 1995.

[42] Cohen, L., Time-Frequency Analysis, Prentice Hall, Englewood Cliffs, New Jersey, 1995.

[43] Ziomek, L.J., Underwater Acoustics, Academic Press, Orlando, FL., 1985.

[44] Ziomek, L.J., A Scattering Function Approach to Underwater Acoustic Detection and Signal Design, Ph.D. Thesis, Penn State University, Oct. 1981.

[45] Chaiyasena, P. Sibul, L.H., and Banyaga, A., "Wavelet Transforms, Wideband Ambiguity Functions, and Group Theory", *Proc. 26th Asilomar Conf. on Signals Systems, and Computers*, Pacific Grove, CA., Oct. 1992.

[46] Sibul, L.H., Chaiyasena, P., and Fowler, M.L., "Signal Ambiguity Functions, Wigner Transforms, and Wavelets", *Proc. of International Conf. on Signal Processing and Digital Filtering*, Lugano, Switzerland, pp. 214-217, 1990.

[47] Weiss, L.G., Young, R.K., Sibul, L.H., and Banyaga, A.,"Group Theoretic Aspects of Signal Processing in the Time-Frequency and Time-Scale Domains", *Conference on Info. Sciences and Systems, Princeton University*, March 21-24, 1996.

[48] Tague, J.A., Estimation-Correlation, Modeling and Identification in Adaptive Array Processors, Ph.D. Thesis, Penn State University, 1987.

[49] Tague, J.A., and Sibul, L.H., "Estimator-Correlator Array Processing, Theoretical Theoretical Underpinnings and Adaptive Implementation", *Multidimensional Systems and Signal Processing*, 2:55-68, 1991.

[50] Price, R., "Optimum Detection of Random Signals in Noise With Application to Scatter-Multipath Communications", *IRE Trans. On Information Theory*, IT 2:125-135, 1956.

[51] Candy, J.V., Signal Processing, The Model Based Approach, McGraw-Hill, New York, 1986.

[52] Jazwinski, A., Stochastic Processes and Filter Theory, Academic Press, New York, 1970.

[53] Aoki, M., Optimization of Stochastic Systems, Academic Press, New York, 1967.

[54] Anderson, B.D. and Moore, J.B., Optimal Filtering, Prentice Hall, Englewood Cliffs, New Jersey, 1979.

[55] Kailath, T., "Innovations Approach to Detection and Estimation Theory", *Proc. IEEE*, Vol. 58, 1970.

[56] Van Trees, H.L., Detection, Estimation, and Modulation Theory, Part I, Wiley, New York, 1968.

[57] Fisher, R.A., "Theory of Statistics and Estimation", *Proc. Cambridge Philosophical Society*, Vol. 22, 700-720, 1925.

[58] Fisher, R.A., "On the Mathematical Foundations of Theoretical Statistics", *Proc. Cambridge Philosophical Society*, Vol. 22, 700-720, 1925.

[59] Altes, R.A., Methods of Wideband Signal Design for Radar and Sonar Systems, Ph.D. Thesis, University of Rochester, New Your, 1970.

[60] Hillsley, K.L., "Cramer Rao Lower Bound for Time-Scale", Personal Communication, November 1998.

[61] Ricker, D.W., "Constrained Bandwidth Waveforms With Minimum Dilation Sensitivity:, *IEEE Trans. On Aero. And Elec. Systems*, Vol. 29, No. 3, pp. 606-626, July, 1993.

[62] Ricker, D.W., "The Doppler Sensitivity of Large TW Phase Modulated Waveforms", *IEEE Trans on Signal Processing*, Vol. 40, No. 10,(2406-2413) Oct. 1992

[63] Qin, Q,., Wong, K., and Luo, Z., "Joint Time Delay and Doppler Stretch Estimation Using Wideband Signals", *Proc. IEEE Workshop on Statistical Signal and Array Processing*, pp.18-21, 1992.

[64] Gohberg, I., Goldberg, S., Basic Operator Theory, Birkhauser, Boston, 1981.

[65] Oppenhein, A.V., and Schafer, R., Discrete Time Signal Processing, Prentice Hall, Englewood Cilffs, New Jersey, 1984.

[66] Haykin, S., Adaptive Filter Theory, Prentice Hall, Englewood Cliffs, New Jersey, 1986.

[67] Noble, B., Applied Linear Algebra, Prentice Hall, Englewood Cliffs, New Jersey, 1967.

[68] Ricker, D.W., "An Iterative Least Squares Approach to Scattering Function Estimation", ARL IM# 84-104, June, 1984.

[69] Matuson, M.A., The Equivalence of the SVD Pseudo-Inverse and Spectrum Division Method of Deconvolution, Ph.D. Thesis, April, 1985.

[70] Matuson, M.A., "SVD Pseudo-Inverse Deconvolution of Two Dimensional Arrays", ARL TM# 85-107, June 1995.

[71] Interstate Electronics Corporation, Signal Processing Techniques, 1979.

[72] Marion, J.B., Classical Dynamics of Systems and Particles, Academic Press, New York, 1970.

[73] Bierman, J.G., Factorization Methods for Discrete Sequential Estimation, Academic Press, New York, 1977.

[74] Schwartz, S.C., "The Estimator-Correlator for Discrete Time Problems", *IEEE Trans. on Info. Theory*, Vol. IT-23, No. 1, pp. 93-100, January, 1997.

[75] Fogel, A. and Schwartz, S.C., "Listing Forms of the Discrete-Time Estimator-Correlator Detector", *IEEE Trans. on Info. Theory*, Vol. IT-29, No. 2, pp. 296-299, March 1993.

[76] Babst, M.S., Wideband Communications in High-Velocity Multipath Fading Channels, Ph.D. Thesis, The Pennsylvania State University, 1997.

[77] Blake, A., "Contour Tracking by Stochastic Propagation of Conditional Density," *In. Proc. European Conf. Computer Vision*, Cambridge UK, pp. 343-356, 1996.

[78] Lowe, D.G., "Robust Model-Based Motion Tracking Through The Integration of Search and Estimation," *Int. Journal of Computer Vision*, 8(2):113-122, 1992.

[79] Kass, M., Witkin, A., ands Terzopoulos, D., "Snakes: Active Contour Models", *Proc. 1st Int. Conf. on Computer Vision*, 259-268, 1987.

[80] Huttenlocker, D.P., Noh, J.J., and Rucklidge, W.J., "Tracking Non-Rigid Objects in Complex Scenes," *Proc. 4th Int. Conf. on Computer Vision*, 93-101, 1993.

[81] Harris, C., "Tracking With Rigid Models," In Active Vision, Blake, A., and Yuille, A., editors, 59-74, MIT, 1992.

[82] Lucas, B. D., Generalized Image Matching by the Method of Differences, Ph.D. Thesis, Computer Science Dept., Carnegie-Mellon University, Autumn, 1984.

[83] Johnson A.E., and Hebert, M., Recognizing Objects by Matching Oriented Points Technical Report CMU-RI-TR-96-04, Carnege-Mellon University, May, 1996.

[84] Drumheller, D.M., Probabilistic Data Association With the Inclusion of Attribute Information, Ph.D. Thesis, The Pennsylvania State University, 1989.

[85] Wang, L.H., Hsueh, L., "Using Range Profiles for Data Association in Multiple Target Tracking", *IEEE Trans. On Aerospace And Electronic Systems*, pp. 445-450, January, 1996.

[86] Frenkel, L., Feder, M., "Recursive Estimate-Maximize (EM) Algorithms for Time Varying Parameters With Applications to Multiple Target Tracking", *Int. Conf on Acoustics, Speech, and Signal Processing*, pp. 2068-2071, Vol. 3, May, 1995.

[87] Hsueh, J.L., Wang, Y.D., and Wang, H.W., "Matching Score Properties Between Range Profiles of High-Resolution Radar Targets," *IEEE Trans. On Antennas and Propagation*, Vol. 44.4, pp. 444-452, April, 1996.

[88] Candy, J.V. and Sullivan, E.J., "Model-Based Environmental Inversion: A Shallow Water Ocean Application," Journ. Acoust. Soc. Am., 98, pp 1446-1454, 1995.

[89] Candy, J.V., and Sullivan, E.J., "Passive Localization in Ocean Acoustics: A Model Based Approach," Journ. Acoust. Soc. Am., 98, pp 1455-1471, 1995.

APPENDIX A

Derivation of the J_{11} Term of the Fisher Information Matrix

In this section a derivation of the J_{11} term of the information matrix is provided in order to illustrate the methods used in the derivation of all of the components.

Beginning with the equation for the J_{11} term from Chapter 3

$$J_{11} = -E\left[2c\,\mathrm{Re}\left[\frac{\partial L}{\partial \tau}\frac{\partial L^*}{\partial \tau} + L\frac{\partial^2 L^*}{\partial \tau^2}\right]\right] \tag{A.1}$$

and the detector

$$L(s,\tau) = \int_{-\infty}^{\infty} r(t)\sqrt{s}\,f^*(s(t-\tau))dt \tag{A.2}$$

also needed is the echo model for r(t) as given by

$$r(t) = \tilde{b}\sqrt{E_t}\,[U(x)f(t)] + n(t) \tag{A.3}$$

where E_t is the transmitted energy and $\widetilde{b}$ is a random variable, white, Gaussian distributed, and zero mean. Also, n(t) is a zero-mean,white, Gaussian randon variable.

Here

$$[U(x)f(t)] = \sqrt{s}\, f(s(t-\tau)) \tag{A.4}$$

Substituting A(3)into (A.2), inserting the results into (A.1) and taking the prescribed derivatives

$$J_{11} = \left[2c\left[2\sigma_b^2 E_t \iint [U(x)f(t)][U(x)f(u)]^* \frac{\partial}{\partial\tau}[U(x)f(t)]^* \frac{\partial}{\partial\tau}[U(x)f(u)]dt\,du \right]\right]$$

$$+ \left[2c \iint N_0\delta(t-u)\right]\frac{\partial}{\partial\tau}[U(x)f(t)]^* \frac{\partial}{\partial\tau}[U(x)f(u)]dt\,du \tag{A.5}$$

$$+ \left[2c\left[2\sigma_b^2 E_t \iint [U(x)f(t)][U(x)f(u)]^*[U(x)f(t)]^* \frac{\partial^2}{\partial\tau^2}[U(x)f(u)]dt\,du \right]\right]$$

$$+ \left[2c\left[N_0 \iint \delta(t-u)[U(x)f(u)]^* \frac{\partial^2}{\partial\tau^2}[U(x)f(u)]dt\,du \right]\right]$$

Now, the second and 4th term in (A.5) cancel as we notice that

$$[U(x)f(u)]^* \frac{\partial^2}{\partial \tau^2}[U(x)f(u)] = -\frac{\partial}{\partial \tau}[U(x)f(t)]^* \frac{\partial}{\partial \tau}[U(x)f(u)] \quad \text{(A.6)}$$

If it is assumed that

$$\int [U(x)f(t)dt = 1 \quad \text{(A.7)}$$

With the 2nd and 4th terms in (A.5 accounted for, we are left with

$$J_{11} = 4c\sigma_b^2 E_t \,\mathrm{Re}\left[\left|\int_{-\infty}^{\infty} [U(x)f(t)\frac{\partial}{\partial \tau}[U(x)f(t)]^* dt\right|^2 + \int_{-\infty}^{\infty}[U(x)f(t)]^* \frac{\partial^2}{\partial \tau^2}[U(x)f(t)]dt\right] \quad \text{(A.8)}$$

Now, to reduce the first term in (A.8), we use Parsevals Relation to change to the frequency domain

$$\left|\ \right|^2 = \int_{-\infty}^{\infty}\int_{-\infty}^{\infty} \sqrt{s}f(s(t-\tau))e^{-j\omega t}dt\left[\frac{\partial}{\partial \tau}\int_{-\infty}^{\infty}\sqrt{s}f(s(t-\tau))e^{-j\omega t}dt\right]^* d\omega \quad \text{(A.9)}$$

Using the substitutions,

$$x = s(t-\tau) \quad \text{(A.10)}$$

Integrate Equation (A.10) to obtain

$$\left| \right|^2 = \left| s \int_{-\infty}^{\infty} j\left(\frac{\omega}{s}\right) F\left(\frac{\omega}{s}\right) F^*\left(\frac{\omega}{s}\right) d\frac{\omega}{s} \right|^2 \tag{A.11}$$

Which is,

$$\left| \right|^2 = s^2 \left(\frac{\overline{\omega}}{s}\right)^2 \tag{A.12}$$

Now, turning our attention to the second term, it is seen that following the same procedure, that is using Parsevals relation and making the same substitution using (A.10)

$$J_{11} = \overline{\omega}^2 - \overline{\omega^2} \tag{A.13}$$

Which is the same as for the narrow band case, this tells us that the CRLB for time scale is inversely proportional to the mean squared bandwidth.

TR Distribution List for "*A Kalman Filtering Approach to Wideband Scattering Function Estimation and Updating*," By Michael J. Roan - May 1999

Attn: Director
Defense Advanced Research Projects Agency
3701 N. Fairfax Drive
Arlington, VA 22203-1714

Attn: Library
Superintendent
Naval Postgraduate School
Monterey, CA 93943-5000

Naval Undersea Warfare Center Division
Attn: Library
Code 8219
Newport, RI 02841-5047

Naval Surface Warfare Center
Attn: Library
Carderock Division
Bethesda, MD 20084-5000

Attn: Library
Naval Command, Control and
Ocean Surveillance Center
RDT&E Division
San Diego, CA 92152-5000

Director
Attn: Library
Applied Research Laboratories
The University of Texas at Austin
Austin, TX 78712

Naval Surface Weapons Center
Attn: Library
10901 New Hampshire Avenue
Silver Spring, MD 20902-5000

Defense Technical Information Center
8725 John J. Kingman Road #944
Fort Belvoir, VA 22060-6217

Director
Attn: Library
Applied Physics Laboratory
John Hopkins University
Laurel, MD 20707

Naval Surface Warfare Center
Attn: Library
Coastal Systems Station
Dahlgren Division
Panama City, FL 32407-5000

Naval Undersea Warfare Center Division
Attn: Library
Keyport, WA 98345-0580

Naval Surface Warfare Center
Attn: Library
Carderock Division Detachment
Annapolis Laboratory
Annapolis, MD 21402-5067

Attn: Library
Naval Undersea Warfare Center Detachment
New London, CT 06320

Marine Physical Laboratory, P-001
Attn: Library
Scripps Institution of Oceanography
University of California, San Diego
San Diego, CA 92152-6400

Office of Naval Research
Attn: Library
Ballston Tower 1
800 North Quincy St.
Arlington, VA 22217

Space and Naval Warfare Systems Command
Attn: Library
Washington, D.C. 20363-5100

Naval Surface Warfare Center
Attn: M. M. Sevik, Code 700
David Taylor Model Basin
Carderock Division
Bethesda, MD 22084-5000

Applied Physics Laboratory
Attn: Library
University of Washington
1013 N.E. 40th St.
Seattle, WA 98105

Office of Naval Research
Ballston Tower 1
800 North Quincy St.
Arlington, VA 22217-5660
Attn: S. Lekoudis, ONR 333
Ms. Nancy Harned, ONR 321 US
Dr. John Tague, ONR 321 US
Ms. Khine Latt, ONR 333
Dr. Kam Ng, ONR 333
Dr. Neil Kerr, ONR 311

Commander
Department of the Navy
Program Executive Office
Undersea Warfare
2531 Jefferson Davis Highway
Arlington, VA 22242-5169
Attn: Mike Traweek
Code ASTO-D3

Dr. James Candy
Lawrence Livermore National Laboratory
7000 East Avenue
Livermore, CA 94550-9234

Dr. Edward L. Titlebaum
Electrical Engineering Department
University of Rochester
Rochester, NY 14620

Applied Research Laboratory
The Pennsylvania State University
P.O. Box 30
State College, PA 16804
Attn: F. W Symons
L. G. Weiss
R. L. Tutwiler
M. J. Gustafson
J. J. Kisenwether
T. W. Hilands
L. H. Sibul
D. W. Ricker
M. J. Roan
R. K. Young
M. R. Keller
K. L. Hillsley
SP Files
ARL Library (2 copies)